


Review

The Structures and Compositions Design of the Hollow Micro–Nano-Structured Metal Oxides for Environmental Catalysis

Jingxin Xu ^{1,†}, Yufang Bian ^{2,†} , Wenxin Tian ¹, Chao Pan ^{1,*}, Cai-e Wu ³, Leilei Xu ^{2,*}, Mei Wu ^{4,*} and Mindong Chen ^{2,5,*}

- ¹ State Key Laboratory of Low-Carbon Smart Coal-Fired Power Generation and Ultra-Clean Emission, China Energy Science and Technology Research Institute Co., Ltd., Nanjing 210023, China; xjx_0718@163.com (J.X.); twxtim@gmail.com (W.T.)
 - ² Collaborative Innovation Centre of the Atmospheric Environment and Equipment Technology, School of Environmental Science and Engineering, Nanjing University of Information Science & Technology, Jiangsu Key Laboratory of Atmospheric Environment Monitoring and Pollution Control, Nanjing 210044, China; bianyufang@emails.bjut.edu.cn
 - ³ College of Light Industry and Food Engineering, Nanjing Forestry University, Nanjing 210037, China; wucaie@njfu.edu.cn
 - ⁴ National & Local Joint Engineering Research Center for Mineral Salt Deep Utilization, Huaiyin Institute of Technology, Huaian 223003, China
 - ⁵ School of Environment and Energy Engineering, Anhui Jianzhu University, Hefei 230009, China
- * Correspondence: pcxyz@139.com (C.P.); leileixu88@gmail.com (L.X.); meiwu@hyit.edu.cn (M.W.); chenmdnuist@163.com (M.C.)
- † These authors equally contributed to this work.

Abstract: In recent decades, with the rapid development of the inorganic synthesis and the increasing discharge of pollutants in the process of industrialization, hollow-structured metal oxides (HSMOs) have taken on a striking role in the field of environmental catalysis. This is all due to their unique structural characteristics compared to solid nanoparticles, such as high loading capacity, superior pore permeability, high specific surface area, abundant inner void space, and low density. Although the HSMOs with different morphologies have been reviewed and prospected in the aspect of synthesis strategies and potential applications, there has been no systematic review focusing on the structures and compositions design of HSMOs in the field of environmental catalysis so far. Therefore, this review will mainly focus on the component dependence and controllable structure of HSMOs in the catalytic elimination of different environmental pollutants, including the automobile and stationary source emissions, volatile organic compounds, greenhouse gases, ozone-depleting substances, and other potential pollutants. Moreover, we comprehensively reviewed the applications of the catalysts with hollow structure that are mainly composed of metal oxides such as CeO₂, MnO_x, CuO_x, Co₃O₄, ZrO₂, ZnO, Al₃O₄, In₂O₃, NiO, and Fe₃O₄ in automobile and stationary source emission control, volatile organic compounds emission control, and the conversion of greenhouse gases and ozone-depleting substances. The structure–activity relationship is also briefly discussed. Finally, further challenges and development trends of HSMO catalysts in environmental catalysis are also prospected.

Keywords: hollow-structured metal oxides; environmental catalysis application; structures and compositions; structure–performance correlation



Citation: Xu, J.; Bian, Y.; Tian, W.; Pan, C.; Wu, C.-e.; Xu, L.; Wu, M.; Chen, M. The Structures and Compositions Design of the Hollow Micro–Nano-Structured Metal Oxides for Environmental Catalysis. *Nanomaterials* **2024**, *14*, 1190. <https://doi.org/10.3390/nano14141190>

Academic Editor: Alexey Pestryakov

Received: 4 June 2024

Revised: 23 June 2024

Accepted: 29 June 2024

Published: 12 July 2024



Copyright: © 2024 by the authors. Licensee MDPI, Basel, Switzerland. This article is an open access article distributed under the terms and conditions of the Creative Commons Attribution (CC BY) license (<https://creativecommons.org/licenses/by/4.0/>).

1. Introduction

With the occurrence of the global industrial revolutions and subsequent development of the economy, huge amounts of fossil fuels, such as naphtha and coal, have been consumed. As a result, a large number of atmospheric and aquatic environmental pollutants, such as carbon monoxide (CO), nitrogen oxides (NO_x), etc., have been discharged into the

environment and are harmful to the health of human beings [1,2]. The removal of these pollutants via environmental catalysis strategy is therefore of great importance from the viewpoint of environmental protection.

Broadly speaking, all the catalytic processes reducing and removing pollutant emissions and recycling resource utilization of the waste can be ascribed to the category of environmental catalysis, such as the below conditions: (a) eliminating the atmospheric, water, and indoor pollutants (e.g., CO [3], SO_x [4], NO_x [5], formaldehyde [2], toluene [6] and 4-Nitrophenol [7], etc.); (b) reducing the harmful substances generated in the energy conversion processes (e.g., supported metal catalysts are used to reduce polycyclic compounds and the biphenyls produced by the pyrolysis of industrial waste plastics) [8]; (c) converting the waste into useful resource [9]. The development of the efficient catalysts is considered the key factor of environment catalysis. In recent decades, structural engineering has attracted global widespread attention, and bridges the interplay between properties and performance.

At present, noble metals and transition metal oxide-supported catalysts are widely used in all kinds of environment catalytic processes [10]. Moreover, studies of catalysts have indicated that the catalytic activities of removing pollutants have been greatly related to various factors, such as the properties of the supports (e.g., specific surface area, porous structure, lattice oxygen mobility, etc.), the characteristics of the active centers (e.g., morphology, crystal face, dispersion, etc.), and the metal–support interaction (e.g., the adsorption of oxygen species, low-temperature reducibility, the ability to activate the reactants, the interaction between metals, etc.) [11].

Therefore, the catalytic ability could improve by adjusting the morphology, spanning from the atomic scale to the microarchitecture, and the spatial organization of components of the support [12,13]. As for the hollow micro–nano structured materials, they are defined as a type of functional nanomaterials with void spaces inside different shells [14]. In addition, the scarcity and cost of materials are also considered to be important concerns when developing new catalysts. The outstanding interfacial properties and higher atom utilization efficiency of HSMOs can be envisaged in potential catalysis application. Therefore, it is reasonable to design and construct novel catalysts with hollow structures in the viewpoint of atom economy.

With the in-depth study of hollow micro–nano structures, the HSMOs have received more and more attention in the field of environmental catalysis. HSMOs have advantageous physical properties such as high specific surface areas, tunable pore sizes, synergistic interaction, adjustable morphology, space utilization, abundant defects, adjustable surface chemistry, and low density, etc. Additionally, further advantages, such as high loading capacity, good surface penetration, water resistance, strong metal–support interaction (SMSIs), and magnetism, can be achieved by controlling their structure and composition. As a result, these have been widely used in many environmental catalysis reactions, including methane combustion [15], water–gas shift [16], CO oxidation [17], CO conversion [18,19], toluene oxidation [20,21], chlorinated aromatic compound oxidation [22], formaldehyde oxidation, etc. [23]. The summary of the application of HSMOs in the elimination of environmental pollutants is shown in Table 1.

Furthermore, HSMOs are also widely used in lithium-ion batteries [24,25], gas sensors [26], energy-related systems [27], and heterogeneous catalysts, etc. [28–30]. Recently, some excellent reviews have given comprehensive descriptions and discussions of HSMOs, showing their fascinating performance, fabrication, and properties [31–34]. However, these reviews did not comprehensively cover the composition and structure design of HSMOs or their applications in the field of environmental catalysis. Therefore, this review summarizes the different aspects of the application of HSMOs to environmental catalysis. In light of this, the synthetic strategies are only briefly introduced in this review. These strategies can be classified into four different types, including hard-templating, soft-templating, self-templated, and template-free methods. Therefore, this review will mainly focus on the recent progresses in the application of the HSMOs as the efficient catalysts and/or supports

in the field of environmental catalysis, which performed lots of superiorities compared with the traditional counterparts. To highlight the catalytic performance of HSMOs, we focus on the catalytic activity as the main performance descriptors rather than the stability and selectivity.

Table 1. Summary of the application of HSMOs in the elimination of environmental pollutants.

Items	Details
Automobile and stationary sources emission	Catalytic oxidation of CO NH ₃ -SCR removal of NO _x Catalyst for automobile three-way catalytic (TWC) reaction Catalyst for diesel oxidation catalytic (DOC) reaction
Volatile organic compounds (VOCs)	Catalytic oxidation of toluene Catalytic oxidation of vinyl chloride (VC) Catalytic oxidation of formaldehyde (HCHO)
Greenhouse gases	Catalytic conversion of CO ₂ Catalytic conversion of CH ₄
Other potential pollutants	Hydrogenation of 4-nitrophenol (4-NP) Catalytic oxidation of 1,2-dichlorobenzene (o-DCB) Catalytic oxidation of dyes (e.g., acid orange 7(AO7), methylene blue) Photocatalytic degradation of pharmaceuticals (e.g., aceta-minophen, norfloxacin (NOR), tetracycline (TC), and ciprofloxacin) Photocatalytic degradation of organic pollutions (e.g., phenol)

2. The Application of HSMO Catalysts in Environmental Catalysis

2.1. Automobile and Stationary Sources Emission Control

The untreated exhaust gases of automobiles, chemical plants, and coal-fired power plants such as CO, NO_x, SO_x, and other harmful gases, have caused serious environmental problems and human health issues [35,36]. As it is well known, CO is a toxic atmospheric pollutant that is both flammable and explosive, whilst NO_x and SO_x can cause acid rain and photochemical smog, which negatively affect human respiratory system. In order to alleviate the related pollutants' emissions, various strategies, such as adsorption, absorption, catalytic oxidation, incineration, plasma destruction, and photocatalysis, etc., have been widely investigated. It is clear that catalytic oxidation has been considered to be the most effective method because of its unique advantages, such as its high efficiency and cleanliness [36,37]. Therefore, lots of efforts have been devoted to the development of efficient catalysts to control the emissions of automobile and stationary sources. Meanwhile, HSMO-based catalysts provide promising and valuable chances to develop advanced catalysts due to the advantages of HSMOs in terms of their low density, large surface-to-volume ratios, reduced mass transport length, and high loading capacity.

2.1.1. Catalytic Oxidation of CO

Industrial and automobile CO emissions have been increasing year upon year. The removal of CO emissions has become an important concern because of their high toxicity to human health and the living environment. The catalytic oxidation of CO has been considered the most effective treatment method [10]. The HSMOs of various structures have been used to catalyze CO oxidation in the past two decades. The hollow interior space of HSMOs is expected to effectively reduce the density of the material and enhance the permeability of the material. As a result, they can provide gaseous reactants with large specific surface areas for the absorbance and mass transference of the CO molecules to the active center. In addition, the extended contact time between CO molecules and the active center have potentially positive impacts on the whole catalytic process.

The 'lattice oxygen' mechanism believes that the oxygen supply ability of metal oxides is a key factor influencing catalytic reactions [38]. To date, numerous catalysts have been investigated in the preliminary study of CO oxidation. Among these catalysts, Ceria (CeO₂), with its cubic fluorite structure, has been considered a key promoter of catalytic CO

oxidation. Therefore, the catalysts for CO oxidation are divided into the hollow micro/nano-structured CeO₂-based materials (HMNCMs) and other HSMOs and highlighted in this subsection. For HMNCMs, CeO₂ performs variable oxidation states, and has good redox properties and a high storage/release oxygen capacity thanks to its abundant oxygen vacancy, the redox property of Ce³⁺/Ce⁴⁺, and its structural integrity [39]. Studies of CeO₂ morphology control for the catalytic oxidation of CO can be traced back to 2006 [40]. Lots of studies have focused on the shape-controlled synthesis of Ce-based nanomaterials and their corresponding catalytic applications [41,42]. Ce-based nanomaterials can obtain a controllable morphology through the reasonable regulation of reaction conditions [43]. To date, many Ce-based catalysts with hollow structures have been successfully designed and fabricated [44–52], which accelerate the process of their practical application [53]. However, there is no complete report on the application of HMNCMs toward the catalytic CO oxidation.

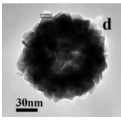
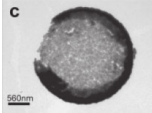
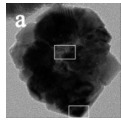
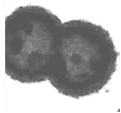
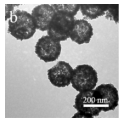
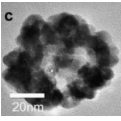
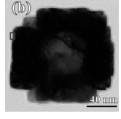
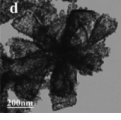
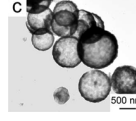
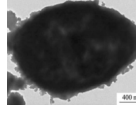
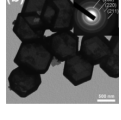
It is worth noting that lots of HMNCMs with different compositions and morphologies have been developed since 2012 [54–58]. The HMNCMs could be divided into the pure CeO₂ hollow structure, the composite binary or multiple CeO₂ hollow structures, the multi-element Ce-based hollow structure, and the Ce-based hollow structure-doped with noble metals according to the composition. The critical factors of reaction conditions, the possible formation mechanism on the morphology and assembly of the HMNCMs, and the CO oxidation catalytic activities have been investigated in previous studies. The amazing progress of hollow micro/nano-structures have been largely driven by the development of analytical technologies and the simultaneous development of template materials [32]. Therefore, in order to clearly prospect and outlook the development and changes, the related information and details about HMNCMs and other HSMOs were summarized.

- Pure CeO₂ hollow structure

The previous investigation into CeO₂ with a hollow structure morphology revealed that the exposed special crystal facets, small CeO₂ crystal sizes, and a significantly deformed structure in the boundary area were key factors for the improved CO oxidation activity [50]. Additionally, the oxygen storage capacity of CeO₂ is greatly related to the morphology or surface structure [45,59]. Therefore, it is of great necessity to explore and develop CeO₂ with hollow structure. Studies have shown that {100} surface ceria nanocrystals performed a higher CO oxidation activity than those with {111} surface-dominant [60,61], which was related to the lattice oxygen migration of {100}/{110}-dominated surface structures [59,62]. Han et al. [63] fabricated the CeO₂ hollow structure catalyst with a significant improvement in the catalytic CO oxidation activity. The reason for this was that the CeO₂ hollow structure exposed more {001} faces, which have more dangling bonds on the surface and internal Ce atoms. Therefore, the CeO₂ with abundant dangling bonds, mesoporosity, oxygen vacancies, and high surface areas were beneficial to their catalytic performance in CO oxidation.

There are also other pure CeO₂ hollow structures, including CeO₂ hollow nanocones [64], CeO₂ hollow microspheres [65–67], and CeO₂ hollow dodecahedrons [68]. A summary of pure CeO₂ with various hollow structures is presented in Table 2. Among them, Li et al. [68] found that the CO catalytic activity of the cracked hollow CeO₂ dodecahedrons was significantly lower than that of the hollow CeO₂ dodecahedrons due to the presence of oxygen vacancy defects and the permeability of the shell. The hollow CeO₂ dodecahedrons and the CeO₂ hollow nanocones exhibited excellent CO catalytic activity, which was ascribed to the homogeneously dispersed particles with mesoporous structures comprising the highly specific BET surface area morphological features. However, the catalytic activity of these CeO₂ hollow structures still does not meet the requirements of industrial applications because the hollow catalyst possesses the disadvantage of a structural collapse as well as low activity. Therefore, CO oxidation catalysts require a stable structure to achieve excellent catalytic stability.

Table 2. Pure CeO₂ with various hollow structures and the catalytic performances of their CO catalytic oxidation.

Synthesis Method	S _{BET} (m ² g ⁻¹)	Catalytic Performance	Morphology	Ref.
One-pot template-free route	14.7	T ₅₀ = 280 °C		[46]
Hydrothermal process	22.0	—		[47]
Template-free method	—	T ₅₀ < 270 °C		[49]
Surfactant-assisted solvothermal synthesis	74.0	—		[54]
Self-template hydrothermal synthesis	36.7	—		[67]
Template-free method	19.6	—		[69]
Template-free method	106.4	T ₈₀ < 310 °C		[63]
Solvothermal or hydrothermal route	147.6	T ₉₅ = 250 °C		[64]
Ultrasonic-spray-assisted synthesis	75.8	T ₁₀₀ = 280 °C		[66]
Yeast cells as templates	38.7	T ₉₀ = 372 °C		[65]
One-step liquid phase reaction	128.0	T ₁₀₀ = 170 °C		[68]

Furthermore, compared with other hollow-structured CeO₂, hollow CeO₂ dodecahedrons performed the best CO oxidation catalytic activity because of the incorporation of Co species [68]. Although the CeO₂ itself cannot achieve a high catalytic CO oxidation activity, it can incorporate other metals as structural and/or electronic promoters to improve its catalytic activity and stability with the priority of not destroying the hollow

structure. Based on these basic studies, HMNCMs doped with transition metals have been further developed.

- The composite binary or multiple CeO₂ hollow structure

It was reported that the synergistic effect created by incorporating the transition metal (Co, Cu, Mn, Ni, and Fe) into CeO₂ could greatly improve the catalytic activity [70–73]. In Table 3, we summarize the composite binary or multiple CeO₂ materials with various compositional, hollow structures, and the catalytic parameters for CO catalytic oxidation. The changes in the physical properties of hollow catalysts with different structures will increase the catalytic CO oxidation activity. For example, the Co₃O₄-CeO_{2-x} hollow multi-shell structure (HOMS) could achieve the complete conversion at 166.9 °C, while the complete conversion temperature of Co₃O₄-CeO_{2-x} (Co/Ce = 4/1) nanoparticles (NPs) was 206 °C [70]. For hollow mesoporous Co₃O₄-CeO₂ composite nanotubes with open-ends, the non-closed structure can accelerate the reactants to enter the hollow structure of the catalyst to contact more active centers, accounting for the 100% CO conversion at 145 °C [71].

Table 3. The binary or multiple CeO₂-based materials with various compositions, hollow structures, and catalytic parameters for CO catalytic oxidation.

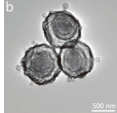
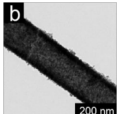
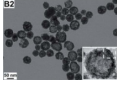
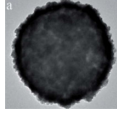
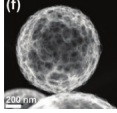

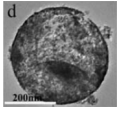
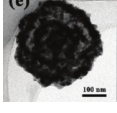
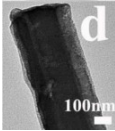
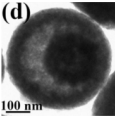
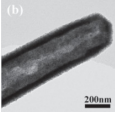
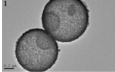
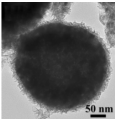
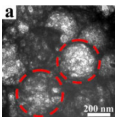
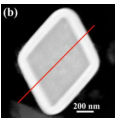
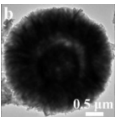
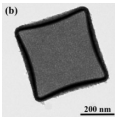
Doped Metals	Material	Synthesis Method	S _{BET} (m ² g ⁻¹)	Total CO Conversion Temperature	Morphology	Ref.
Co	Co ₃ O ₄ -CeO _{2-x}	Sequential templating approach	55.2	166.9 °C		[70]
	Co ₃ O ₄ -CeO ₂	Self-templating method	44.8	145 °C		[71]
Cu	(Cu doping) CeO ₂	One-step solvothermal process	165.5	21 °C		[74]
	CeO ₂ -CuO _x	Self-assembled approach	98.7	112 °C		[75]
	CuCe-L	Aerosol-assisted synthesis	48.0~58.6	120 °C		[76]
	CuO@CeO ₂	Surface Etching Strategy	36.0	—		[77]
	CuO@CeO ₂	Template-free synthesis	90.0	60 °C		[78]
	CuO/CeO ₂ -8%	Two-step route	24.9	130 °C		[79]

Table 3. Cont.

Doped Metals	Material	Synthesis Method	S_{BET} ($\text{m}^2 \text{g}^{-1}$)	Total CO Conversion Temperature	Morphology	Ref.
	Ce-MOF CeO ₂ -CuO	Assistance of selective etching	86.7	98 °C		[80]
Cu	CeO ₂ -MO _x (M = Cu, Co, Ni)	Wet-chemical approach	—	160 °C		[81]
	Ce-Mn Binary Oxide	Interfacial reaction-directed synthesis	202.0	T ₅₀ = 120 °C		[55]
	MnO ₂ /CeO ₂ -MnO ₂	Sacrificial templates	103.1	206 °C		[82]
	CeO ₂ @MnO ₂	Wet-chemical synthetic strategy	98.3	230 °C		[83]
Mn	CeO ₂ -MnO _x	Hard template-assisted solution combustion	115.2	160 °C		[84]
	Mn ₂ O ₃ @CeO ₂	Wet-chemical process	54.5	220 °C		[85]
	CeO ₂ -MnO _x	Pyrolyzing Ce-Mn coordination polymers	77.8	~250 °C		[86]
Fe	Fe ₂ O ₃ /CeO ₂	PB-based wet chemical approach	73.9	~230 °C		[87]

As shown in Figure 1, the Co catalytic CO oxidation mechanism was addressed by the Langmuir–Hinshelwood (L-H) model, which contained the four following steps [71]: (1) The CO was adsorbed into the interface of Co₃O₄ and CeO₂. (2) The CO₂ molecule was formed with the oxygen vacancy left due to the extraction of surface oxygen by CO. (3) The O₂ reacted with the oxygen vacancy and the amount of adsorbed O₂ increased, with the dissociation of O₂ into the O₂[−] ion radical, which promoted the enhancement of the CO oxidation. (4) The O₂[−] ion radical reacted with the CO molecule and the CO₂ molecule was formed. The oxygen vacancy was a vital part for the dissociation of O₂ in the CO oxidation reaction, which linked with the metal nanoparticles size, the oxidation states, and the oxidation states of the catalyst.

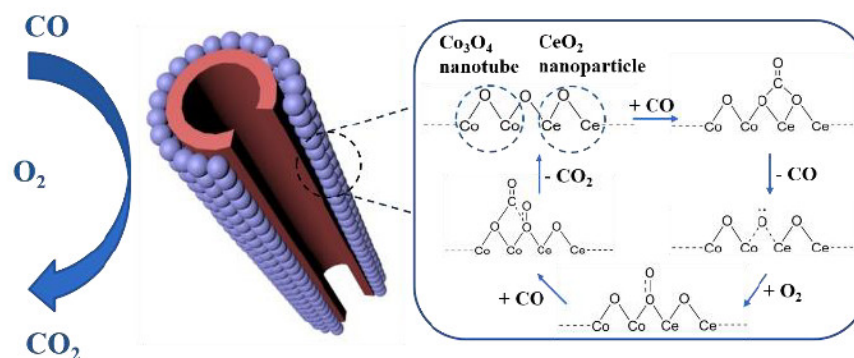


Figure 1. Schematic of the reaction mechanism for CO oxidation. Figure reproduced from ref. [71].

As a new type of composite materials, the hollow composite materials have attracted increasing attention. Liu et al. fabricated the $\text{CeO}_2\text{-CuO}_x$ hollow nanospheres with loos and a rough surface, which demonstrated that they had a more unique structure because Cu species were more inclined to concentrate on the surface of CeO_2 hollow spheres compared with the pristine CeO_2 [74]. In addition, the Cu species was the active site of $\text{CeO}_2\text{-CuO}_x$ composite hollow spheres in terms of catalytic CO oxidation [75]. The structural stability of the $\text{CuO}_x/\text{CeO}_2$ interface is also a very important concern for Cu-doped CeO_2 catalysts. The sintering of the surface CuO_x during the reaction often causes changes in the surface copper species and crystal structure of cerium oxide, which in turn affect the catalytic activity.

The active center theory believes that the corners, steps, edges, dislocations, defects, and other discontinuities on the catalyst surface would modify the nature of the adsorbed species and the dynamics of the surface reactions [88]. Their catalytic activities are usually higher than those on a flat surface. As a result, these sites are considered active centers. As shown in Table 3, abundant steps were exhibited on the surface of the novel litchi-peel-like hierarchical hollow copper–ceria microspheres, which was crucial for the improvement in catalyst activity [76]. The excellent catalytic activity could be attributed to the step-stabilized strong interaction between CuO_x species and CeO_2 and the abundant surface steps in litchi-peel-like samples that act as adsorption sites for oxygen.

Many researchers believed that the copper–ceria catalyst was a sort of promising alternative that could substitute for noble metal catalysts due to its low cost and decent catalytic activity [78]. Therefore, the spiny yolk@shell CuO@CeO_2 cubes with a hedgehog-like surface composed of large spiny CuO crystal whiskers [77], triple-shelled CuO/CeO_2 hollow nanospheres [79], and hollow-multiporous wall CeO_2 -supported CuO catalysts [78] were prepared. The hollow-multiporous wall CeO_2 supported CuO catalysts for CO oxidation with a T_{100} of around 60°C . However, its stability test was not so excellent compared to other Cu-doped CeO_2 catalysts.

It is common practice to improve the catalytic activity of HMNCMs by incorporating Mn. Zhang et al. [82] prepared $\text{MnO}_2@\text{CeO}_2\text{-MnO}_2$ composite hollow spheres exhibiting a superior catalytic performance by the facile three-step method, which employed carbon spheres (CSs) as sacrificial templates. Chen et al. prepared $\text{CeO}_2\text{-CuO}$ with a core–shell structure [80] and porous/hollow-structured $\text{CeO}_2\text{-MnO}_x$ [84] to promote the performance of the catalytic CO oxidation. Liu et al. [81] fabricated $\text{CeO}_2\text{-MO}_x$ ($M = \text{Cu, Co, Ni}$) composite yolk–shell nanospheres by the general wet-chemical approach. After this, they fabricated a series of $\text{MCo}_2\text{O}_4@\text{CeO}_2$ ($M = \text{Ni, Cu, Zn, Mn}$) core@shell nanospheres [80], double-shelled $\text{Fe}_2\text{O}_3/\text{CeO}_2$ boxes [87], $\text{CeO}_2@\text{MnO}_2$ core@shell nanospheres [83], $\text{Mn}_2\text{O}_3@\text{CeO}_2$ core@shell cubes [85], and $\text{CeO}_2\text{-MnO}_x$ hollow 3D porous architecture [86].

Obviously, the doped metal Cu of Ce-based materials played a pivotal role in catalytic reaction. However, the comparison of catalytic activities toward the CO oxidation of the and hollow-multiporous wall CeO_2 supported CuO catalysts and the $\text{CeO}_2\text{-CuO}_x$ hollow nanospheres indicated that the adjustable morphology of catalysts endows the catalyst to rationalize a multitude of factors, such as the synergistic interaction, high surface area,

space utilization, high loading capacity, superior pore permeability, and abundant inner void space.

- The multi-element Ce-based hollow structure

Additionally, multi-metal doped Ce-based CO oxidation catalysts have also been extensively studied. Some parameters of the hollow structure, such as the composition and wall thickness, are related to the synergy between metals. Liu et al. [89] reported the hollow CeO_2 - Cu_2O , core-shell $\text{NiO}@\text{Cu}_2\text{O}$, and hollow CeO_2 - NiO - Cu_2O cages (Figure 2). The multicomponent metal oxides with a hollow structure exhibited a lower CO oxidation temperature than Cu_2O cubes.

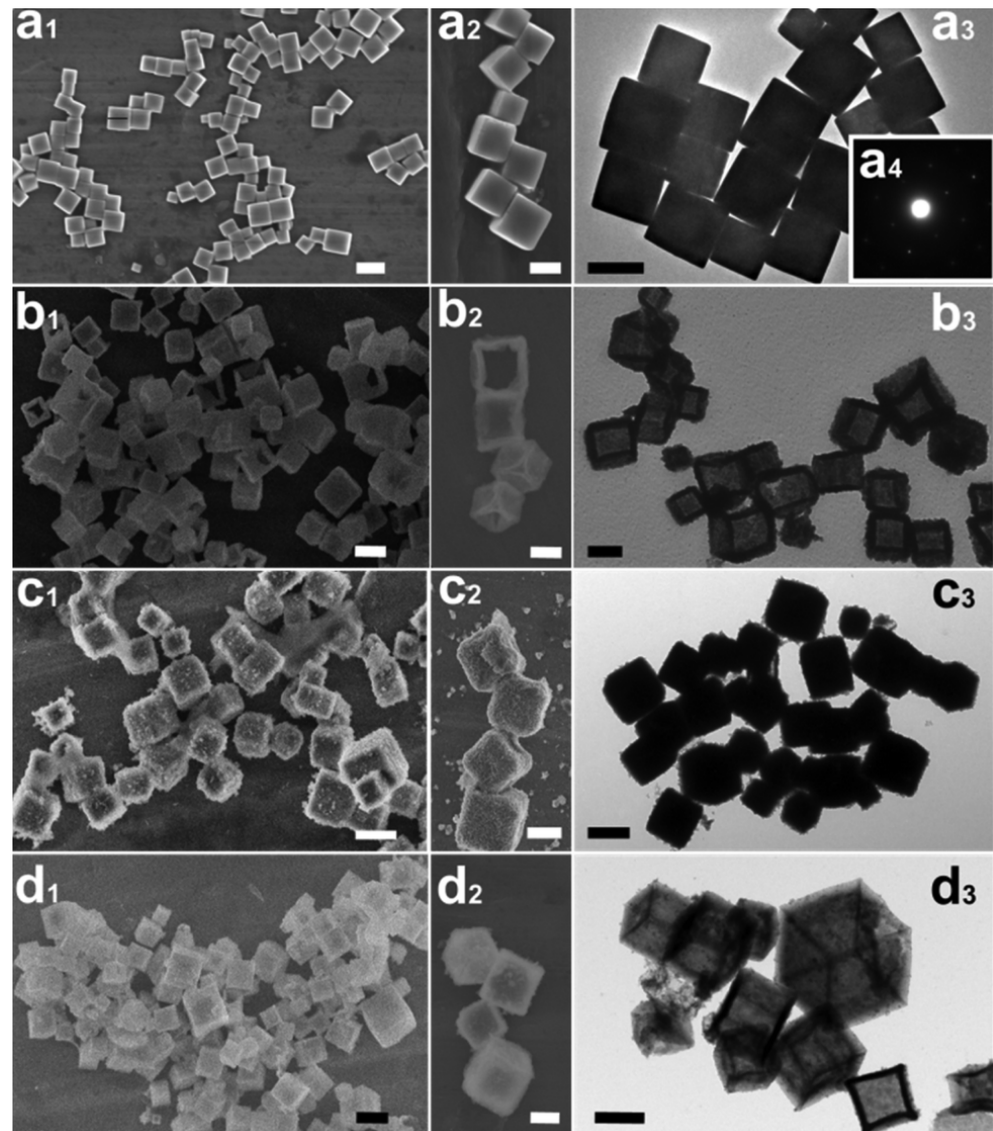


Figure 2. The SEM (x1 and x2) and TEM (x3) images of the Cu_2O cubes, composite CeO_2 - Cu_2O (1), $\text{NiO}@\text{Cu}_2\text{O}$ (2), and CeO_2 - NiO - Cu_2O (3). (x = a, b, c and d for Cu_2O and composites 1–3, respectively) The scale bar is 800 nm in parts x1 and x3, and it is 500 nm in part x2. Figure reproduced from ref. [89]. (a₁,a₂) The SEM images of Cu_2O cubes; (a₃) The TEM images of Cu_2O cubes; (a₄) The SAED pattern of Cu_2O cubes; (b₁,b₂) The SEM images of composite CeO_2 - Cu_2O ; (b₃) The TEM images of composite CeO_2 - Cu_2O ; (c₁,c₂) The SEM images of composite $\text{NiO}@\text{Cu}_2\text{O}$; (c₃) The TEM images of composite $\text{NiO}@\text{Cu}_2\text{O}$; (d₁,d₂) The SEM images of composite CeO_2 - NiO - Cu_2O ; (d₃) The TEM images of composite CeO_2 - NiO - Cu_2O .

Cheng et al. [90] synthesized NiCo₂O₄@CeO₂ core@shell nanotubes with a tunable shell thickness through the layer-by-layer coating method and employed these materials as the high-performance catalyst of the CO oxidation reaction. The NiCo₂O₄@CeO₂-2 (2 represented the molar ratio of Ce/(Ni + Co)), which showed the highest catalytic activity: over 50% of CO can be oxidized at a low temperature of 100 °C, and the final T₁₀₀ (100% conversion temperature) was about 150 °C. The effect of different shell structures on catalytic performance was studied. The results showed that the two-phase interface area of NiCo₂O₄@CeO₂-1 with the thinnest CeO₂ shell will decrease, which weakens the synergistic effect between CeO₂ and NiCo₂O₄.

- Ce-based hollow structure doped with noble metals

Huge challenges such as the low thermal stability and loss of catalytic activity due to sintering still need to be solved in catalytic applications. This was attributed to the noble metal nanoparticles which tend to aggregate during the process of catalytic reaction, causing the rapid decay of catalytic activity and stability [12]. The decentralized function of HMNCMs is a critical advantage for noble metal materials. Thus, designing and fabricating HMNCMs to suppress the aggregation and sintering of noble metal nanoparticles is an effective and promising solution [63,91]. The summary of the Ce-based hollow structure doped with noble metals is presented in Table 4.

Table 4. CeO₂-based hollow structure doped with noble metals with various compositions, structures, and their catalytic performances of CO catalytic oxidation.

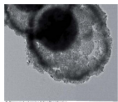
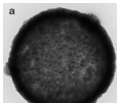
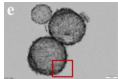
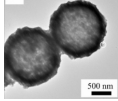
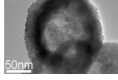
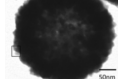
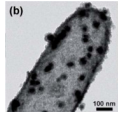
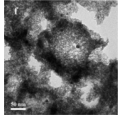
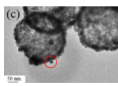
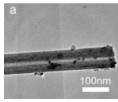
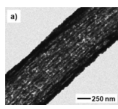
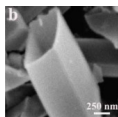
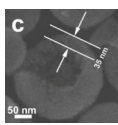
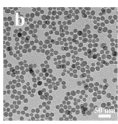
Doped Noble Metal	Material	Synthesis Method	S _{BET} (m ² g ⁻¹)	Catalytic Performance	Morphology	Ref.
	Pd@CeO ₂	Template-assisted and solvothermal alcoholysis strategy	73.3	T ₉₀ = 2 °C		[92]
Pd	h-Pd-CeO ₂ NCSs	Polymer-templated synthesis	59.3	T ₈₀ = 130 °C		[91]
	MnO ₂ -Pd-CeO ₂	Multi-assembly method	128.0	T ₉₀ = 90 °C		[93]
	Au/CeO ₂ -ZnO	Chemical reaction	32.4	T ₁₀₀ = 60 °C		[94]
Au	Au/CeO ₂	One-step template-free strategy	145.0	T ₉₂ = 25 °C		[95]
	Au/CeO ₂	Template-free method	23.9	T ₉₀ = 185 °C		[96]

Table 4. Cont.

Doped Noble Metal	Material	Synthesis Method	S_{BET} ($\text{m}^2 \text{g}^{-1}$)	Catalytic Performance	Morphology	Ref.
Au	Au@CeO ₂	In situ redox reaction	—	$T_{100} = 21 \text{ }^\circ\text{C}$		[97]
	Au@CeO ₂ -ZrO ₂	Electrostatic attraction-induced deposition method	—	$T_{100} = 130 \text{ }^\circ\text{C}$		[98]
	Au/CeO ₂	Hard template synthesis method	77.8	$T_{100} = 81 \text{ }^\circ\text{C}$		[3]
	Au/CeO ₂	Conventional solvothermal+ method auto-redox method	—	$T_{100} = 73 \text{ }^\circ\text{C}$		[99]
Pt	Pt _{encap} /CeO ₂	Template-based procedure	—	—		[57]
	CeO ₂ -Pt	Interfacial reactions	62.3	$T_{100} = 93 \text{ }^\circ\text{C}$		[100]
	Pt/CeO ₂	One-pot template-free solvothermal method	190.1	$T_{100} = 155 \text{ }^\circ\text{C}$		[101]
	Pt/CeO ₂ @SiO ₂	Microemulsion method	146.2	$T_{100} = 162 \text{ }^\circ\text{C}$		[102]

The noble metal NPs act as the active catalytic sites for CO oxidation. The role of hollow ceria as support is primarily to stabilize noble metal NPs to prevent their sintering during catalytic reactions. In addition, ceria also works as an electronic modulator for the loaded noble metal NPs [92,95,97]. The interior void space of hollow CeO₂-ZnO microspheres fabricated by Xie et al. [94] can be clearly observed in Table 4. The Ce-OZn linkages formed at the interface between CeO₂ and ZnO nanoparticles, which was conducive to strengthening interfacial interactions and CO adsorption. Consequently, the catalytic activity of CO oxidation over the CeO₂-ZnO composite hollow microspheres was greatly improved due to the synergistic effect between CeO₂ and ZnO. They loaded the Au nanoparticles on the surfaces of the CeO₂-ZnO composite hollow microspheres by the deposition-precipitation method to further improve the CO oxidation catalytic activity.

Many HMNCMs have been used as the support for Au nanoparticles, such as Au@CeO₂-ZrO₂ with a hollow core-shell structure [98], Au/CeO₂ hollow nanospheres [3], Au/CeO₂ nanotubes [99], and sandwich hollow-structured CeO₂@Au@CeO₂-MnO₂ [103]. Compared to non-hollow-structured core-shell Au@CeO₂ nanocomposites [104], these hollow-structured catalysts exhibited a higher catalytic activity for CO oxidation.

HMNCMs loaded with Pd can effectively prevent particle migration and deactivation by separating precious metal NPs in the small cavities [91]. As shown in Figure 3a, (1) Pd NPs were fully deposited on the surface of RF polymer spheres to form RF@Pd structure;

(2) RF@Pd particles were exposed to the solution containing Ce^{3+} and hexamethylenetetramine (HTMA) to form RF@Pd@CeO₂; (3) Hollow Pd–CeO₂ nano-composite spheres (NCSs) were fabricated by calcination to eliminate the polymer templates.

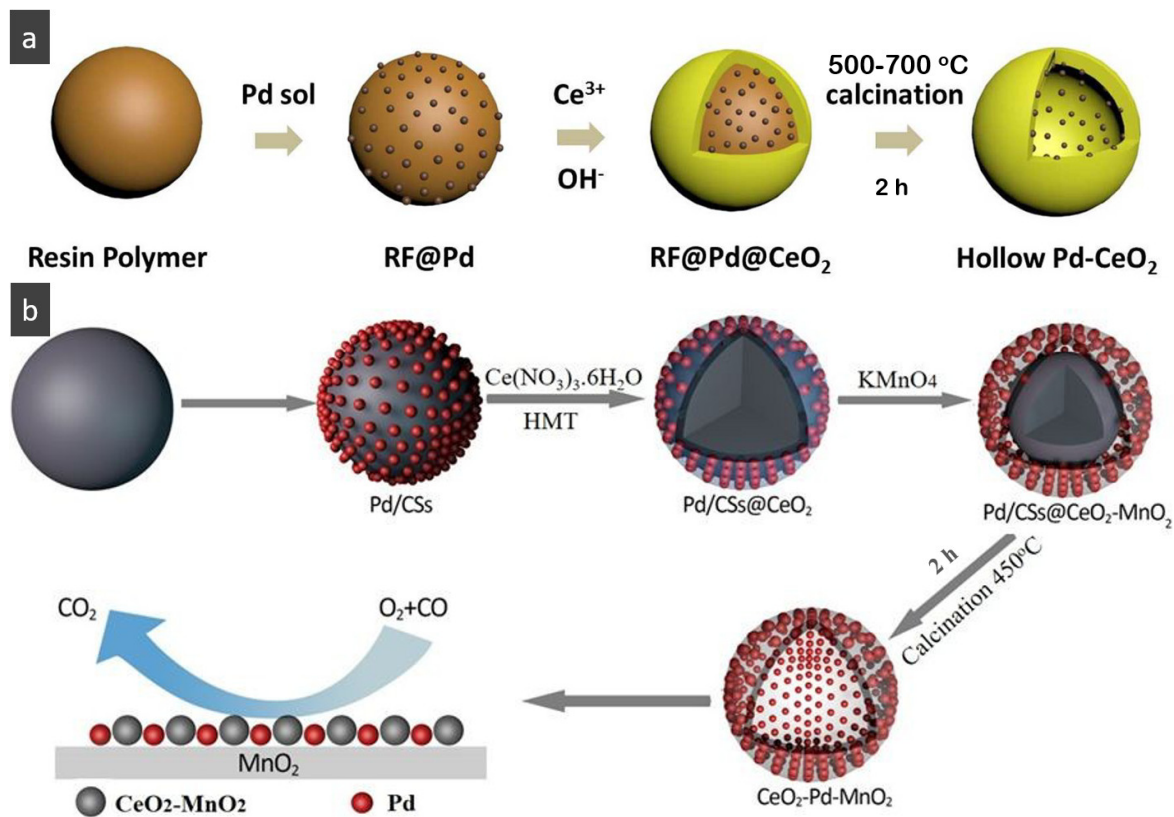


Figure 3. (a) The formation process of the hollow Pd–CeO₂ nano-composite sphere reproduced from ref. [91]; (b) Schematic illustration of the synthesis process for sandwich-like MnO₂–Pd–CeO₂ hollow spheres. Figure reproduced from ref. [93].

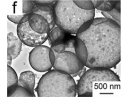
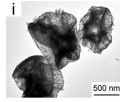
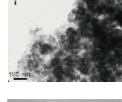
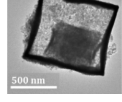
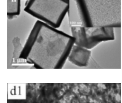
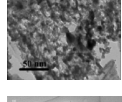
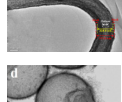
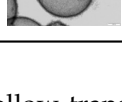
For other HMNCMs doped with metallic Pd NPs, Zhang et al. [93] prepared sandwich-like MnO₂–Pd–CeO₂ hollow spheres by depositing Pd nanoparticles on the outer surface of the MnO₂ shell, before coating it with CeO₂, which had an anchoring effect on the outermost layer (Figure 3b). The hollow spheres exhibited excellent stability and CO oxidation activity due to the sandwich structure and the strong synergy between Pd and the layered porous MnO₂–CeO₂ shell.

There are also many works which have incorporated metal Pt NP into HMNCMs to improve their catalytic activity. Wang et al. [100] found that Pt cations on the CeO₂–Pt interface could make the Pt–CO bond weak, which made the reduction in oxygen easy during the CO oxidation reaction. Additionally, the CeO₂–Pt nanotube composites also had excellent thermal stability, even when calcined at a high temperature up to 700 °C. This demonstrated that the hollow structure could prevent the migration and sintering of Pt NPs. Similarly, the CeO₂ hollow sphere embedded with Pt (Pt/CeO₂ HS) [101] and Pt/CeO₂@SiO₂ catalysts with the porous/hollow structure [102] exhibited high activity and excellent durability in terms of CO oxidation. The significant increase in the CO conversion rate was attributed to the presence of internal voids in the material, which enhanced the chemisorption of CO on the Pt sites.

- Other HSMOs

The rational morphological design and component optimization of other metal oxides doped in HMNCMs such as Fe₂O₃, Co₃O₄, CuO, etc., have also been studied. Based on this, other HSMOs applied to CO oxidation are summarized in Table 5.

Table 5. Other HSMOs with various compositional, structure, and their catalytic performances of CO catalytic oxidation.

Materials	Synthesis Method	S_{BET} ($\text{m}^2 \text{g}^{-1}$)	T_{100} of 100% CO Conversion	Morphology	Ref.
$\alpha\text{-Fe}_2\text{O}_3$ hollow microspheres	Ultrasonic-spray-assisted synthesis method	49.3	320 °C		[66]
Co_3O_4 hollow microspheres	Ultrasonic-spray-assisted synthesis method	37.6	260 °C		[66]
H- Co_3O_4 @H-C	Reduction–oxidation pyrolysis process	104.0	130 °C		[105]
Hollow nanostructure Co_3O_4	Self-sacrificial template strategy	40.6	130 °C		[106]
Core–shell nanostructure Co_3O_4	self-sacrificial template strategy	56.1	90 °C		[106]
Au/ $\alpha\text{-Fe}_2\text{O}_3$ -Hollow Catalysts	Hydrothermal–thermal decomposition process	10.9	—		[107]
Hollow In_2O_3 @Pd- Co_3O_4 core/shell nanofibers	Coaxial electrospinning	30.0	57 °C		[108]
MnO_2 - Co_3O_4 hollow spheres	“Kirkendall effect” method	123.0	135 °C		[109]

As displayed in Table 5, Li et al. [66] prepared the hollow transition metal oxide microspheres (CeO_2 , $\alpha\text{-Fe}_2\text{O}_3$, and Co_3O_4) via a general ultrasonic-spray-assisted synthesis method for catalytic CO oxidation. The catalytic activity expressed by the CO conversion of these hollow/mesoporous transition metal oxide microspheres followed the following sequence: Co_3O_4 hollow microspheres > CeO_2 hollow microspheres > $\alpha\text{-Fe}_2\text{O}_3$ hollow microspheres. Therefore, Co_3O_4 was demonstrated to be an efficient catalyst for the oxidation of CO.

The other hollow-structured Co_3O_4 catalysts include the H- Co_3O_4 @H-C (hollow Co_3O_4 NPs embedded in hollow carbon shell) [105], hollow and core–shell nanostructure Co_3O_4 [106]. The activities of these hollow-structured Co_3O_4 catalysts were improved by introducing hollow structures into the Co_3O_4 NPs. The hollow nanostructure Co_3O_4 provided more abundant active sites which are beneficial to the catalytic activity compared to the core–shell nanostructure Co_3O_4 . However, the core–shell Co_3O_4 exhibited greater long-term stability than the hollow nanostructure Co_3O_4 . This may be ascribed to the shell structure being prone to collapse without Co_3O_4 cores providing support points. Therefore, HSMOs could be designed with hollow structures to increase the oxygen vacancies and provide abundant active sites to improve the catalyst activity. The stability of the hollow structure could be increased by structural adjustment.

Moreover, second active metal oxides can be addicted to catalysts using metal–support interactions to improve the general catalytic performance. Zeng et al. [107] synthesized the Au/ $\alpha\text{-Fe}_2\text{O}_3$ catalysts with a varied hollow structure, which displayed the high catalytic performance of CO oxidation. Comparing $\alpha\text{-Fe}_2\text{O}_3$ supports with the spindle, rod, and

hollow rod structures, the hollow α -Fe₂O₃ nanoparticles exhibited the best activity due to the strong Au–support interaction with the Au nanoparticles.

For hollow micro/nanostructured materials doped with metallic Pd NPs, Du et al. [108] fabricated the hollow In₂O₃@Pd–Co₃O₄ core/shell nanofiber catalyst with a higher CO oxidation activity ($T_{90} = 56$ °C) and lower activation energy. Additionally, they also confirmed that the ultra-thin shell structure and structural defects of In₂O₃@Pd–Co₃O₄ increased the redox capability. The high content of Pd²⁺, the small proportion of Co³⁺, and the increase in chemisorbed oxygen species were also possible reasons for the improvement in its catalytic performance. Moreover, the L-H mechanism could effectively explain the catalytic CO oxidation over the In₂O₃@Pd–Co₃O₄ catalyst. The possible CO oxidation reaction mechanism over the In₂O₃@Pd–Co₃O₄ catalyst is described in Figure 4a. Firstly, CO and O₂ molecules were adsorbed onto the surface of the catalyst; secondly, Pd²⁺ and Co³⁺ activated the adsorbed CO molecules, and formed CO_(ads); then, the oxygen adsorbed on the surface was captured to convert CO_(ads) into CO_{2(ads)}; then, the CO_{2(ads)} was converted into the CO₂ and the oxygen vacancies of the sample were regenerated; finally, the O₂ in the reactant supplemented the oxygen vacancies, and the absorbed oxygen was also regenerated. The Pd²⁺ is the main active sites for CO oxidation. According to the XPS measurement, the oxidation states of Pd were Pd⁰⁺ and Pd²⁺. The surface atomic ratio of Pd²⁺/(Pd⁰⁺ + Pd²⁺) was 51.6% and the In³⁺ oxidation state of In was presented in the catalysts.

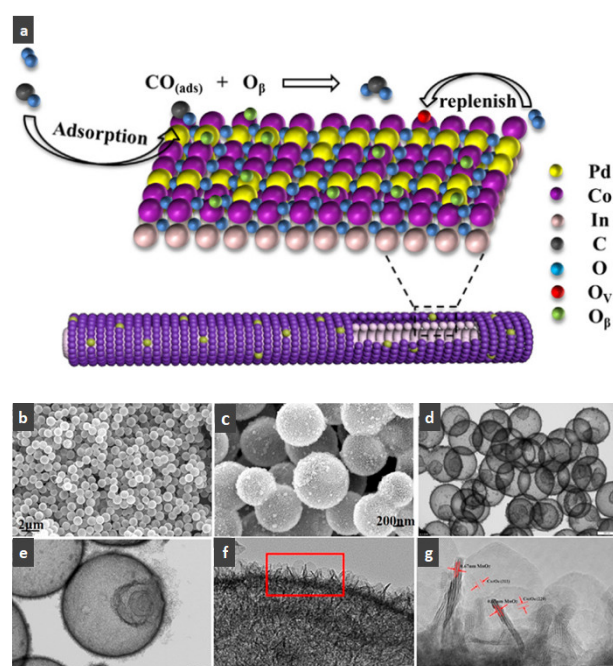


Figure 4. (a) The reaction mechanism of CO oxidation over the In₂O₃@Pd–Co₃O₄ catalyst reproduced from ref. [108]; (b,c) SEM images, (d–f) TEM images, and (g) HRTEM images of the MnO₂–Co₃O₄ hollow spheres reproduced from ref. [109].

As shown in Figure 4b–f, the Co–Mn composite hollow spheres [109] were successfully prepared through a ‘Kirkendall effect’ method. The unique surface structure of the MnO₂–Co₃O₄ composite oxides could expose the abundant catalytic active sites of the interface between Co₃O₄ and MnO₂ (Figure 4f). The Co₃O₄ nanoparticles with the ultra-thin nanosheet structure can be observed in Figure 4g, which could provide plentiful surface oxygen species and the strong adsorption ability of CO to improve the catalytic performance. The high content of Co³⁺ and Mn⁴⁺ facilitated the formation of oxygen vacancies in the catalysts. Therefore, the multi-shelled MnO₂–Co₃O₄ hollow spheres exhibited a reliably high activity for CO oxidation due to its strong synergistic effect and the abundant oxygen vacancies between Co₃O₄ and MnO₂.

Generally, traditional metal oxide-based catalysts can achieve acceptable CO catalytic activity at high temperatures, while noble metal-based catalysts can achieve them at relatively low reaction temperatures. However, the high cost of precious metal catalysts limits their availabilities and wide applications [10]. Therefore, it is both greatly necessary and urgent to develop the ‘noble-metal-free’ catalyst with the low-temperature catalytic performance of CO oxidation.

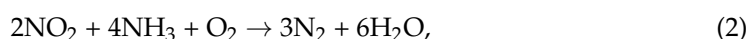
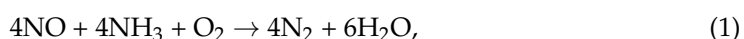
In summary, HSMOs were widely used to catalyze the CO oxidation reactions, while more attention was paid to HMNCMs due to the advantageous physical properties such as the high specific surface areas, big pore volumes, synergistic interaction, abundant defects, adjustable morphology, space utilization, and low density, etc. In addition, ceria is a very important oxygen storage material because of the reversible valence couple in $\text{Ce}^{4+}/\text{Ce}^{3+}$ and the high mobility of oxygen vacancies. There are generally two sources of oxygen vacancies in CeO_2 , specifically, the intrinsic oxygen vacancies and the foreign oxygen vacancies generated by doping the heteroatoms.

Firstly, the pure CeO_2 hollow structure was considered a promising catalyst for CO oxidation. The improved CO oxidation activity of the pure CeO_2 hollow structure depended on a critical factor, such as the exposed special crystal faces, small CeO_2 crystal sizes, and significantly deformed structure in the boundary area. Afterward, with the growing tendency towards the fabrication of nanomaterials, more and more studies have focused on HMNCMs, including the composite binary, multiple CeO_2 hollow structure, and Ce-based hollow structure doped with noble metals. Hereafter, the multi-element Ce-based hollow structure emerged only recently. CeO_2 can generate a strong synergistic effect with other components in the catalytic process. Other HSMOs have similarly received a research process as HMNCMs. Therefore, the strong synergistic effect of transition metal oxides has been widely reported in the field of CO catalytic oxidation using the hollow structure of HSMOs to increase the exposed surface area of the active center to the reactants.

It is generally believed that catalysts with multi-shell hollow structures can obtain a better structure and catalytic stability than the single-shell counterpart because the multi-shell layers possess different supporting functions and the outer shell has a protective effect on the inside shell. Compared with single-shell hollow metal oxides, the multi-shell structure has a larger specific surface area, easier diffusion kinetics, higher bearing capacity, and lower density. Modifying the surface of the hollow structure by manufacturing defects, adding active metal components, and reducing the thickness of the hollow structure wall can greatly improve the catalytic activity. The hollow structure can greatly facilitate the internal diffusion of reactants and the external diffusion of products during the reaction [86]. In addition, increasing the number of shells of the hollow structure can improve the thermal stability of the hollow structure [110].

2.1.2. NH_3 -SCR Removal of NO_x

The emission of nitrogen oxides (NO_x) is mainly derived from the high temperature combustion of fuel such as the coal combustion process in power plants and mobile transportation, or in stationary sources such as glass furnace and ceramics factory. [111] They constitute one of the main factors responsible for causing environmental problems, such as acid rain, ozone layer holes, and photochemical smog [112]. The elimination of NO_x air pollutants has become one of the public’s main concerns. To date, two methods have been applied to eliminate NO_x by HSMOs catalysts: the oxidation method and the low-temperature selective catalytic reduction of NO_x with NH_3 (NH_3 -SCR) (Equations (1) and (2)).



In fact, the NO catalytic oxidation will enhance the SCR process via ‘fast’ SCR reaction: $4\text{NH}_3 + 2\text{NO} + 2\text{NO}_2 \rightarrow 4\text{N}_2 + 6\text{H}_2\text{O}$ [113,114]. To be specific, the fast SCR reaction can be inspired by the partial oxidation of NO into NO_2 [115,116]. In addition, a suitable NO/NO_2

ratio is demanded for the oxidation method. However, the ratio of NO in the flue gas accounts for 95% of the NO_x . Therefore, the catalytic oxidation of NO to NO_2 plays an important role in the technique to eliminate NO_x .

The hollow structure of the functional material has various advantages, such as high porosity, low density, good permeability, large specific surface area, better gas transfer, more active sites in the SCR of NO_x , and outstanding reactant shuttle space [114]. Because the above characteristics can be optimized by various methods, considerable efforts have been devoted to the development of high-efficiency and environmentally friendly denitrification catalysts, which can work well at low temperatures ($<250\text{ }^\circ\text{C}$) [117,118]. However, previous studies reported that the reaction of SO_2 and NH_3 on the catalyst surface would deposit NH_4HSO_4 over the catalyst surface in the presence of oxygen. As a result, the active sites were blocked [5]. Therefore, the urgent challenges for industrial flue gas denitrification catalysts are to prevent the deactivation of active sites on the catalyst surface from the toxicity caused by SO_2 , alkali metals, as well as active metal oxide nanoparticles aggregating at high temperatures [114].

- Single-component HSMOs catalysts

In the past decade, manganese oxide (MnO_x) has attracted extensive attention as a low-temperature NH_3 -SCR catalyst due to its various types of active unstable oxygen. The active oxygen species is the main factor affecting its catalytic performance; meanwhile, the morphological structure also greatly affects the catalytic performance of manganese oxide (MnO_x). For example, Shao et al. [113] reported that the hollow structure of MnO_2 could significantly enhance the catalytic oxidation activity of NO due to the cavity structure providing the shuttle space for oxidation (Figure 5a,b). The adsorption and conversion rate of the reactants were greatly improved. As a result, the NO oxidation effect of MnO_x with hollow morphology was much better than that of $\text{MnO}_2\text{-C}$ with amorphous morphology.

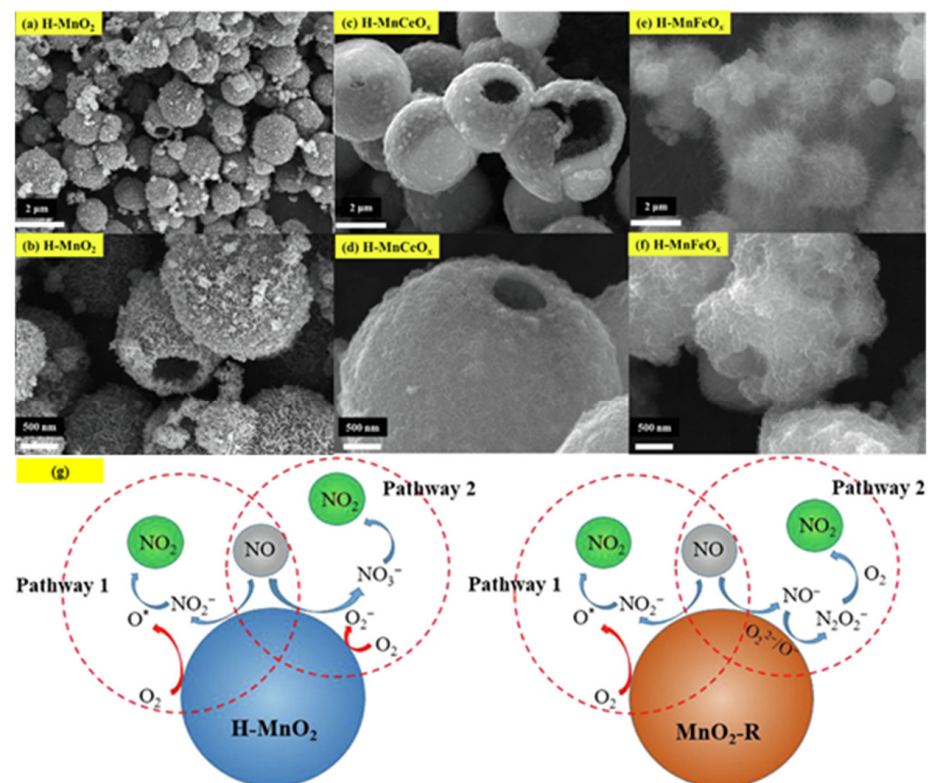


Figure 5. (a–f) SEM images of the MnO_x with hollow morphology; (g) Reaction pathways of NO oxidation over H-MnO₂ and MnO₂-R catalysts reproduced from ref. [113].

The oxidation reaction pathways of NO on H-MnO₂ and MnO₂-R (rod-like morphology) through various characterization techniques are shown in Figure 5g. It is widely believed that the reaction pathway 1 ($\text{NO} \xrightarrow{\text{Mn}^{n+}} \text{NO}_2^- \xrightarrow{\text{O}_2} \text{NO}_2$) is the main path of NO conversion, which occurred on both H-MnO₂ and MnO₂-R surfaces. For H-MnO₂, in reaction pathway 2, the NO initially converted into NO₃⁻ on the catalyst surface. Subsequently, they were oxidized to NO₂ by O species. However, the NO could be converted into NO⁻ and N₂O₂²⁻ by the abundant chemisorbed oxygen (O₂²⁻ or O⁻ species), and then oxidized to NO₂.

- Multi-component HSMOs catalysts

However, there are also some disadvantages of pure MnO_x catalysts, such as low N₂ selectivity at high temperature, poor SO₂ tolerance, and a narrow operation window [118]. To date, it has been reported that the use of metal dopants or promoters is a very common method to improve the SO₂ resistance of HSMOs catalysts [112]. To improve the performance of NO oxidation, they continued to try doping the Ce and Fe into H-MnO₂ (Figure 5c–f) and MnO₂-R. The result indicated that the mixed-metal oxide doped with the second metal had a positive effect on the catalytic oxidation of NO. Fe doping (H-MnFeO_x) displayed the highest NO conversion, i.e., 89.8% at 220 °C. This was because of the rambutan-like morphology of H-MnFeO_x, which could provide more active sites.

In addition, the MnO_x-CeO₂ binary oxide has always been widely investigated as a catalyst of NH₃-SCR reaction. [117]. The main reason is that the hollow structure provides a huge specific surface area, higher reducibility, and sufficient acid sites for reactants [119]. Additionally, the uniformly distributed high content of Mn⁴⁺ [120] and oxygen vacancies [121] were also the possible reasons. Additionally, the porous multi-shell hollow sphere can accelerate the diffusion rate of gas into the internal space. Ma et al. [122] prepared the CeO₂-MnO_x composite with a multi-shell hollow structure (Figure 6a–d). The catalyst with three-layer hollow spheres presented the best performance with 100% conversion in the 150–250 °C range. As shown in Figure 6e, the multiple collisions of reactant gases between the shells were more likely to occur in the catalyst with a multi-shell structure. Therefore, the catalytic activity of the catalysts followed the order of three shells > double shells > single shell > NPs.

There are more MnO_x catalysts with hollow morphologies combined with other metal oxides for the NH₃-SCR reaction, among which the typical hollow sphere morphologies were usually used. For instance, the triple-shelled NiMn₂O₄ hollow spheres were synthesized by a self-assembly method, which showed the low-temperature activity of the NH₃-SCR reaction with complete NO_x conversion at 125 °C [123]. The excellent catalytic performance was attributed to the plentiful active Mn⁴⁺ and surface adsorbed oxygen of the spherical NiMn₂O₄ material. The hollow nanotube structure of MnCoO_x catalyst (MnCoO_x-HNT) [114] was used to catalyze the low-temperature SCR process of NO_x. The hollow nanotube structure could effectively protect the active sites on the inner surface from SO₂ or alkali metal pollution. In addition to this, the catalyst surface possessed large amounts of OH groups, which acted as sacrificial sites for anchoring SO₂ and alkali metals on the surface of the catalyst. In addition, another special hollow structure catalyst, such as the urchin-like MnO_x@PrO_x hollow core-shell structure catalyst [124], was fabricated using a sacrificial templating method. The MnO_x@PrO_x catalyst with a hollow core-shell structure exhibited excellent low-temperature NH₃-SCR activity with a maximum NO conversion of 99% at 120 °C due to the abundant Lewis acid sites and the excellent reducibility generated by the interaction between MnO_x and PrO_x. Furthermore, the special core-shell structure of the catalyst brought about the superior SO₂ and H₂O tolerance.

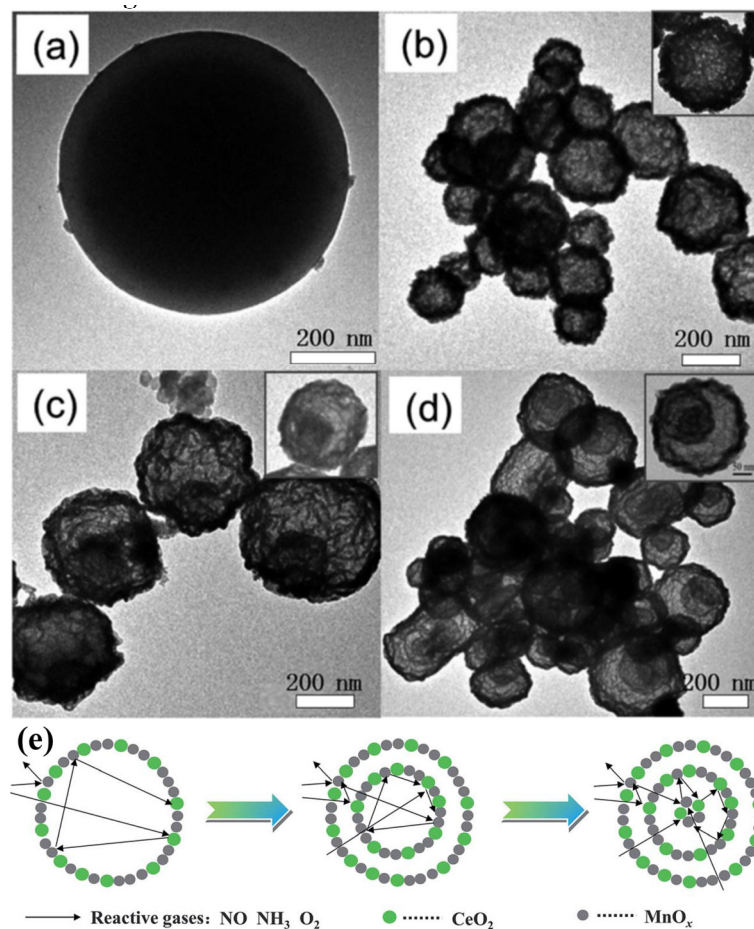


Figure 6. TEM images of the $\text{CeO}_2\text{-MnO}_x$ hollow spheres with various shell numbers obtained at different heating rates: (a) before calcination; (b) single-shell, $2\text{ }^\circ\text{C min}^{-1}$; (c) double-shell, $5\text{ }^\circ\text{C min}^{-1}$; (d) triple-shell, $10\text{ }^\circ\text{C min}^{-1}$. Insets show the corresponding individual hollow sphere; (e) Proposed collision processes of reactive gases against hollow spheres with different shells. Figure reproduced from ref. [122].

For the low-temperature $\text{NH}_3\text{-SCR}$ catalysts, Ce-based catalysts have also been investigated. The morphology design of the hollow structure CeO_2 catalyst is beneficial to improve the performance of the denitration catalyst. The CeO_2 shell can serve as the effective barrier for the aggregation of the nanoparticles. Meanwhile, the CeO_2 shell can also improve the tolerance of SO_2 and H_2O by inhibiting the formation of ammonium nitrate and sulfates [125]. The CeMoO_x catalysts with hollow structure were investigated, such as Mo-doped CeO_2 hollow microspheres [126] and Sn-modified CeMoO_x electrospun fibers [127]. The results presented that the strong redox ability, an abundance of Brønsted acid sites, plenty of chemisorbed oxygen species, and a high content of Ce^{3+} were the main factors for the excellent catalytic performance.

Thereafter, the hollow-structured CeO_2 $\text{NH}_3\text{-SCR}$ catalyst, such as the hollow-structured $\text{CeO}_2\text{-TiO}_2$ catalysts [112], Cr–Ce composite catalysts with the double-shelled hollow morphology [128], $\text{CeO}_2\text{@Fe-ZSM-5}$ catalyst with hollow structure [129], hollow-structured $\text{WO}_3\text{@CeO}_2$ catalyst [130] porous $\text{Ce}_x\text{Nb}_{1-x}$ oxide hollow nanospheres [131], and $\text{P}_x\text{-Ce}_{0.3}\text{-Zr-Ti}$ nano-hollow spheres [132] have been developed and fabricated. The structures of these catalysts exhibited the hollow spheres. The high $\text{NH}_3\text{-SCR}$ activity on the hollow cavity structure catalyst was attributed to the large cavity size, increased curvature radius, abundant active oxygen species, defects, acidic strength, and increased surface proportion of Ce^{3+} .

To summarize, HSMOs have been used to catalytically remove NO_x with NH_3 -SCR due to its unique physiochemical properties. For the catalytic oxidation activity of NO, MnO_x with a hollow structure has been frequently examined as a promising catalyst due to their various types of active unstable oxygen and the cavity structure could provide the shuttle space for oxidation. Additionally, transitional metals and rare earth metals doped into Mn-based oxides have been widely studied to overcome the disadvantages of MnO_x , such as the low N_2 selectivity at high temperature, poor SO_2 tolerance, and narrow operation window. The exceptional catalytic activities of the Mn-based materials principally originate from the redox characteristics of MnO_x and the presence of oxygen vacancies. In addition, Mn-based materials and Ce-based materials with a hollow structure, which contains sufficient acid sites with large amount of active surface oxygen (O_s), are crucial for low-temperature catalytic NH_3 -SCR. The increase in the curvature radius of the curved hollow spheres surface is an acceptable strategy.

2.1.3. Catalyst for Automobile Three-Way Catalytic (TWC) Reaction and Diesel Oxidation Catalytic (DOC) Reaction

The main source of air pollution and secondary pollution is the soot particles emitted by mobile diesel engines. Therefore, it is necessary to develop high-performance catalysts that can oxidize soot at a low temperature [133]. However, both TWC and DOC should eliminate all these harmful components, such as CO, NO, hydrocarbons (HCs), and soot, at the same time [134,135]. NO_2 is beneficial to soot combustion, as is water vapor, which is also another key factor influencing the catalytic effect of soot combustion catalysts [136].

The hollow-structured metal oxide catalysts of the oxidation of CO and NO have reached a significantly high level of activity. The hollow structures are feasible due to the significantly improved soot–catalyst contact in the fields of automobile three-way catalysts (TWCs) and diesel oxidation catalytic (DOC) reaction [134,137,138]. Additionally, the development of the TWCs with strong interactions between metals and metal oxides to prevent the sintering of metal nanoparticles have been a research hotspot. For example, the soot or NO oxidation was performed on the CeMnCu ternary composite oxides with hollow structures prepared by different methods [136]. The results indicated that the addition of the third metal oxide, high BET surface area, small metal oxide hollow-structure grain size, uniform element distribution, and low-average-valence Ce was essential for improving the reducibility and catalytic activity of soot combustion. The hollow structure of the nanoparticles in each CMC-Cp-x (CMC: CeMnCu, Cp: co-precipitation) could expose large amounts of lattice oxygen to the (sub-) surface to promote the migration of lattice oxygen, which is very important for catalytic oxidation (Figure 7a–f).

In addition, Feng et al. [139] prepared the trepang-like hierarchical structured $\text{CeO}_2@\text{MnO}_2$ nanocomposite oxide with a width of 60 nm by hydrothermal method. The special structure of MnO_2 short nanorods on the surface of the hollow spindle CeO_2 (Figure 7g,h) was beneficial in terms of accelerating the oxidation of soot and achieving a high catalytic activity with T_{50} at 373 °C (5% O_2 /500 ppm NO). The main reason for this was that this unique structure could provide more active sites and increase the accessible opportunities between the catalyst and the soot.

For other hollow-structured catalysts for eliminating soot particles, $\text{La}_{0.63}\text{Sr}_{0.27}\text{K}_{0.1}\text{CoO}_{3-\delta}$ nanotubes with a hollow structure were synthesized by doping some Sr^{2+} to inhibit the grain growth during the heat treatment at a high temperature [140]. The soot particles have more contact chances between the catalyst and reaction gas within the hollow structure. As a result, the $\text{La}_{0.63}\text{Sr}_{0.27}\text{K}_{0.1}\text{CoO}_{3-\delta}$ catalyst displayed high activity in terms of soot oxidation with T_{50} at 359 °C in 5% O_2 and 2000 ppm NO. Additionally, the hierarchical hollow structure [HHS] assembled from the porous NiCo_2O_4 nanosheets was also attributed to abundant active oxygen species [141]. Therefore, the temperature at 50% soot conversion (T_{50}) of NiCo_2O_4 nanosheets could be achieved as low as at 354 °C. Therefore, the application of hollow structures in the field of automobile TWC reaction and DOC reaction is valid, but still needs to be developed diligently.

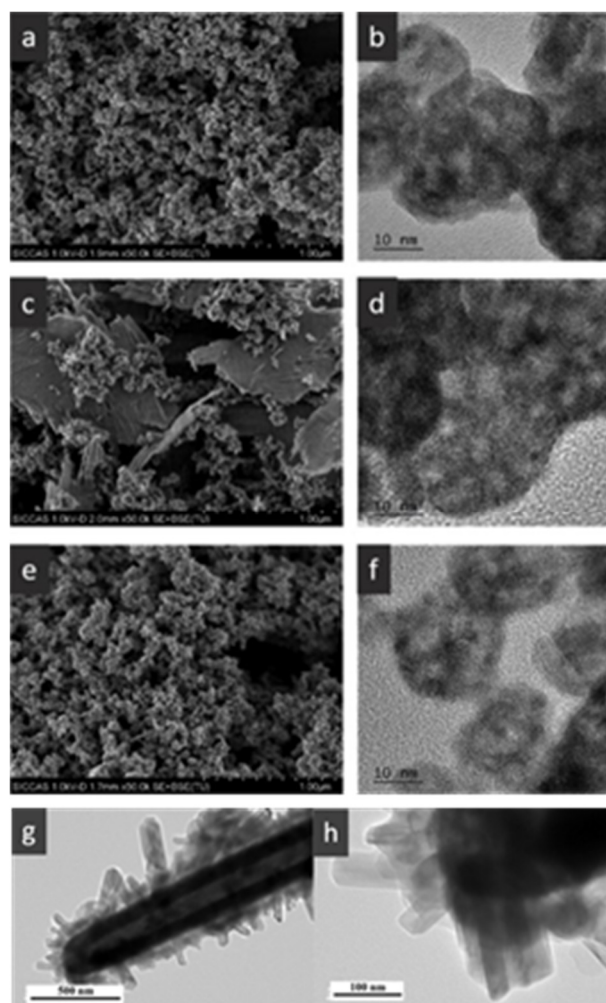


Figure 7. (a,c,e) SEM images of the CMC-Cp-a, -b, and -c, respectively; (b,d,f) TEM images of the CMC-Cp-a, -b, and -c, respectively (Ce/Mn/Cu molar ratio of 84/16/16 (CMC-Cp-a), 84/8/8 (CMC-Cp-b) or 84/32/16 (CMC-Cp-c)) reproduced from ref. [136]; (g,h) TEM images of the CeO₂@MnO₂ reproduced from ref. [139].

2.2. Volatile Organic Compounds Emission Control

Volatile organic compounds (VOCs) are considered air pollutants that are greatly harmful to human health, and refer a class of substances composed of various organic compounds with a boiling point in the range of 50 °C–260 °C at room temperature. Meanwhile, outdoor sources are the main part of the anthropogenic emission sources of VOCs, including chemical industries, transportation, petroleum refineries, dry cleaners, food processors, and textile manufacturers, etc. [142]. Excess VOCs are emitted by indoors and natural resources, such as solvents and cleaning products, restaurant and domestic cooking, office supplies, printers, heat-exchanger systems, etc. [143]. Additionally, VOCs also participate in the formation of photochemical smog and the depletion of the ozone layer, which are responsible for the climate and environmental changes [144]. The catalytic recovery technologies of volatile organic compounds, such as the catalytic combustion [144], catalytic decomposition at room temperature [145], catalytic oxidation, [23], and photocatalytic mineralization, etc. [143], have been widely considered as the most promising post-treatment technologies to control the emissions of VOCs [146]. Recently, the catalytic oxidation of VOCs has received more and more attention. Therefore, it is urgent to develop excellent catalysts with advanced low-temperature activity for VOCs through structural engineering.

2.2.1. Catalytic Elimination of Toluene

The aromatic hydrocarbons, such as benzene and toluene, are the toxic and carcinogenic volatile organic compounds in the discharged exhaust gas [147]. HSMOs are expected to catalyze the oxidation of these VOCs with high efficiency due to the large surface area and abundant oxygen vacancies, which are essential for the improvement of the catalytic oxidation of toluene [147,148]. Nevertheless, HSMOs have been widely used in the field of the catalytic elimination of aromatic hydrocarbons. In recent years, various excellent metal oxide catalysts with hollow structures have been developed for the catalytic elimination of toluene and have shown good low-temperature catalytic activity, stability, reusability, and excellent water tolerance [149–151]. However, hollow-structured metal oxides have different morphologies and compositions. Thus, the metal oxide catalysts with hollow structures for toluene oxidation reported in the summary are exhibited in Table 6. The metal oxide catalysts could be divided into single-component metal oxide catalysts with hollow structures, hollow-structured metal-oxide-supported catalysts, and hollow-structured binary metal oxide catalysts.

Table 6. Summary of toluene oxidation over the reported metal oxide catalysts with hollow structures.

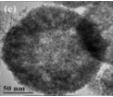
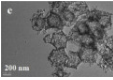
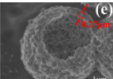
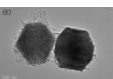
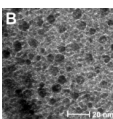
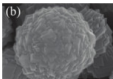
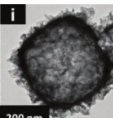
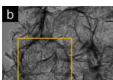
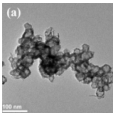
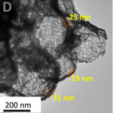
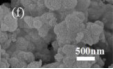
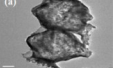
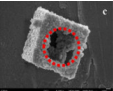
Catalysts	Synthesis Method	S_{BET} ($\text{m}^2 \text{g}^{-1}$)	Reaction Conditions	Catalytic Performance			Morphology	Ref.
			Toluene Concentration, Weight Hourly Space Velocity (WHSV)	T_{90} ($^{\circ}\text{C}$)	T_{100} ($^{\circ}\text{C}$)	E_a (kJ mol^{-1})		
CeO ₂ hollow sphere	Hydrothermal methods	130.2	1000 ppm, 48,000 mL g ⁻¹ h ⁻¹	207	—	55.0		[147]
Hollow Co ₃ O ₄ polyhedral nanocages	Thermal treatment of ZIF-67 templates	74.3	12,000 ppm, 21,000 mL g ⁻¹ h ⁻¹	259	280	77.9		[152]
Flower-like MnO ₂ hollow microspheres	Interface reaction method	214.0	3000 ppm, 15,000 mL g ⁻¹ h ⁻¹	237	—	—		[151]
Manganese oxide polyhedra with hollow morphologies	Hydrothermal route	90.0	1000 ppm, 32,000 mL g ⁻¹ h ⁻¹	—	240	—		[153]
Pt/ZrO ₂ (0.57)	Modified Stöber process	285.0	1000 ppm in a total air flow of 100 mL min ⁻¹	172	—	—		[144]
Pt/H-MnO ₂	Carbon spheres template method	54.0	1000 ppm, 60,000 mL g ⁻¹ h ⁻¹	180	—	—		[154]
Nanocage-shaped Co _{3-x} Zr _x O ₄ loaded with Pt	Template method	23.5	50 ppm, 36,000 mL g ⁻¹ h ⁻¹	165	—	66.2		[20]
Pd-Modified NiCoO _x hollow nanospheres	Hard template method	162.1	500 ppm, 36,000 mL g ⁻¹ h ⁻¹	—	190	—		[6]

Table 6. Cont.

Catalysts	Synthesis Method	S_{BET} ($\text{m}^2 \text{g}^{-1}$)	Reaction Conditions		Catalytic Performance		Morphology	Ref.
			Toluene Concentration, Weight Hourly Space Velocity (WHSV)	T_{90} ($^{\circ}\text{C}$)	T_{100} ($^{\circ}\text{C}$)	E_a (kJ mol^{-1})		
hollow microsphere CuMnO_x	One-pot preparation	193.3	1000 ppm, 30,000 $\text{mL g}^{-1} \text{h}^{-1}$	237	—	55.7		[155]
MnCeO_x -OH hollow structure	Carbon spheres as hard templates	88.4	1000 ppm, 36,000 $\text{mL g}^{-1} \text{h}^{-1}$	237	—	98.9		[156]
$\text{Ce}_{0.03}\text{MnO}_x$ hollow microsphere	Redox co-precipitation method	51.2	1000 ppm, 20,000 $\text{mL g}^{-1} \text{h}^{-1}$	—	225	90.4		[157]
Hollow $\text{Mn}_x\text{Co}_{3-x}\text{O}_4$ Polyhedron	Controlling heating rates	59.7	3000 ppm, 30,000 $\text{mL g}^{-1} \text{h}^{-1}$	188	195	57.4		[158]
Hollow CoInO_x nanocube	SiO_2 template strategy	36.0	3000 ppm, 30,000 $\text{mL g}^{-1} \text{h}^{-1}$	178	—	41.6		[150]

- Single-component metal oxide catalysts with hollow structure

The morphology of catalysts with hollow structures consisting of a single-metal oxide component, such as CeO_2 , Co_3O_4 , and MnO_2 , has been extensively studied. For example, Feng et al. [147] prepared CeO_2 with different morphologies (rod, cube, and hollow sphere) for catalytic toluene combustion at low temperature. Among these catalysts, the CeO_2 hollow sphere exhibited the best tolerance to water and toluene combustion activity with T_{90} at 207 $^{\circ}\text{C}$, which was an improvement compared to the CeO_2 rod and CeO_2 cube. The excellent catalytic performance of the CeO_2 hollow sphere led to more active surface oxygen and better redox properties on the catalyst due to the larger surface area and more surface oxygen vacancies. Similarly to hollow Co_3O_4 polyhedral nanocages, the other reason for the high activity were the strongest OH groups and the higher atomic ratio of $\text{Co}^{3+}/\text{Co}^{2+}$ on the catalyst surface [152].

Manganese oxides (MnO_x) are among the most active oxides for catalytic VOCs oxidation. Furthermore, a study showed that Mn was the main activity center of toluene oxidation [155]. The probable reaction pathway for the toluene oxidation of the MnO_x polyhedra with a hollow structure was proposed. At the start, toluene molecules were adsorbed on the surface of the catalysts, and then partly oxidized into benzyl alcohol, which might subsequently transform into benzaldehyde and benzoic acid. With the increasing temperature, the benzene ring was opened to form the maleic anhydride and was further oxidized to carbon dioxide and water [153].

Moreover, the structure–activity of this important transition metal oxide has been widely studied. The VOC decomposition of MnO_x was ascribed to the outstanding adsorption capacity, high mobility of oxygen, the higher average oxidation state (AOS) of Mn, and abundant OH groups [159,160]. The low-temperature reducibility of the catalyst was attributed to the high content of Mn^{4+} , which facilitated the occurrence of the redox cycle and promoted the activation of the surrounding surface lattice oxygen, thus enhancing the mobility of oxygen species with the participation of oxygen vacancies. Additionally, Gu et al. [151] prepared the hierarchically structured flower-like MnO_2 hollow microspheres with low-temperature activity and high thermal stability, resulting from its large specific surface area ($214 \text{ m}^2/\text{g}$), abundant oxygen vacancies, improved reducibility, high num-

ber of acidic sites, and strong acidity. The adsorption and activation of gaseous toluene molecules were further promoted by these features, thus exhibiting remarkable activity for toluene catalytic oxidation at low temperature. The mechanism for explaining the results was proposed as shown in Figure 8, which was a complete cycle synergizing the Brønsted acid site and oxygen vacancy for toluene oxidation. Initially, the gas toluene was adsorbed and activated on Brønsted acid sites. Then, it reacted with the surrounding active oxygen species to produce carbon dioxide and water and complete a catalytic cycle. Meanwhile, the molecular oxygen could be activated on the oxygen vacancies, which would be generated with the consumption of active oxygen species. And, the activated surface lattice oxygen could also participate in the reaction.

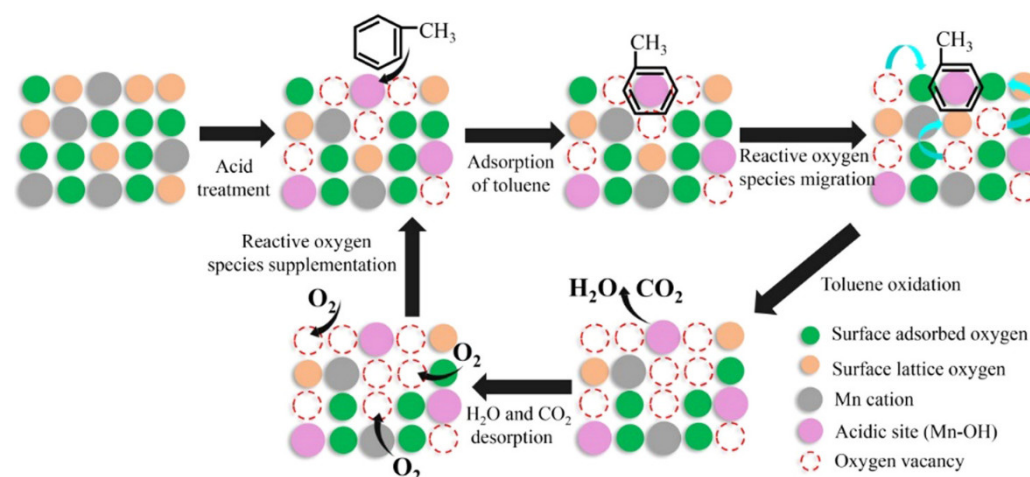


Figure 8. Schematic diagram of the complete reaction cycle for the catalytic oxidation of toluene on MnO_2 -1.2. Figure reproduced from ref. [151].

For the oxidation elimination of VOCs, post-plasma catalysis (PPC) is also an important catalytic technology. The insufficient adsorption of gas and low catalytic activity at room temperature for the complete oxidation of toluene are still challenges in post-plasma catalysis (PPC). At the same time, hollow structures are a special morphology for metal oxides and have attracted considerable attention due to their well-defined interior voids, high specific surface areas, and superior permeation properties. Yang et al. [159] described a simple one-step template-free hydrothermal method for the preparation of the hierarchical hollow urchin structured MnO_2 , which is displayed in Figure 9a–f. The post-plasma catalytic decomposition of toluene was conducted at room temperature. As a result, hollow urchin α - MnO_2 exhibits a higher toluene decomposition, CO_2 selectivity, and carbon balance compared with solid urchin α - MnO_2 . The toluene decomposition, CO_2 selectivity and carbon balance over hollow urchin α - MnO_2 reach up to $\sim 100\%$, $\sim 59\%$, and $\sim 81\%$ at an SIE of 240 J/L, respectively, which indicated the higher activity in comparison to the non-thermal plasma (NTP) process (the initial concentration of toluene was kept at 105 ppm with a gas flow rate of 150 mL min^{-1}). As shown in Figure 9g,h, the major degradation pathways of toluene over the hollow urchin α - MnO_2 catalyst during the post-plasma catalytic process consisted of two steps: (1) the plasma-induced ring-opening destruction of toluene in the gas phase (Figure 9g); and (2) the adsorption and conversion of toluene and organic byproducts into CO_2 and H_2O on the surface of the catalyst (Figure 9h).

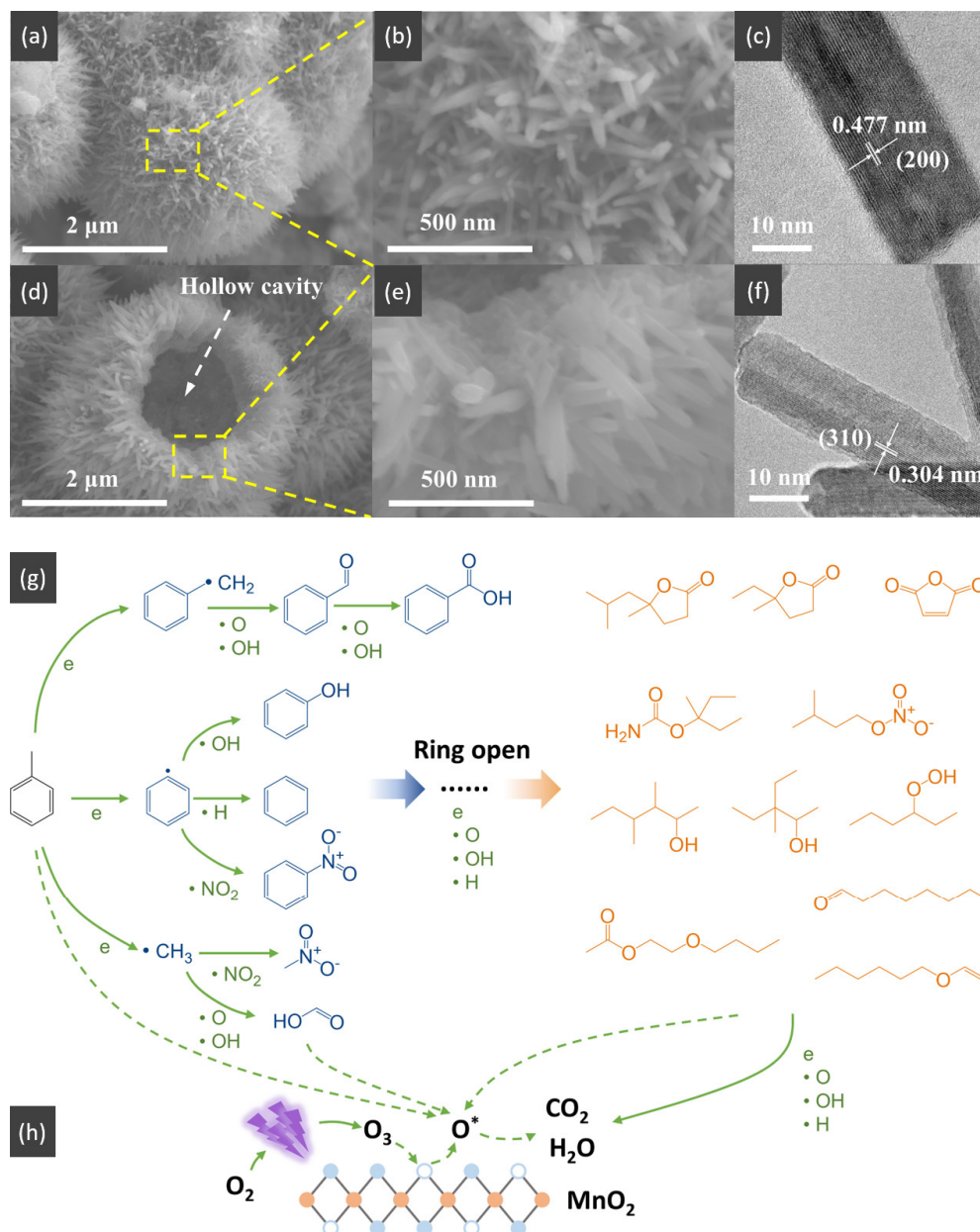


Figure 9. SEM and HRTEM images of: (a–c) solid-urchin and (d–f) hollow-urchin MnO₂. Plausible reaction pathways for toluene decomposition in the PPC (post-plasma catalysis) process are also given: (g) NTP (non-thermal plasma)-induced gas-phase reactions in the DBD (dielectric barrier discharge) reactor and (h) catalytic reactions on the surface of MnO₂ in the catalytic reactor. Figure reproduced from ref. [159].

- Hollow-structured metal oxides supported catalysts

As can be observed in Table 6, the catalytic activity of single-component metal oxides is significantly lower than that of multi-component catalysts. Metal Pt and Pd noble-based catalysts have been widely investigated in the catalytic oxidation of toluene. Additionally, noble metals exhibit much higher activity in the combustion of toluene compared with transition metal oxides (mainly CoO_x, MnO_x, etc.), which was attributed to the advantages of a hollow structure such as large surface areas and space inside, abundant oxygen vacancies, SMSIs, etc.

To optimize the dispersion and chemical state of Pt species, Kondratowicz et al. [144] deposited Pt species into the hollow ZrO_2 spheres as support using the bottom-up strategy and impregnation with PtCl_4 or the reduction of PtCl_4 in an ethylene glycol solution. In contrast with the materials produced by the bottom-up strategy, the catalyst produced by the polyol technique had a better catalytic activity in terms of toluene combustion due to the larger Pt nanoparticles with higher stabilization and the dispersion of the metallic Pt phase. Moreover, the more reactive oxygen would generate on the surface Pt site.

Mo et al. [154] prepared a series of different MnO_2 crystal structures (α -, β -, γ -, and hollow- MnO_2). Compared with α -, β -, and γ - MnO_2 , the H- MnO_2 catalyst exhibited a superior high level of activity with T_{90} at 230 °C for toluene oxidation due to the abundant surface O_{ads} species on the catalyst with the well-defined hollow structure. Then, these catalysts were decorated by Pt NPs on the MnO_2 crystal structures. The Pt/ α - MnO_2 catalyst showed the best performance for catalytic toluene combustion ($T_{90} = 170$ °C), which was attributed to the SMSIs between the Pt nanoparticles and the supports. The surface oxygen vacancies and the mobility of the surface lattice oxygen would be improved by the SMSIs, thus leading to the deep oxidation of the toluene molecules to CO_2 and H_2O .

Qu et al. [6] presented the h- NiCoO_x catalyst with large surface areas, abundant surface hydroxyl groups and numerous oxygen vacancies, which exhibited a superior catalytic activity compared with single metal oxides (Co_3O_4 and NiO) and NiCoO_x nanosheets. After being loaded with Pd particles, the 2.0 wt% Pd/h- NiCoO_x demonstrated an especially high performance for toluene oxidation with approximately 100% conversion achieved at 190 °C. In comparison with h- NiCoO_x , the temperature is lower by 60 °C. Mechanisms based on the Mars-van Krevelen model [161] for the toluene oxidation reaction over Pd/metal oxide catalysts are presented in Figure 10a. The proposed system was followed as: (1) after the toluene molecules were adsorbed on the catalyst surface, it was activated to form the dehydrogenated intermediates with the promotion of surface hydroxyl groups on the catalyst [162]. (2) The activated lattice oxygen species were migrated to react with the intermediates due to the existence of oxygen vacancies and mixed-valence states, such as in the $\text{Co}^{3+}/\text{Co}^{2+}$ and $\text{Ni}^{3+}/\text{Ni}^{2+}$ pairs, and then, it could be reoxidized by the gaseous oxygen [161,162]. (3) The dehydrogenated intermediates and toluene were completely oxidized from CO_2 and H_2O .

Wang et al. [20] reported that hollow nanocage-shaped $\gamma\text{Pt}/\text{Co}_{3-x}\text{Zr}_x\text{O}_4$ catalysts show significant activity for complete toluene catalytic oxidation. The key points of the preparation with the solution-phase cation exchange method for designing this catalyst were constructing solid-solution supports by doping Zr into the Co_3O_4 lattice, and subsequently loading Pt. The SEM images of the materials are displayed in Table 6. After Pt nanoparticle loading, the 2.0 wt% Pt/ $\text{Co}_{2.73}\text{Zr}_{0.27}\text{O}_4$ catalyst achieved complete toluene catalytic oxidation at 180 °C, which was the best catalytic activity among these $\gamma\text{Pt}/\text{Co}_{2.73}\text{Zr}_{0.27}\text{O}_4$ samples. In Figure 10b, which shows the proposed mechanisms of toluene decomposition and catalytic oxidation over 2.0 wt% Pt/ $\text{Co}_{2.73}\text{Zr}_{0.27}\text{O}_4$, the steps are as follows: firstly, because the Pt metal on the catalyst surface was more active, the toluene molecule favorably adsorbed onto it and was then activated as a dehydrogenation intermediate. Afterward, the major intermediates such as benzaldehyde and benzoate were formed due to the dehydrogenation intermediate reacting with active oxygen species, and finally, was completely oxidized to CO_2 and H_2O . Additionally, the rapid activation of O_2 molecules benefited from the Pt metallic atoms and the active oxygen species produced by the generated oxygen vacancies.

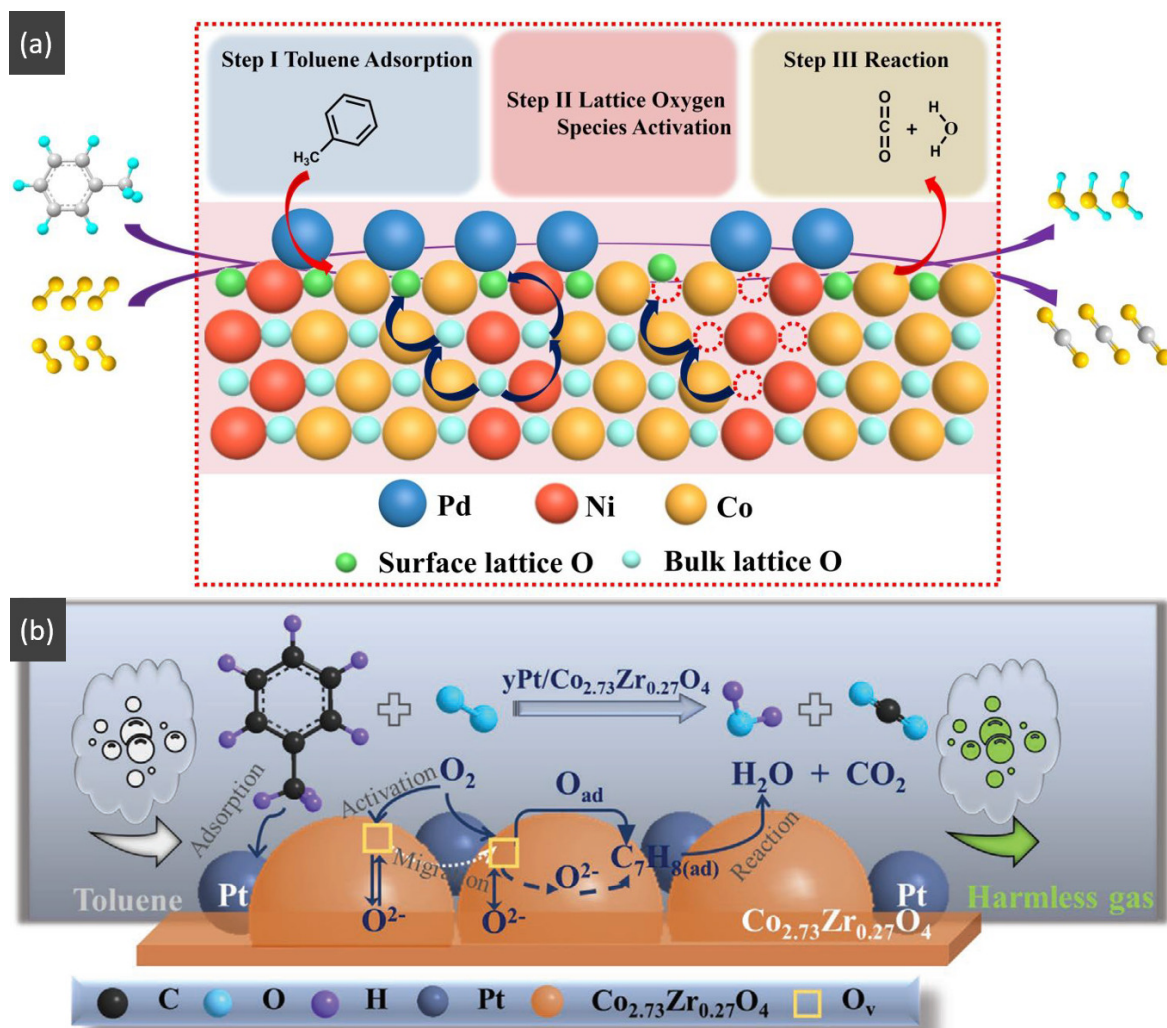


Figure 10. (a) The schematic illustration of the reaction mechanism for toluene oxidation over Pd/metal oxide catalysts reproduced from ref. [6]; (b) Proposed mechanism for enhanced catalytic oxidation toward toluene over 2.0 wt% Pt/Co_{2.73}Zr_{0.27}O₄ reproduced from ref. [20].

- Hollow-structured binary metal oxide catalysts

The economic inapplicability of precious metals limits their application and development. Thus, transition metal oxides such as Co, Mn, etc., are expected to replace metal Pt and Pd due to their low cost and high availability when the outstanding catalytic activity for toluene oxidation is proven. Moreover, the addition of other metals could significantly improve the catalytic activity of toluene due to the synergistic effect [163].

Li et al. [156] prepared hollow-structured Mn–Ce binary oxides using carbon spheres as hard templates and applied for catalytic toluene combustion. The MnCe–OH catalyst exhibited the highest catalytic performance for toluene combustion with T₉₀ at 237 °C in comparison with the MnCe–H and MnCe sample (obtained from acidic- or alkali-treated carbon spheres) attributed to the thinner and more porous shell, enhanced low-temperature reducibility, and moderate surface components (abundant Mn⁴⁺ and surface adsorbed oxygen). Furthermore, a large number of the defects with the Ce addition, surface adsorption oxygen, and the surface Mn⁴⁺ species of the Ce_aMnO_x hollow microsphere with hierarchical structure were formed by redox co-precipitation method [157]. The catalytic performance for toluene combustion was significantly improved in terms of its high stability = and water resistance, even under the condition of 5 vol.% H₂O of Ce_{0.03}MnO_x. The possible reaction mechanism for toluene catalytic oxidation over Mn–Ce binary oxides

was offered based on in situ DRIFTS analyses. The oxidation of toluene underwent the following consecutive steps: initially, toluene molecules were transformed into aldehydic, then into benzoate species, and the CO_2 and H_2O were formed finally.

Additionally, adding a second metal element to the hollow structure to improve the catalytic activity is closely related to the preparation method. Xiao et al. [155] reported the hollow-microsphere CuMnO_x catalysts synthesized by an expeditious salt hydrolysis-driven redox-precipitation protocol for toluene combustions. As shown in Figure 11a, to fabricate the CuMnO_x with molecular-scale homogeneity and a high dispersion of Cu^{2+} and Mn^{2+} , the hydrolysis driving redox method was used to raise their atomic utilization efficiency compared with the co-precipitation method. The HR-2Mn1Cu (hydrolysis-driven redox-precipitation protocol) showed the lowest toluene conversion temperature with T_{50} and T_{90} of 228 °C and 237 °C, respectively, and the toluene conversion at 240 °C was much higher than that of other catalysts. The excellent activity of the HR-2Mn1Cu was ascribed to the formation of a long-range disordered mesostructure with the uniform introduction of copper ions by the hydrolysis-driven redox co-precipitation. With the corrosion of H_2O_2 , the surface hollow structure and accumulative pores were formed, which then increased the high specific surface area and accessibility of surface edge sites and inner atoms of HR sample.

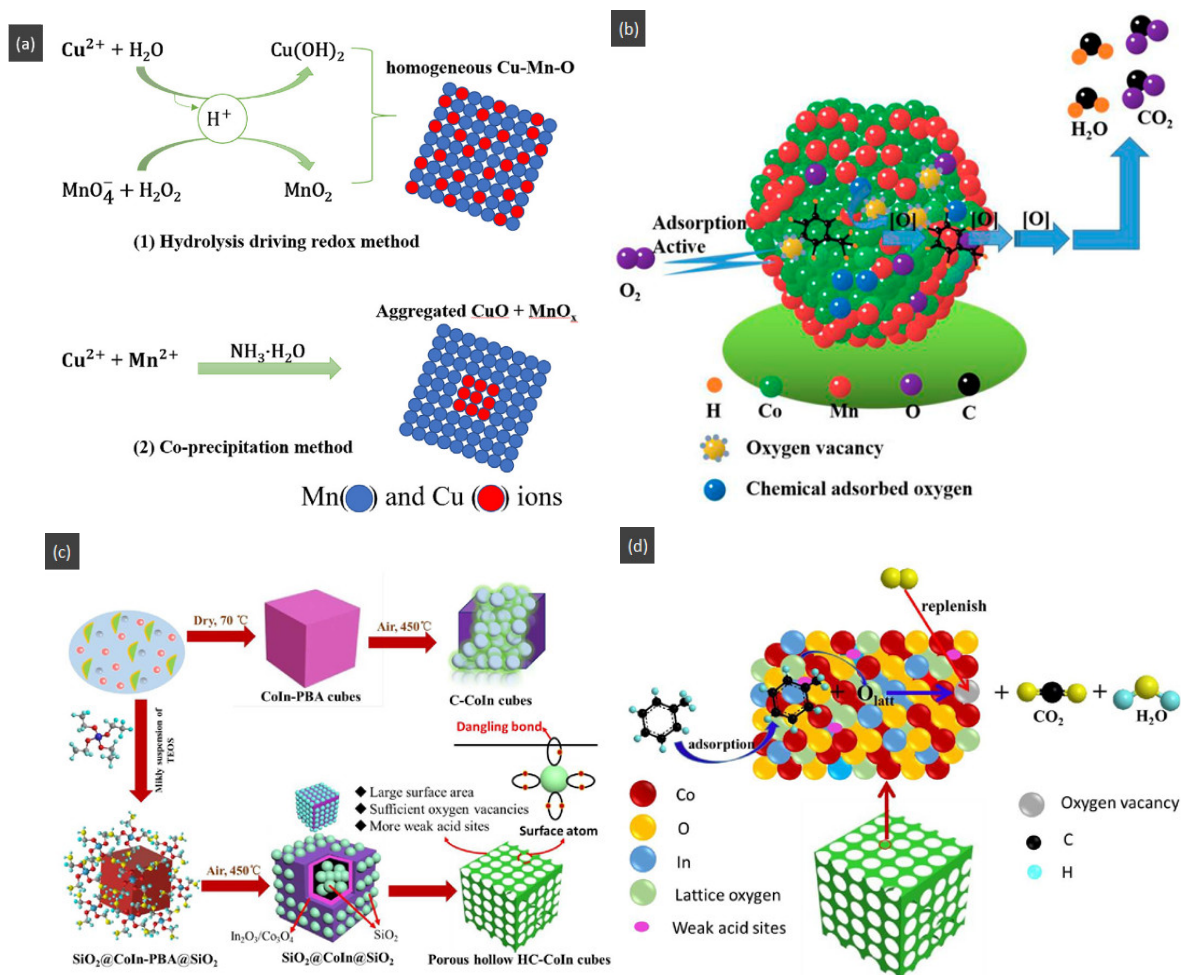


Figure 11. (a) Illustration of two pathways to synthesize the Cu–Mn oxide reproduced from ref. [155]; (b) Schematic of the oxidation of toluene on $\text{Mn}_x\text{Co}_{3-x}\text{O}_4$ reproduced from ref. [158]; (c) The formation schematic of the porous hollow HC-CoInO_x nanocube; (d) The proposed reaction mechanism over the CoInO_x catalyst reproduced from ref. [150].

Temperatures and heating rates are important heating decomposition conditions for precursors, based on the application of hollow Co_3O_4 polyhedral nanocages [152]. Zhao et al. [154] successfully fabricated the hollow $\text{Mn}_x\text{Co}_{3-x}\text{O}_4$ polyhedron (HW- $\text{Mn}_x\text{Co}_{3-x}\text{O}_4$) by controlling heating conditions to optimize the decomposition of Mn@Co-ZIFs precursors. The HW- $\text{Mn}_x\text{Co}_{3-x}\text{O}_4$ displayed remarkable catalytic oxidation performance for toluene with T_{100} occurring at 195 °C due to the high surface atomic ratio of $\text{Co}^{2+}/(\text{Co}^{3+} + \text{Co}^{2+})$, an abundance of surface-adsorbed oxygen with the largest specific area, and a minimum crystallite size. In addition, the possible reaction mechanism was proposed and followed the L-H mechanism different from hollow Co_3O_4 polyhedral nanocages. The complete redox cycle [164] is shown in Figure 11b, and the steps were as follows: firstly, the toluene molecule reacted with the chemically adsorbed oxygen after being adsorbed onto the surface of the catalyst. Secondly, the benzaldehydic species were produced and converted into CO_2 and finally H_2O . Meanwhile, oxygen vacancies were produced by the catalysts to form the new chemically adsorbed oxygen.

The hollow-structured material made good progress, but the synthesis of the hollow-structured cubic metal oxides faces huge challenges. As shown in Figure 11c, the SiO_2 template strategy was applied to prepare hollow the CoInO_x nanocube (HC- CoInO_x) [150] for the catalytic combustion of toluene. The formation process of the construction of a hollow structure indicated that using the porous SiO_2 template can greatly increase its surface area to produce a large number of surface dangling bonds and provide more oxygen vacancies and surface weak acid sites, which would play important roles in improving the oxidation activity of materials. Thus, the hollow HC- CoInO_x nanocube exhibited an excellent catalytic performance ($T_{90} = 178$ °C). The proposed reaction mechanism over the hollow HC- CoInO_x catalyst for the toluene oxidation process is shown in Figure 11d, which preferred the Mars–van Krevelen mechanism. The redox cycle includes the following steps: firstly, toluene molecules reacted with the adjacent lattice oxygen after adsorbing onto the metal active sites and then formed CO_2 , H_2O , and an oxygen vacancy. Subsequently, the gas O_2 molecules were reabsorbed and replenished into this oxygen vacancy, and then reacted with another toluene molecular as before.

In summary, there is no doubt that the optimization of the hollow structure highly improved the catalytic activity of single-component metal oxide catalysts. However, there are bottlenecks to this improvement. The introduction of noble metals is known to further enhance the activity. For the supported catalyst, the precious metal was the active site to activate the O_2 molecules, and the active oxygen species were produced by the generated oxygen vacancies of the HSMOs [20]. Additionally, to make full use of the advantages of the hollow structure (high specific surface areas, big pore volumes, abundant defects, adjustable morphology, space utilization, low density, and the metal–support interactions, etc.) [159], the toluene catalytic oxidation reaction is crucial.

In order to maximize the toluene catalytic oxidation activity of the HSMOs, the incorporation of other active metal elements has been used to adjust the structure–activity relationship. The key factors for the oxidation of toluene on the catalyst are the surface reaction [158], the high number of acidic sites [151], and the supply of active oxygen by the abundant oxygen vacancies [150]. As for binary metal oxide catalysts, the catalytic oxidation of toluene over the metal oxides with a hollow structure is related to various influencing factors, such as the concentration of surface oxygen vacancies [20], the thickness and the porosity of the shell [156], abundant surface hydroxyl groups [6] and Mn^{4+} species [157], and so on. Based on these synthesis methods and experimental investigations, the hollow-structured metal oxide catalysts with high activity and durability at the component level could be designed and fabricated.

2.2.2. Removal of Other Volatile Organic Compounds (VOCs)

Formaldehyde (HCHO) has been considered a carcinogenic and toxic volatile organic compound (VOC), which widely exists in wood adhesives, furniture, preservatives and disinfectants, textiles, dyes, cigarette smoke, and other materials we encounter daily [23].

As a dangerous indoor pollutant, HCHO at a very low concentration can also pose a huge threat to human health [165]. In addition, chlorinated volatile organic compound pollutants (CVOCs) also include chlorinated volatile organic compounds which have high chemical stability, severe toxicity, and potential carcinogenicity [166]. The removal of pollutants in the air or indoors using catalytic oxidation technology has been considered one of the most promising technologies for addressing this issue.

Compared with traditional catalytic materials, HSMOs have attracted significant attention for addressing catalytic VOC oxidation due to certain advantages such as their large specific surface area, low density, high loading capacity, outstanding interior voids, good surface permeability, excellent permeation properties, and high mobility. Furthermore, HSMOs are good candidates for catalyst support.

The related catalytic elimination method, catalytic performance, synthesis method, and structural properties of the previously reported metal oxide catalysts with hollow structures in catalytic oxidation are summarized in Table 7. As can be observed, the application range of hollow-structured oxide catalysts in the field of VOC removal is gradually expanding due to their outstanding advantages. The catalysts were prepared by different methods and metal oxides led to the exhibition of various morphologies, such as hollow spherical structures, hollow nanoboxes, hollow chains, and core-shell nanospindles.

Table 7. Summary of catalytic activities in the VOC oxidation of reported metal oxide catalysts with hollow structures.

Catalysts	Synthesis Method	Textural Properties		Reaction Conditions	X (%)	T (°C)	Ref.
		S _{BET} (m ² g ⁻¹)	Pore Volume (cm ³ g ⁻¹)				
K _x MnO ₂ hollow nanospheres	Soft chemistry route	40.7	0.09	100 ppm HCHO, 20 vol % O ₂ , GHSV = 50,000 h ⁻¹	80	100	[167]
MnO ₂ hollow spheres	Hard templating method	104.0~236.0	0.40~0.80	100 ppmv HCHO in dry air, GHSV 30,000 h ⁻¹	99.7	90	[23]
Au/MnO ₂ hierarchical hollow microsphere	Hydrothermal method and sol-gel method	52.3	0.16	200 ppm HCHO in air, GHSV 30,000 mL·g ⁻¹ _{cat} ·h ⁻¹	59.2	25	[168]
Pt/C@MnO ₂ composite hierarchical hollow microspheres	Hydrothermal method with hollow carbon spheres as a sacrificial template	153.0	0.37	HCHO solution (38% mass concentration)	90.5	—	[2]
Hierarchical Pt/WO ₃ nanoflakes assembled hollow microspheres	Solution method	23.0	0.12	HCHO solution (38% mass concentration), 260 ppm HCHO concentration	97	—	[165]
Hierarchically macro-mesoporous Pt/γ-Al ₂ O ₃ composite hollow microspheres	Chemically induced self-transformation method	114.0	0.37	HCHO solution (38%)	—	—	[169]
Hierarchical Pt/NiO hollow microspheres	Template-free approach	50.8	0.11	HCHO solution (38%)	—	—	[170]
Pt/CoSn(OH) ₆ hollow nanoboxes	—	—	—	HCHO solution (38%), ~180 ppm HCHO concentration	80.1	—	[171]
Hollow chains mesoporous Pt/TiO ₂ (R _{Pt-nominal} were 0.5 wt%)	Microwave-hydrothermal route	132.0	0.29	HCHO solution (38%)	—	—	[145]
Fe ₂ O ₃ @SnO ₂ core-shell nanospindles	—	108.0	0.18	HCHO aqueous solution (38 wt%, contains 10–15 wt% methanol)	95.99	—	[172]
RuCoO _x /Al ₂ O ₃ hollow microspheres	Soft-template method	193.0	0.39	Gas containing 0.1% vinyl chloride in air, weight hourly space velocity (WHSV) of 30,000 mL·g ⁻¹ ·h ⁻¹	90	345	[166]

- Hollow nanospheres

For vinyl chloride (VC) catalytic oxidation, Wang et al. [166] synthesized hollow alumina microspheres (Al_2O_3 -hms) as the support for ruthenium/cobalt binary oxides to prepare the catalyst. The $\text{RuCoO}_x/\text{Al}_2\text{O}_3$ -hms exhibited the highest VC oxidation activity with T_{50} at 310°C and T_{90} at 345°C compared with $\text{RuO}_x/\text{Al}_2\text{O}_3$ -hms, $\text{CoO}_x/\text{Al}_2\text{O}_3$ -hms, and Al_2O_3 -hms. The SMSI effects between metal nanoparticles and Al_2O_3 -hms support varied the low-temperature reducibility, the abundance of surface oxygen, lattice oxygen mobility, and the metal valence state distribution over $\text{RuCoO}_x/\text{Al}_2\text{O}_3$ -hms catalysts.

Manganese oxides (MnO_x) were the transition metal oxides with multiple crystalline phases and oxidation states, which have been extensively investigated due to their high reductive degree in high oxidation states (Mn^{4+} and/or Mn^{3+}). Chen et al. [167] synthesized manganese oxide honeycomb and hollow nanospheres via a simple soft chemistry route for the effective removal of HCHO. The catalytic activity of K_xMnO_2 nanospheres for HCHO oxidation was improved by changing the KMnO_4/OA molar ratio to form the hollow structure. The 100% HCHO conversion temperature (T_{100}) of the hollow K_xMnO_2 nanospheres was 80°C , and the T_{100} of honeycomb nanospheres was 85°C , which, due to the HCHO, would adsorb and retain for a longer period in the hollow structure.

Boyjoo et al. [23] prepared the MnO_2 hollow spheres by the redox (CPR) method to control the manganese oxide precipitation coated on SiO_2 spheres (Figure 12). The $\text{Mn}[\text{P}]\text{N}$ ('Mn' stands for MnO_2 , 'P' for permanganate $\text{Mn}(\text{VII})$ solution, and 'N' for nitrate $\text{Mn}(\text{II})$ solution; the letter between the square brackets [] represents the solution that was added dropwise) was performed best with T_{50} and T_{90} of 75.6°C and 99.7°C , respectively, which was attributed to the highest surface area. The $\text{Mn}[\text{P}][\text{N}]$ maintained a high 75% conversion up to 90 h of reaction due to the high concentration of oxygen vacancies to continuously regenerate hydroxyl species on the surface of the birnessite sheets. Moreover, the hydroxyl radicals replenished from the water would be helped to complete the oxidation of formaldehyde.

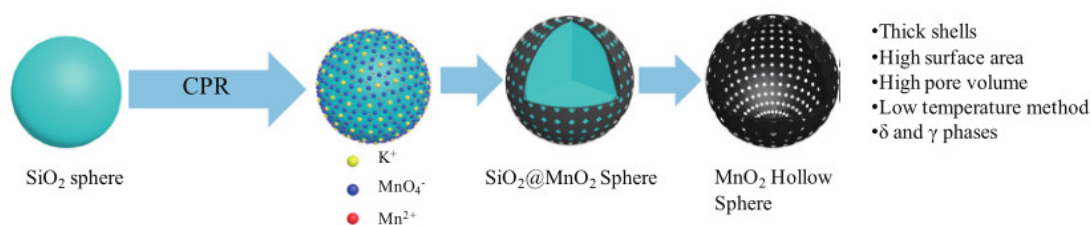


Figure 12. Brief description of the hard templating method to synthesize the MnO_2 hollow sphere. Figure reproduced from ref. [23].

Furthermore, the adoption of a hollow spherical structure with hierarchical structures to modify the surface of metal oxides has received more attention due to open the hierarchical architecture endowed abundant surface sites for the diffusion and adsorption of reactants as well as the high active metal dispersion [2]. For example [168], MnO_2 hierarchical hollow microspheres (MnO_2 -S3) with a crystalline structure of γ - MnO_2 were prepared using the hydrothermal method; then, the Au nanoparticles were dispersed on the surfaces of hollow MnO_2 microspheres using the sol-gel method. The Au/MnO_2 -S3 showed the highest activity with 59.2% conversion, achieved at 25°C , among the Au/MnO_2 samples. Therefore, another effective method was to load noble metals to improve the catalytic activity.

Pt with high activity and good stability is typically used to decompose HCHO, even at room temperatures [173]. This was attributed to the fact that the metal Pt with the negative charge could provide more active sites for HCHO oxidation, probably due to facilitating the electron transfer and the formation of active oxygen [174]. The HCHO conversion efficiency of the hierarchical WO_3 nanoflakes, comprising assembled hollow microspheres, was only 3% within 60 min, and the HCHO conversion efficiency was 97% of WO_3 -Pt1.0 (within

60 min) (1.0 represents the weight percentage of Pt loaded in the samples) [165]. This result indicates that WO_3 was inert for the catalytic oxidation of HCHO, and Pt played a key role in the HCHO decomposition. Furthermore, Sun et al. [2] prepared a hierarchical core-shell Pt/ MnO_2 -HCS (hollow carbon spheres) composite sphere through the template-assisted hydrothermal method and reductive deposition of Pt NPs (Figure 13a–d). Compared with MnO_2 -MS (MnO_2 microsphere), the Pt/ MnO_2 -HCS sample exhibited a higher HCHO decomposition efficiency of 90.5% within 60 min.

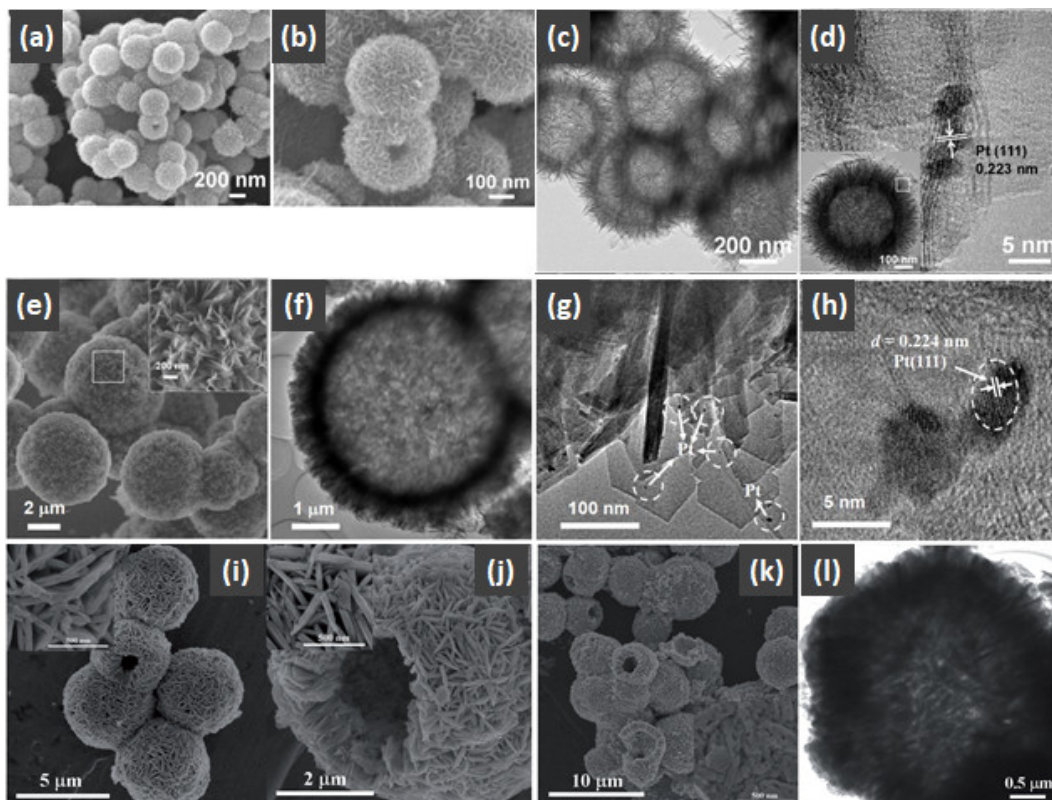


Figure 13. FESEM images of the MnO_2 -HCS (a,b). TEM ((c) and inset of (d)) and HRTEM (d) images of the Pt/ MnO_2 -HCS reproduced from ref. [2]; (e–h) Structural characterization of the Pt/ $\gamma\text{-Al}_2\text{O}_3$; SEM (e), high magnification SEM (inset in (e)), TEM (f,g), and HRTEM (h) images of the PHAO sample reproduced from ref. [169]; (i–l) SEM images and the corresponding high-magnification SEM images (insets) of the samples: Ni80 (i), Ni400 (j), and Ni600 (k); TEM image of the Ni400P sample (l) reproduced from ref. [170].

The other special hierarchical macro-mesoporous hollow structure, such as that of the $\gamma\text{-Al}_2\text{O}_3$ hollow spheres (HAO), was assembled with nanosheets on the surface and then PHAO (Pt- hollow $\gamma\text{-Al}_2\text{O}_3$ spheres) was fabricated by depositing small Pt NPs on the surfaces of the nanosheets, which were used for HCHO oxidation (Figure 13e–h) [169]. Among all the catalysts, PHAO was the most active catalyst in terms of HCHO oxidation and demonstrated a highly improved performance.

As shown in Figure 13i–l, Qi et al. [170] prepared hierarchical Pt/NiO hollow microspheres through the template-free approach, and loaded Pt by the combined NaOH-assisted impregnation of NiO with NaBH_4 reduction. In contrast to Ni400G (the as-prepared sample heated to 400 °C which was ground into a fine powder using an agate mortar to destroy the hollow spheres), the Ni400P (with a calcination temperature at 400 °C) achieved a higher catalytic activity due to the hierarchical hollow spheres assembled by a large number of nanosheets and the bimodal macro-mesoporous structures. And, this phenomenon also reflected the two following points: (1) the diffusion and transport of gas molecules would be blocked in the pores generated by the disorderly stacked nanosheets; (2) it is

difficult for the growth and cluster of Pt nanoparticles because of the lack of a hierarchical macro-mesoporous structure.

- Other hollow-structured metal oxides

To oxidate HCHO, Qi et al. [145] prepared a highly efficient Pt/TiO₂ catalyst using TiO₂ hollow chains as support material, and found that the hollow chain-like structure with numerous mesopores, great pore volume, and a high surface area remarkably improved its catalytic activity. Additionally, the uniform CoSn(OH)₆ hollow nanoboxes with an abundance of surface hydroxyl groups and plenty of catalytic oxidation sites also provided superior support in order to disperse the Pt metals [171].

Lv et al. [172] reported using the Fe₂O₃@SnO₂ core-shell nanospindles as the support for loading Pt nanoparticles, which were prepared by assembling SnO₂ shells over Fe₂O₃ cores (Figure 14a–d). Compared to the Pt/Fe₂O₃ and Pt/SnO₂ catalysts, the Pt/Fe₂O₃@SnO₂ shows enhanced room-temperature HCHO oxidation activity with the 95.99% removal ratios of HCHO after 1 h. By analyzing the DFT simulation results, an excellent catalytic performance was ascribed to the fast adsorption and activation of the reactant O₂ by the Fe₂O₃ surface, and the SnO₂ surface is beneficial for the desorption of the resultant H₂O. Also, the synergetic combination of the individual oxide building blocks produced by the hetero-structure was another reason for the observed enhanced catalytic capability.

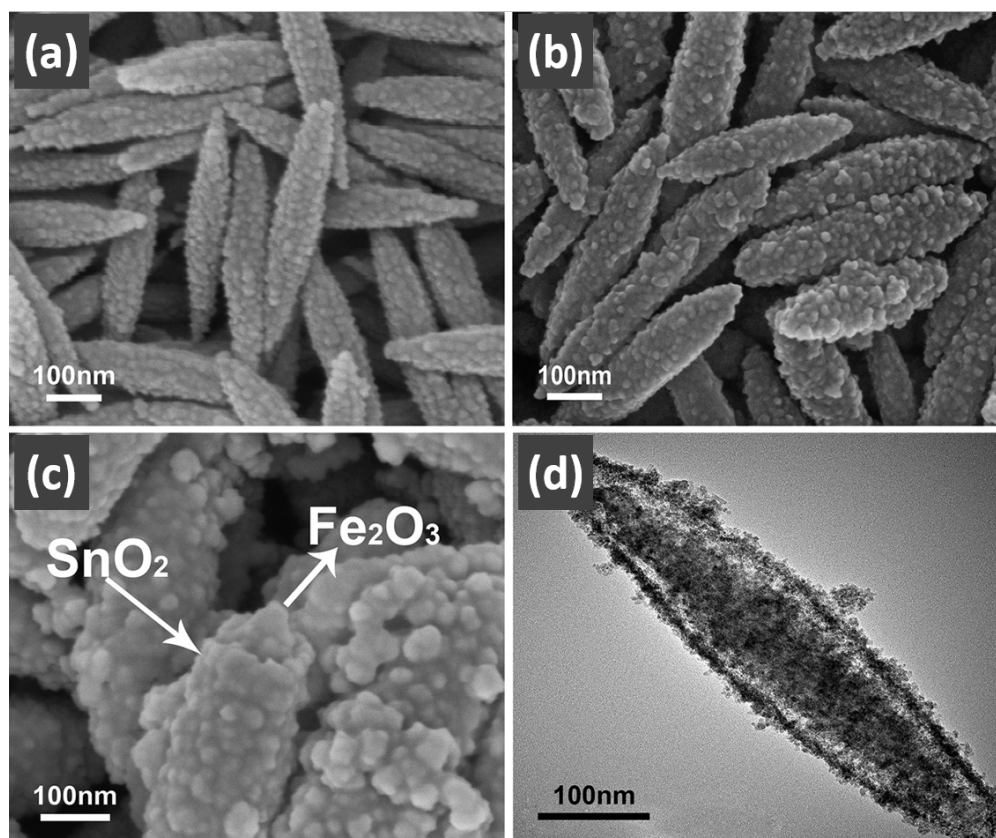


Figure 14. The SEM and TEM images of the prepared Fe₂O₃ (a) and Fe₂O₃@SnO₂ (b–d) reproduced from ref. [172].

Generally, metal supports loaded with noble metal are widely used catalysts for the catalytic oxidation of volatile organic compounds. However, the dispersion degree of noble metal on metal oxides is critical to catalytic activity. Metal oxides with a hollow structure have shown their advantages, such as their large specific surface area, low density, high loading capacity, outstanding interior voids, good surface permeability, and high

mobility, etc. The low-temperature oxidation performance of catalysts for the removal of volatile organic compounds is due to the two following key factors: (1) the synergistic effect between the noble metal particles and the support; and (2) the abundance of surface sites for the diffusion and adsorption of reactants.

2.3. Removal of Other Pollutants

2.3.1. Catalytic Conversion of CO₂

As it is well known, global warming is caused by massive emissions of greenhouse gases [175]. Carbon dioxide has been considered the main greenhouse gas responsible for global warming [176,177]. Meanwhile, CO₂ can also be a promising and economical carbon source for synthesizing organic compounds [178,179]. Thus, the incorporation of CO₂ into epoxides [175], the synthesis of symmetrical or asymmetrical urea compounds [180] and formic acid and its derivatives [181] from CO₂, the synthesis of acetic acid via methanol hydrocarboxylation with CO₂ and H₂ [182], as well as the recycling of CO₂ through the hydrogenation or reforming processes, etc. [183], are considered promising approaches. In some of these processes, catalysts have been extensively researched and developed because they can reduce processing costs. Researchers are keen to enhance the catalytic activity using metal oxides with special surface characteristics [175]. Moreover, the hollow nano-microstructures of metal oxide materials strongly affects their efficiency due to the composition and size of such structures, the various pore sizes, and the fine structure of the spherical shells. Thus, the application of HSMOs is one of the solutions for catalysts to achieve a high performance.

Spinel-type composite metal oxides have been widely used for the incorporation of CO₂ and CS₂ into epoxides due to their various advantages, such as their mixed-metal oxidation state, chemical stability, excellent synergistic performance, economical cost, and simple preparation process [9,175,176]. In terms of ingredients, catalysts with nanocrystalline aluminum-derived spinel structures are widely employed due to their high thermal stability, high mechanical resistance, hydrophobicity, and low surface acidity. The hollow spinel-type composite metal oxides, such as nano-CuAl₂O₄ hollow spheres [175], nanoporous triple-shelled CuAl₂O₄ hollow spheres [179], and multi-shell hollow CoAl₂O₄ microspheres [9], have been promising catalysts for the cycloaddition of CO₂ to epoxides. For instance, the copper–alumina spinel hollow sphere decorated the unique structures of the nanoflake with a triple-shell structure [179], as displayed in Figure 15a–c, which highly improved the catalytic activity for the cycloaddition of CO₂ at atmospheric pressure due to the good accessibility of interior active sites in the hollow structure. Additionally, another hollow-structured catalyst with an excellent performance for the cycloaddition of CO₂ and epoxide under solvent-free conditions is that of hollow marigold CuCo₂O₄ spinel microspheres [176], which have numerous Lewis acidic active sites.

In addition, Witoon et al. [183] prepared a series of CuO–ZnO catalysts for the hydrogenation of CO₂ to methanol by adjusting the chitosan concentration. It was found that the hollow-structured CuO–ZnO catalyst (Figure 15d–f) with the largest surface area (46.2 m² g^{−1}) and the smallest crystallite sizes achieved the highest space–time yield of methanol (135 g kg^{−1} cat · h^{−1}) at 513 K. Tian et al. [184] synthesized the hollow CuO/ZnO/Al₂O₃ composite microspheres using carbonaceous saccharide as the template. The obtained catalysts could achieve an optimum methanol yield of 15.3% with the 24.7% CO₂ conversion at 262 °C.

Other hollow structures were developed from the MOF derivative catalysts. The included hollow-structured Cu@ZrO₂ prevent the sintering of Cu nanoparticles, which leads to the high performance of CO₂ hydrogenation, and to methanol reaction with 5% CO₂ conversion and 85% methanol selectivity at 220 °C [185]. Additionally, the hollow-structured In₂O₃@ZrO₂ effectively improved the catalytic activity of formate intermediates to methanol (STY_{MeOH} of 0.29 g_{MeOH} · g_{cat}^{−1} · h^{−1} at 290 °C) because of the strong In₂O₃–ZrO₂ interaction at the In₂O₃/ZrO₂ heterointerfaces [186].

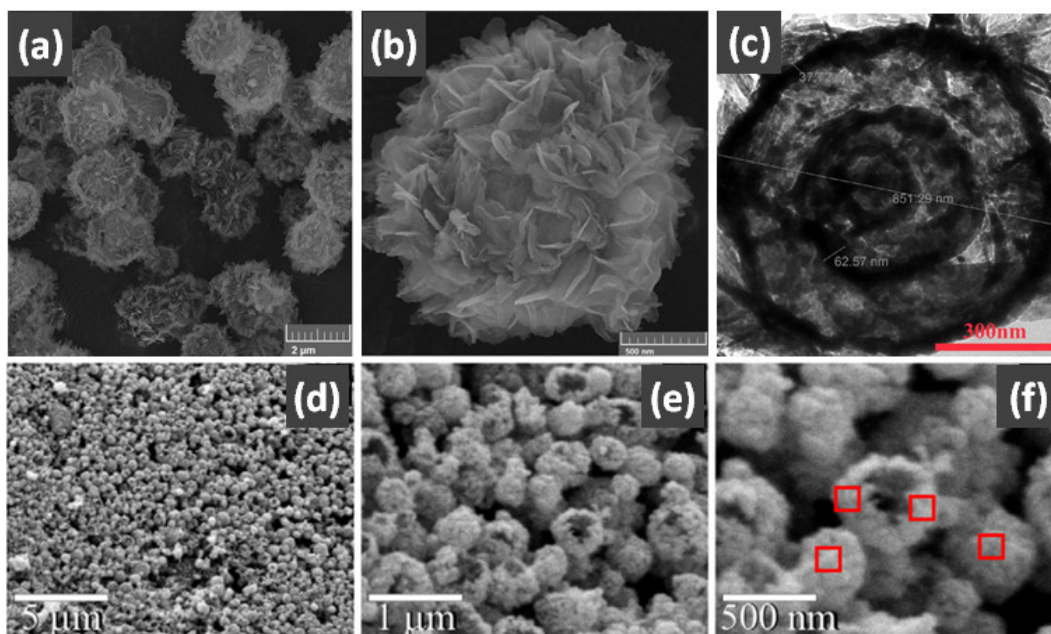
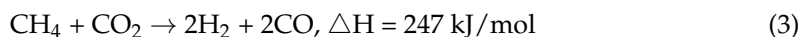


Figure 15. (a,b) FESEM and (c) TEM images of the synthesized CuAl_2O_4 hollow sphere reproduced from ref. [179]; (d–f) SEM images at different magnifications of the CuO-ZnO catalyst reproduced from ref. [183]. The red borders in the figure represent irregular spherical shape of the sample.

2.3.2. Catalytic Conversion of CH_4

The impact of CH_4 , another greenhouse gas, on the environment is 20 times that of CO_2 [187]. The methane dry reforming process (Equation (3)) is a sustainable means of reducing greenhouse gas emissions by simultaneously consuming two kinds of greenhouse gases. It can contribute to both environmental protection and the energy economy [188]:



However, the carbon deposition [189] and active metals sintering [188,190] of catalysts are the main problems arising during the dry reforming of methane (DRM). Recent studies have shown that the application of HSMOs is favorable for the catalysis of DRM [189,191–193].

As it is known to all, HSMOs exhibit advantages including their high loading capacity, superior pore permeability, high specific surface area, abundant inner void space, and low density. Therefore, the promotion of gas diffusion and the high dispersity of active metal nanoparticles were attributed to the hollow structure [191,194]. Additionally, the high metal dispersion over a greater surface area of the support is one particular advantage of supported metal catalysts, showing excellent activity due to the interactions of the metal with the support and the stability of the support at high temperature.

Compared with the one-component system, the incorporation of the second oxide significantly improves the catalytic activity, stability, and anti-catalytic toxicity of the nanostructure, which is due to the synergistic interaction between the two different oxides that would be increased by tuning the composition and morphology of hollow structure. The adjustment of the component benefited from the SMSIs provided sufficient reaction active sites and oxygen vacancies to inhibit the high carbon deposition [195]. Finally, superior catalytic activity and particle sintering resistance would be achieved. Thus, the investigation of HSMOs could remarkably influence the activity, stability, and anti-catalytic toxicity of catalysts for DRM.

2.3.3. Removal of Organic Compounds

To date, HSMOs have shown great potential in the field of the catalytic environmental contaminants, such as the hydrogenation of 4-nitrophenol (4-NP) and the cat-

alytic oxidation of 1,2-dichlorobenzene (*o*-DCB). For the catalytic hydrogenation of 4-NP, Au/CeO₂ catalyst [196], hollow Cu₂O/rGO nanohybrid [197], Au@mesoporous SnO₂ yolk-shell nanoparticles [198], cellulose nanocrystal-supported hollow CuFe₂O₄ nanoparticles (CuFe₂O₄/CNC) [199], and Fe₃O₄@Au hollow spheres, etc. [200], the materials exhibited excellent catalytic activity due to the unique porous structure, were permeable for chemical species, and had large specific surface areas, which induced the easy accessibility of the reactant at the active sites. Furthermore, the good reusability of Fe₃O₄@Au hollow spheres was attributed to its magnetic properties, which resulted in the rapid recycling of catalysts [200].

Except for the Fe₃O₄@Au hollow spheres sample, hollow Fe₃O₄-Au nanocomposites [201] (Figure 16a–f), hollow Fe₃O₄/P(GMA-EGDMA)SO₃H/Au-PPy catalyst [202] (Figure 16g–j), Au/Fe₃O₄@TiO₂ hollow nanospheres [203] (Figure 16k–n), and multi-shelled FeCo₂O₄ hollow porous microspheres/cotton cellulose fibers (CCFs) [204] all exhibited magnetism, and thus their convenient separability and excellent repeatability. Moreover, the superior catalytic performance of FeCo₂O₄ hollow porous microspheres/CCFs was also ascribed to the synergistic effect between magnetic TS-FeCo₂O₄ (triple-shelled) and CCFs. And, the CeO₂@Au@CeO₂-MnO₂ catalyst with the sandwich hollow structure [103] proved the synergistic effect among the components. Additionally, the TS-FeCo₂O₄/CCF materials could act as a photo-catalyst with high catalytic activity, which was attributed to the multiple additional reflections of the incident light which would occur in the multi-shelled hollow structure. Thus, the more efficient utilization of incident light within the interior cavity was realized.

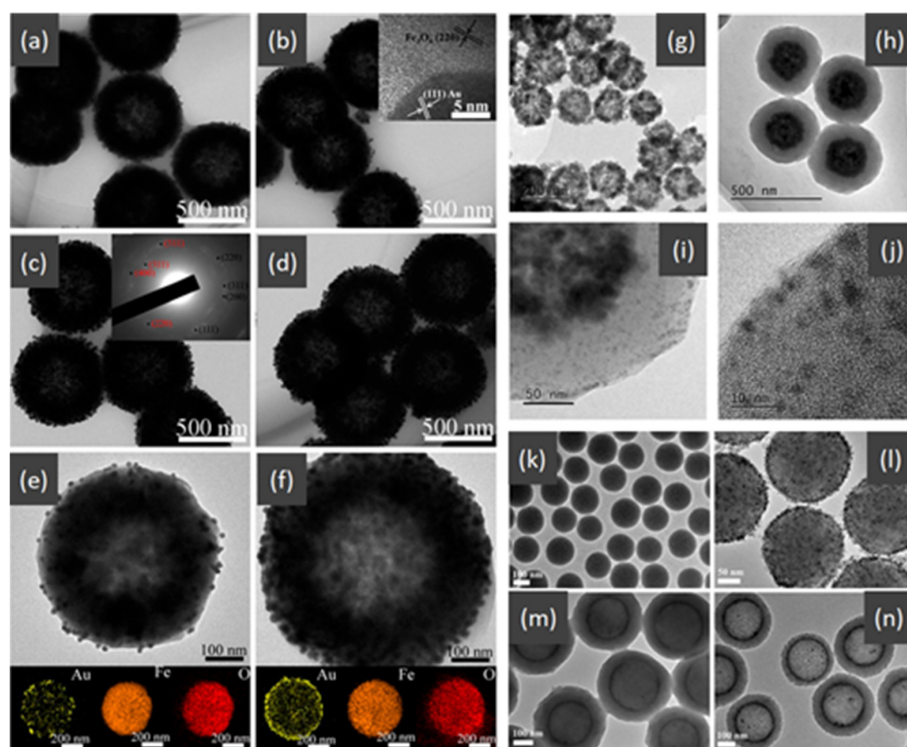


Figure 16. TEM images of the Fe₃O₄-Au 5 mL (a) and Fe₃O₄-Au 20 mL with the HRTEM image (inset) (b); Fe₃O₄-Au 40 mL with the SAED pattern (inset) (c) and Fe₃O₄-Au 60 mL (d); TEM images of single Fe₃O₄-Au 5 mL (e) and Fe₃O₄-Au 60 mL (f) microspheres and corresponding EDS elemental mapping images (Au, Fe, and O). Figure reproduced from ref. [201] TEM images of (g) hollow Fe₃O₄ microspheres, (h) Fe₃O₄/P(GMA-EGDMA) microspheres, and (i,j) Fe₃O₄/P(GMA-EGDMA)SO₃H/Au-PPy microspheres. Figure reproduced from ref. [202]. TEM images of (k) SiO₂ nanospheres, (l) Au/Fe₃O₄/SiO₂, (m) Au/Fe₃O₄/SiO₂@TiO₂, (n) Au/Fe₃O₄@hTiO₂. Figure reproduced from ref. [203].

Furthermore, the $\text{Co}_3\text{O}_4/\text{CoP}$ composite hollow polyhedron [7] was synthesized as a superior catalyst with dramatic efficiency and stability for the reduction of 4-NP through phosphorization calcination. It is believed that the rapid transfer of electrons during the catalytic hydrogenation of 4-NP is crucial, which is supported by the MFe_2O_4 ($\text{M}=\text{Co}, \text{Ni}, \text{Cu}$) hollow spheres [205], the plasmonic Au-loaded hollow porous TiO_2 spheres, etc. [206].

In addition, Wu et al. [207] prepared metal oxides (NiO , CuO , and NiO/CuO) with hollow nanosphere morphology. The five-stage hydrogenation of the 4-NP reaction process over NiO/CuO porous carbon shell (HNSs@C) is illustrated in Figure 17a. The HNSs played a key role in the “electrical” connection between the particles during the electron transfer from the oxidation site to the reduction site [208]. Moreover, the surface with rich interconnected nanobranches could reduce the interface resistance and provide a convenient way for electron transfer.

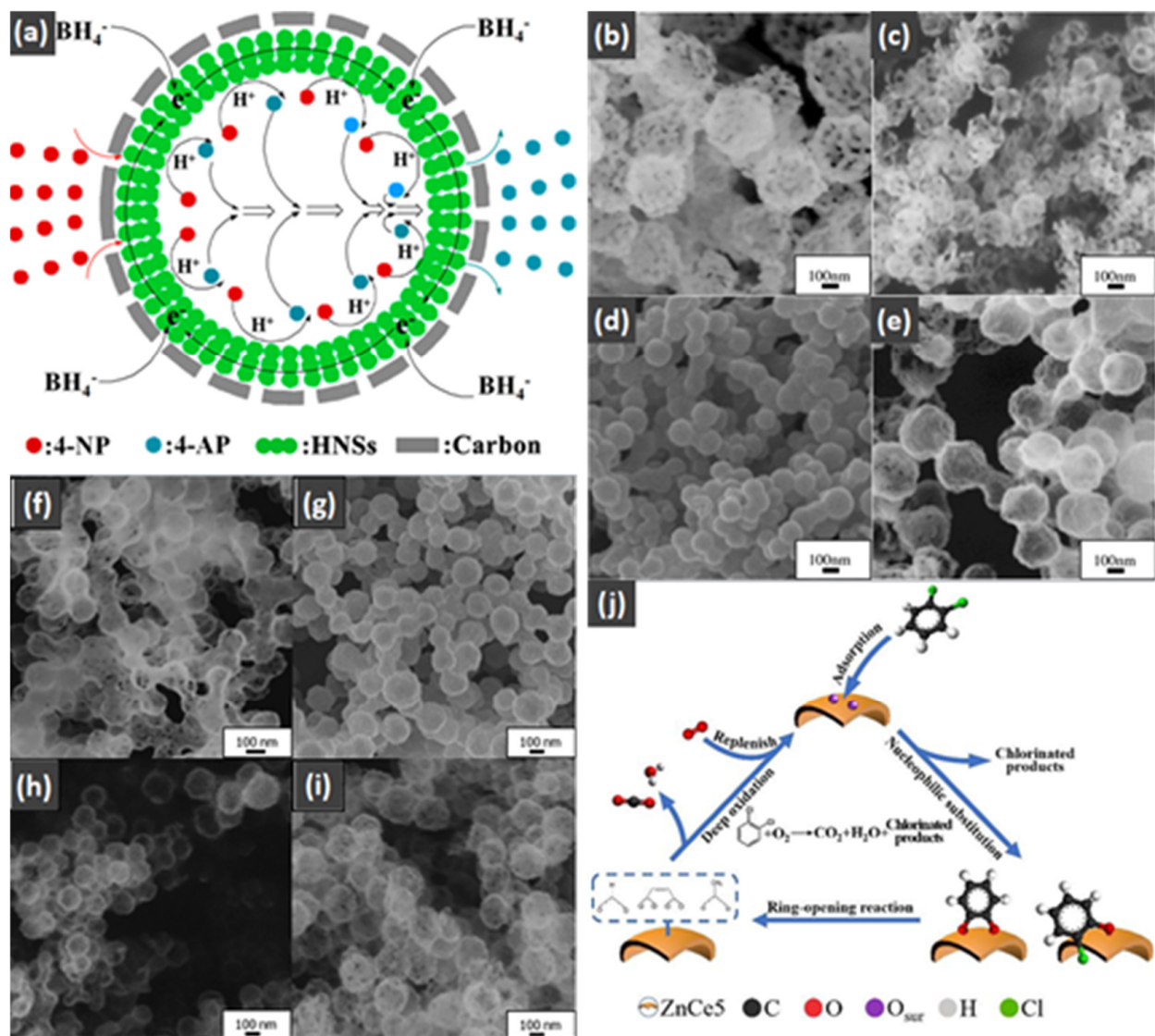


Figure 17. (a) Schematic diagram of the catalytic mechanism of metal oxide HNSs@C for the hydrogenation of 4-NP reaction. Figure reproduced from ref. [207]. SEM images of (b) Fe_2O_3 , (c) FeCa_5 , (d) FeCa_{10} , and (e) FeCa_{20} . Figure reproduced from ref. [209]. SEM images of (f) FeMn_{10} , (g) FeMn_{20} , (h) FeMn_{40} , and (i) FeMn_{80} (represent the molar ratios of $\text{Mn}/(\text{Fe} + \text{Mn})$ are $\sim 10, 20, 40,$ and 80 mol%). Figure reproduced from ref. [22]. (j) Proposed reaction routes of *o*-DCB catalytic oxidation over ZnCe_5 (doped with 5 mol% Ce). Figure reproduced from ref. [210].

For the catalytic oxidation of *o*-DCB, the structure–reactivity relationship has been widely investigated. However, the morphological effect of the hollow structure was rarely discussed. A small amount of data currently available developed demonstrated that the strong performance of the hollow-structured catalysts was attributed to their small crystallite size, the high concentration of surface-active oxygen [22], good low-temperature reducibility, and the synergistic effect between metal oxides [209,210]. As shown in Figure 17b–e, the Ca-doped FeO_x hollow microspheres were fabricated using carbon microspheres as templates [209], and the optimal FeCa10 (the nominal content of Ca was 10 mol%) hollow microspheres achieved a superior catalytic activity, water resistance, stability, and CO₂ selectivity. The hierarchical porous structure of a series of novel Fe–Mn composite oxides with hollow microsphere morphology, as shown in Figure 17f–i, was also one of the properties that resulted in high catalytic activity, CO₂ selectivity, good water-resistant performance, and excellent stability [22].

The oxidation of *o*-DCB over mixed-oxide hollow microspheres occurs to follow the Mars–van Krevelen-like mechanism [209,210]. For example, as shown in Figure 17j, the reaction mechanism of the Ce-doped ZnO hollow microspheres was summarized as the following steps: (1) *o*-DCB was converted into catecholate or phenolate species through nucleophilic substitution after being adsorbed onto the surface ZnCe5; (2) and then ZnCe5 proceeded to inducing the ring opening reaction of catecholate or phenolate species, which facilitated the formation of maleate, acetate, and formate species; (3) CO₂ and H₂O were formed due to the oxidation of a large amount of maleate, acetate, or formate species [210].

HSMOs also have great potential for treating water pollutants such as dyes (e.g., acid orange 7(AO7) [211], methylene blue) [212], pharmaceuticals (e.g., acetaminophen [213], norfloxacin (NOR) [214], tetracycline (TC) [215], and ciprofloxacin) [216], and organic pollutions (e.g., phenol) [217] through the photocatalytic degradation and advanced oxidation processes (AOPs).

For the photocatalytic degradation of pharmaceuticals and organic pollutions, hollow-structured TiO₂ has been widely studied. The hollow mesoporous TiO₂ microspheres were synthesized for the photocatalytic degradation of acetaminophen [213], and the TiO₂ hollow mesoporous nanostructures photocatalytic degradation of phenols [217]. Additionally, the CeO₂/Co₃O₄ hollow microsphere [215] was prepared for the degradation of tetracycline (TC). For the photodegradation of AO7, Fe-doped CeO₂ hollow microspheres [211] as the catalyst were prepared by a simple coprecipitation method using yeast as a bio-template, as shown in Figure 18a–h. Fe-doped CeO₂ hollow microspheres have a higher photocatalytic performance in degrading AO7 aqueous solutions containing H₂O₂ under visible irradiation, which can be attributed to their greater number of oxygen vacancies, higher specific surface area, and lower band gap, in contrast with CeO₂ hollow microspheres and Fe-doped CeO₂ nanoparticles.

Thus, the advantages of HSMOs with respect to the photocatalytic degradation of pharmaceuticals and organic pollutions are given as follows: (1) the addition of substance promoted the separation of electron and hole pairs; (2) the large specific surface area provided more active sites; and (3) the abundant pore structure increased the probability of contact between the catalyst and pollution [217].

For AOPs' treatment of methylene blue, Zhang et al. [212] prepared Fe₃O₄@MnO₂ ball-in-ball hollow spheres (BBHs) with magnetic properties as the catalyst shown in Figure 18i–l. The improved catalytic activity of Fe₃O₄@MnO₂ BBHs was ascribed to the synergistic effect of outer MnO₂ nanosheets and the inner Fe₃O₄ hollow ball. And, the recyclability of the as-prepared catalyst was attributed to the magnetic property.

AOPs have been considered an effective means of water purification. The Fenton reaction is a specific kind of AOP. In addition, the Mn-doped Fe₃O₄ hollow microsphere [218], hollow spheres of Cu–CuFe₂O₄/SiO₂ composite [219], bifunctional hollow mesoporous Fe⁰@C/MnFe₂O₄ [220], and the hollow sphere CuFe₂O₄ [221] have been prepared as Fenton-like catalysts for treating other dyes. These catalysts exhibited a superior catalytic activity for the removal of pollutants, good catalytic stability, and easy magnetic recovery

due to the inherent characteristics of metal oxides and the advantages of a hollow structure, which could provide important instructions to rationally design and synthesize HSMOs for water pollution treatment.

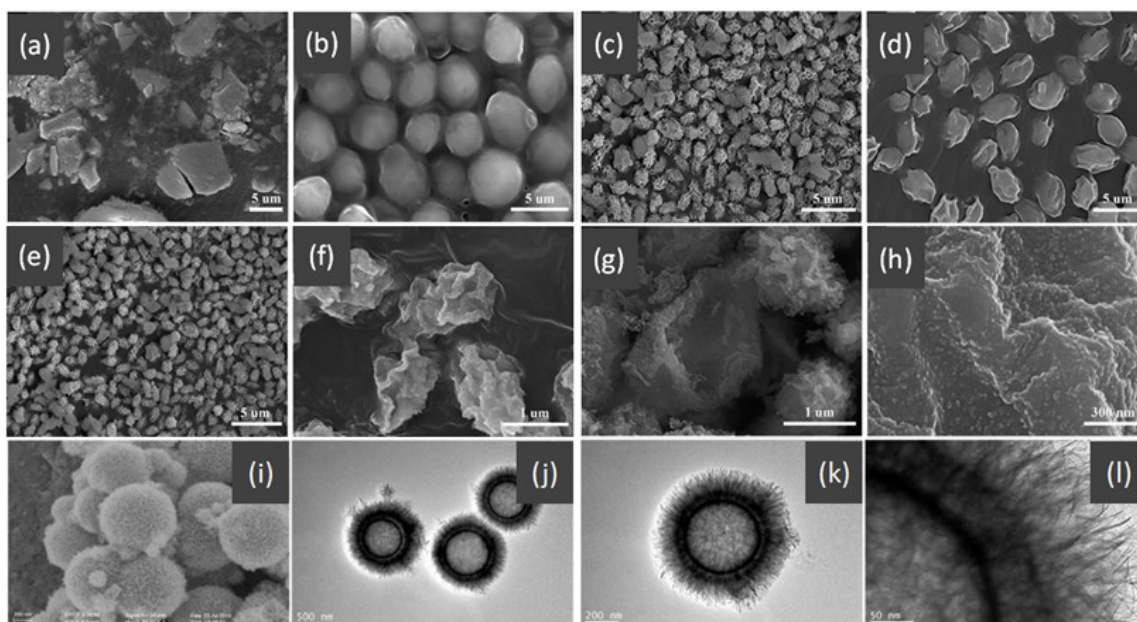


Figure 18. SEM images of the (a) Fe-doped CeO₂ nanoparticles, (b) yeast template, (c) CeO₂ hollow microspheres, and Fe-doped CeO₂ hollow microspheres before (d) and after (e–h) calcination. Figure reproduced from ref. [211]. The SEM image (i) and TEM images (j–l) of Fe₃O₄@MnO₂ BBHs. Figure reproduced from ref. [212].

3. Conclusions and Perspectives

HSMOs have piqued the interest of researchers as a novel type of structure. This structure takes advantage of the intrinsic properties of various metal oxides and fully exploits the various properties of the hollow structure, as well as the benefits of interfacial interaction and the synergistic effects between the metal oxides. Because metal oxide hollow structures have basic properties such as their high loading capacity, superior pore permeability, high specific surface area, abundant inner void space, and low density, they have a wide range of applications in environmental catalysis. We summarized their geometric morphology, metal oxide components, and interior/ulterior architecture from various levels and perspectives in different environmental catalysis processes in order to investigate the structure–performance correlation of HSMOs.

For environmental catalysis, the premise is to realize a highly catalytic performance by enhancing the probability of contact between the catalysts and the reactant, thus exposing more active sites. Countless HSMOs with properties such as a high specific surface areas, big pore volumes, and adjustable morphology have been developed. As the structure–activity relationship becomes clearer in this important field, the excellent catalytic performance is ascribed to the improvement in the properties in terms of magnetic properties, synergistic interaction, abundant defects, sufficient utilization of interior space, sufficient acid/base sites, good redox characteristics, abundant active oxygen, high storage/release capacity of oxygen, a large amount of active surface oxygen (O_S), etc.

However, some aspects of HSMOs still need attention and deserve further study in order to optimize hollow structures in different applications, as described below:

(1) Specific laws of the synergistic effect between metal components of HSMOs. It is generally accepted that the synergistic effect is complex. However, the specific laws of the synergistic effect should be briefly summarized and then these novel laws should be generalized for practically useful synthetic approaches. For example, this could include the

integration of different types of catalytic sites, such as acid, base, redox, oxygen vacancy, and other sites, using the variation of catalyst metal oxide compositions.

(2) Synthesis strategies need to be developed in order to reduce the process complexity and production cost. The synthesis of catalysts with hollow structures typically involves complex steps and elaborate formulations, which are more expensive than the conventional catalysts used in the industry. Therefore, the functional benefits offered by hollow-structured catalysts also come at a cost. In reality, in environmental catalysis, there are more substances that would cause catalyst poisoning and deactivation. To assess the real potential of catalysts, detailed techno-economic analyses and extensive benchmarking studies of the candidate and conventional catalysts are required.

(3) The rational design and optimization of the HSMOs' shell porosity, thickness, and shell number are necessary. The catalytic kinetic behavior and molecular behavior control of HSMOs were regulated by these characteristics. The proper selection of microporous shells with a precise pore structure and size, increasing the number of shell layers, changing the thickness or curvature, etc., could promote selective reactions. The physical and chemical properties of HSMOs are investigated and tuned to enhance their interactions with the reacting gas molecules, thus effectively increasing the reaction rate.

Additionally, pioneering characterization technologies are highly preferred and urgently desired so that the aspects of HSMOs outlined above can be made much clearer with the use of advanced characterization data. Focusing on the structural characteristics of HSMOs, expounding the constitutive relationship between the component composition and its performance could have a guiding significance for the further optimization of the structure of the material, and it is expected to be widely used in the preparation of other HSMO materials. In the future, we can predict that the development of HSMOs for environmental catalysis will eventually intersect with various state-of-the-art fields.

Funding: This research was funded by the National Natural Science Foundation of China (Grant Nos. 22276098, 21976094, and 22176100), the National Key Research and Development Project (Grant No.2018YFC0213802), the Educational Commission of Anhui Province of China (2023AH050173), the National & Local Joint Engineering Research Centre for Mineral Salt Deep Utilization (SF202102), and the State Key Laboratory of Low-carbon Smart Coal-fired Power Generation and Ultra-clean Emission. The APC was funded by State Key Laboratory of Low-carbon Smart Coal-fired Power Generation and Ultra-clean Emission.

Data Availability Statement: Data are contained within the article.

Conflicts of Interest: Authors Jingxin Xu, Wenxin Tian and Chao Pan were employed by the company China Energy Science and Technology Research Institute Co., Ltd. The remaining authors declare that the research was conducted in the absence of any commercial or financial relationships that could be construed as a potential conflict of interest.

References

1. Binas, V.; Venieri, D.; Kotzias, D.; Kiriakidis, G. Modified TiO₂ based photocatalysts for improved air and health quality. *J. Mater.* **2017**, *3*, 3–16.
2. Sun, D.; Wageh, S.; Al-Ghamdi, A.A.; Le, Y.; Yu, J.; Jiang, C. Pt/C@MnO₂ composite hierarchical hollow microspheres for catalytic formaldehyde decomposition at room temperature. *Appl. Surf. Sci.* **2019**, *466*, 301–308. [[CrossRef](#)]
3. Gong, M.; Zhang, J.; Luo, J.-L.; Wang, C.-A. Au/CeO₂ hollow nanospheres with enhanced catalytic activity for CO oxidation. *Int. J. Appl. Ceram. Technol.* **2017**, *14*, 908–914. [[CrossRef](#)]
4. Lin, J.; Huang, J.; Chen, X.; Zheng, Y.; Xiao, Y.; Zheng, Y.; Jiang, L. Key factors for methane combustion over palladium-based catalysts revealed by enhanced and depressed catalytic performance. *Appl. Catal. B* **2024**, *340*, 123283. [[CrossRef](#)]
5. Xu, W.; He, H.; Yu, Y. Deactivation of a Ce/TiO₂ Catalyst by SO₂ in the Selective Catalytic Reduction of NO by NH₃. *J. Phys. Chem. C* **2009**, *113*, 4426–4432. [[CrossRef](#)]
6. Qu, J.; Chen, D.; Li, N.; Xu, Q.; Li, H.; He, J.; Lu, J. Construction of Pd-Modified NiCoO_x Hollow Nanospheres with Surface Hydroxyls and Oxygen Vacancies for Highly Enhanced Catalytic Toluene Oxidation Activity. *ACS Sustain. Chem. Eng.* **2020**, *8*, 10581–10587. [[CrossRef](#)]
7. Liu, X.; Li, X.; Qin, L.; Mu, J.; Kang, S.-Z. Co₃O₄/CoP composite hollow polyhedron: A superior catalyst with dramatic efficiency and stability for the room temperature reduction of 4-nitrophenol. *Appl. Surf. Sci.* **2018**, *434*, 967–974. [[CrossRef](#)]

8. Kim, S.; Park, C.; Lee, J. Reduction of polycyclic compounds and biphenyls generated by pyrolysis of industrial plastic waste by using supported metal catalysts: A case study of polyethylene terephthalate treatment. *J. Hazard. Mater.* **2020**, *392*, 122464. [[CrossRef](#)] [[PubMed](#)]
9. Khalifeh, R.; Sorouri, M.; Damirchi, E.K.; Rajabzadeh, M. Efficient and selective CO₂ and CS₂ conversion to cyclic carbonates and trithiocarbonates by using multishell hollow CoAl₂O₄ microsphere as a unique catalyst under solventless condition. *J. Taiwan Inst. Chem. Eng.* **2020**, *115*, 229–241. [[CrossRef](#)]
10. Cui, Y.; Xu, L.; Chen, M.; Lv, C.; Lian, X.; Wu, C.-E.; Yang, B.; Miao, Z.; Wang, F.; Hu, X. CO Oxidation over Metal Oxide (La₂O₃, Fe₂O₃, PrO₂, Sm₂O₃, and MnO₂) Doped CuO-Based Catalysts Supported on Mesoporous Ce_{0.8}Zr_{0.2}O₂ with Intensified Low-Temperature Activity. *Catalysts* **2019**, *9*, 724. [[CrossRef](#)]
11. Hou, Z.; Pei, W.; Zhang, X.; Zhang, K.; Liu, Y.; Deng, J.; Jing, L.; Dai, H. Rare earth oxides and their supported noble metals in application of environmental catalysis. *J. Rare Earths* **2020**, *38*, 819–839. [[CrossRef](#)]
12. Liu, B.; Yu, S.; Wang, Q.; Hu, W.; Jing, P.; Liu, Y.; Jia, W.; Liu, Y.; Liu, L.; Zhang, J. Hollow mesoporous ceria nanoreactors with enhanced activity and stability for catalytic application. *Chem. Commun.* **2013**, *49*, 3757–3759. [[CrossRef](#)] [[PubMed](#)]
13. Li, Y.; Gan, L.; Si, R. Effect of tungsten oxide on ceria nanorods to support copper species as CO oxidation catalysts. *J. Rare Earths* **2021**, *39*, 43–50. [[CrossRef](#)]
14. Wang, X.; Feng, J.; Bai, Y.; Zhang, Q.; Yin, Y. Synthesis, Properties, and Applications of Hollow Micro-/Nanostructures. *Chem. Rev.* **2016**, *116*, 10983–11060. [[CrossRef](#)] [[PubMed](#)]
15. Guo, G.; Lian, K.; Wang, L.; Gu, F.; Han, D.; Wang, Z. High specific surface area LaMO₃ (M=Co, Mn) hollow spheres: synthesis, characterization and catalytic properties in methane combustion. *RSC Adv.* **2014**, *4*, 58699–58707. [[CrossRef](#)]
16. Zhao, H.; Yao, S.; Zhang, M.; Huang, F.; Fan, Q.; Zhang, S.; Liu, H.; Ma, D.; Gao, C. Ultra-Small Platinum Nanoparticles Encapsulated in Sub-50 nm Hollow Titania Nanospheres for Low-Temperature Water-Gas Shift Reaction. *ACS Appl. Mater. Interfaces* **2018**, *10*, 36954–36960. [[CrossRef](#)] [[PubMed](#)]
17. Jeyavani, V.; Kondhekar, D.; Bhati, M.; Dev, S.; Joshi, K.; Devi, R.N.; Mukherjee, S.P. Remarkable SO₂ and H₂S Resistant Ability on CO Oxidation by Unique Pd/WO₃ 3D Hollow Sphere Nanocatalyst: Correlating Structure–Activity Relationships on SO₂ Exposure. *ACS Appl. Energy Mater.* **2024**, *7*, 1476–1487. [[CrossRef](#)]
18. Wang, Z.; Wei, Y.; Qi, J.; Wan, J.; Wang, Z.; Yu, R.; Wang, D. Mass Transfer Modulation by Hollow Multi-Shelled Structures for High Space-Time Yield Synthesis of Light Olefins from Syngas. *Adv. Funct. Mater.* **2024**, *34*, 2316547. [[CrossRef](#)]
19. Xiao, J.; Cheng, K.; Xie, X.; Wang, M.; Xing, S.; Liu, Y.; Hartman, T.; Fu, D.; Bossers, K.; van Huis, M.A.; et al. Tandem catalysis with double-shelled hollow spheres. *Nat. Mater.* **2022**, *21*, 572–579. [[CrossRef](#)]
20. Wang, M.M.; Chen, D.Y.; Li, N.; Xu, Q.F.; Li, H.; He, J.H.; Lu, J.M. Nanocage-Shaped Co_{3–x}Zr_xO₄ Solid-Solution Supports Loaded with Pt Nanoparticles as Effective Catalysts for the Enhancement of Toluene Oxidation. *Small* **2020**, *16*, 2005715. [[CrossRef](#)]
21. Luo, L.; Huang, R.; Hu, W.; Yu, Z.; Tang, Z.; Chen, L.; Zhang, Y.; Zhang, D.; Xiao, P. Metal–Organic Framework-Derived Hollow CoMn₂O₄ Nanocube Catalysts for Deep Toluene Oxidation. *ACS Appl. Nano Mater.* **2022**, *5*, 8232–8242. [[CrossRef](#)]
22. Ma, X.D.; Wen, J.X.; Guo, H.W.; Ren, G.B. Facile template fabrication of Fe-Mn mixed oxides with hollow microsphere structure for efficient and stable catalytic oxidation of 1,2-dichlorobenzene. *Chem. Eng. J.* **2020**, *382*, 122940. [[CrossRef](#)]
23. Boyjoo, Y.; Rochard, G.; Giraudon, J.-M.; Liu, J.; Lamonier, J.-F. Mesoporous MnO₂ hollow spheres for enhanced catalytic oxidation of formaldehyde. *SM&T* **2019**, *20*, e00091.
24. Wei, W.; Wang, Z.; Liu, Z.; Liu, Y.; He, L.; Chen, D.; Umar, A.; Guo, L.; Li, J. Metal oxide hollow nanostructures: Fabrication and Li storage performance. *J. Power Sources* **2013**, *238*, 376–387. [[CrossRef](#)]
25. Wang, Z.; Zhou, L.; Lou, X.W.D. Metal oxide hollow nanostructures for lithium-ion batteries. *Adv. Mater.* **2012**, *24*, 1903–1911. [[CrossRef](#)] [[PubMed](#)]
26. Sun, Y.F.; Liu, S.B.; Meng, F.L.; Liu, J.Y.; Jin, Z.; Kong, L.T.; Liu, J.H. Metal oxide nanostructures and their gas sensing properties: A review. *Sensors* **2012**, *12*, 2610–2631. [[CrossRef](#)] [[PubMed](#)]
27. Lai, X.; Halpert, J.E.; Wang, D. Recent advances in micro-/nano-structured hollow spheres for energy applications: From simple to complex systems. *Energy Environ. Sci.* **2012**, *5*, 5604–5618. [[CrossRef](#)]
28. Prieto, G.; Tüysüz, H.; Duyckaerts, N.; Knossalla, J.; Wang, G.-H.; Schüth, F. Hollow Nano- and Microstructures as Catalysts. *Chem. Rev.* **2016**, *116*, 14056–14119. [[CrossRef](#)] [[PubMed](#)]
29. Rezaei, F.; Khalifeh, R.; Amrollahi, M.A. Urchin-like double-shelled Pd–PdO/ZnO hollow sphere as an efficient catalyst for the Suzuki-Miyaura reaction. *Mater. Today Chem.* **2020**, *18*, 100353. [[CrossRef](#)]
30. Fu, X.-P.; Yu, W.-Z.; Li, M.-Y.; Si, R.; Ma, C.; Jia, C.-J. Facile Fabrication of CeO₂-Al₂O₃ Hollow Sphere with Atomically Dispersed Fe via Spray Pyrolysis. *Inorg. Chem.* **2021**, *60*, 5183–5189. [[CrossRef](#)]
31. Wang, L.; Wan, J.; Wang, J.; Wang, D. Small Structures Bring Big Things: Performance Control of Hollow Multishelled Structures. *Small Struct.* **2020**, *2*, 2000041. [[CrossRef](#)]
32. Yu, L.; Yu, X.Y.; Lou, X.W.D. The Design and Synthesis of Hollow Micro-/Nanostructures: Present and Future Trends. *Adv. Mater.* **2018**, *30*, e1800939. [[CrossRef](#)] [[PubMed](#)]
33. Feng, J.; Yin, Y. Self-Templating Approaches to Hollow Nanostructures. *Adv. Mater.* **2019**, *31*, e1802349. [[CrossRef](#)] [[PubMed](#)]
34. Hu, J.; Chen, M.; Fang, X.; Wu, L. Fabrication and application of inorganic hollow spheres. *Chem. Soc. Rev.* **2011**, *40*, 5472–5491. [[CrossRef](#)] [[PubMed](#)]

35. Dong, S.; Wang, J.; Tang, X.; Li, J.; Zhang, X.; Liu, B. Low-temperature and stable CO oxidation of in-situ grown monolithic $\text{Mn}_3\text{O}_4/\text{TiO}_2$ catalysts. *J. Alloys Compd.* **2021**, *855*, 157444. [[CrossRef](#)]
36. Xiong, J.; Mei, X.; Liu, J.; Wei, Y.; Zhao, Z.; Xie, Z.; Li, J. Efficiently multifunctional catalysts of 3D ordered meso-macroporous $\text{Ce}_{0.3}\text{Zr}_{0.7}\text{O}_2$ -supported PdAu@ CeO_2 core-shell nanoparticles for soot oxidation: Synergetic effect of Pd-Au- CeO_2 ternary components. *Appl. Catal. B* **2019**, *251*, 247–260. [[CrossRef](#)]
37. Cui, Y.; Xu, L.; Chen, M.; Lian, X.; Wu, C.-E.; Yang, B.; Miao, Z.; Wang, F.; Hu, X. Facilely fabricating mesoporous nanocrystalline Ce–Zr solid solution supported CuO-based catalysts with advanced low-temperature activity toward CO oxidation. *Catal. Sci. Technol.* **2019**, *9*, 5605–5625. [[CrossRef](#)]
38. Sun, H.; Liu, Z.; Chen, S.; Quan, X. The role of lattice oxygen on the activity and selectivity of the OMS-2 catalyst for the total oxidation of toluene. *Chem. Eng. J.* **2015**, *270*, 58–65. [[CrossRef](#)]
39. Montini, T.; Melchionna, M.; Monai, M.; Fornasiero, P. Fundamentals and Catalytic Applications of CeO_2 -Based Materials. *Chem. Rev.* **2016**, *116*, 5987–6041. [[CrossRef](#)] [[PubMed](#)]
40. Sun, C.; Sun, J.; Xiao, G.; Zhang, H.; Qiu, X.; Li, H.; Chen, L. Mesoscale Organization of Nearly Monodisperse Flowerlike Ceria Microspheres. *J. Phys. Chem. B* **2006**, *110*, 13445–13452. [[CrossRef](#)] [[PubMed](#)]
41. Zhang, D.; Du, X.; Shi, L.; Gao, R. Shape-controlled synthesis and catalytic application of ceria nanomaterials. *Dalton Trans.* **2012**, *41*, 14455–14475. [[CrossRef](#)]
42. Sun, C.; Li, H.; Chen, L. Nanostructured ceria-based materials: Synthesis, properties, and applications. *Energy Environ. Sci.* **2012**, *5*, 8475. [[CrossRef](#)]
43. Yuan, Q.; Duan, H.H.; Li, L.L.; Sun, L.D.; Zhang, Y.W.; Yan, C.H. Controlled synthesis and assembly of ceria-based nanomaterials. *J. Colloid. Interface Sci.* **2009**, *335*, 151–167. [[CrossRef](#)] [[PubMed](#)]
44. Chen, F.; Wang, W.; Chen, Z.; Wang, T. Biogenic synthesis and catalysis of porous CeO_2 hollow microspheres. *J. Rare Earths* **2012**, *30*, 350–354. [[CrossRef](#)]
45. Zhang, Y.; Cheng, T.; Hu, Q.; Fang, Z.; Han, K. Study of the preparation and properties of CeO_2 single/multiwall hollow microspheres. *J. Mater. Res.* **2007**, *22*, 1472–1478. [[CrossRef](#)]
46. Yang, Z.; Han, D.; Ma, D.; Liang, H.; Liu, L.; Yang, Y. Fabrication of Monodisperse CeO_2 Hollow Spheres Assembled by Nano-octahedra. *Cryst. Growth Des.* **2010**, *10*, 291–295. [[CrossRef](#)]
47. Ma, J.; Qian, K.; Huang, W.; Zhu, Y.; Yang, Q. Facile One-Step Synthesis of Double-Shelled CeO_2 Hollow Spheres and Their Optical and Catalytic Properties. *Bull. Chem. Soc. Jpn.* **2010**, *83*, 1455–1461. [[CrossRef](#)]
48. Chen, G.; Xu, C.; Song, X.; Xu, S.; Ding, Y.; Sun, S. Template-free Synthesis of Single-Crystalline-like CeO_2 Hollow Nanocubes. *Cryst. Growth Des.* **2008**, *8*, 4449–4453. [[CrossRef](#)]
49. Chen, G.; Zhu, F.; Sun, X.; Sun, S.; Chen, R. Benign synthesis of ceria hollow nanocrystals by a template-free method. *CrystEngComm* **2011**, *13*, 2904–2908. [[CrossRef](#)]
50. González-Rovira, L.; Sánchez-Amaya, J.M.; López-Haro, M.; del Rio, E.; Hungría, A.B.; Midgley, P.; Calvino, J.J.; Berna, S.; Botana, F.J. Single-Step Process to Prepare CeO_2 Nanotubes with Improved Catalytic Activity. *Nano Lett.* **2009**, *9*, 1395–1400. [[CrossRef](#)] [[PubMed](#)]
51. Zhang, D.; Pan, C.; Shi, L.; Huang, L.; Fang, J.; Fu, H. A highly reactive catalyst for CO oxidation: CeO_2 nanotubes synthesized using carbon nanotubes as removable templates. *Microporous Mesoporous Mater.* **2009**, *117*, 193–200. [[CrossRef](#)]
52. Zhang, D.; Yan, T.; Pan, C.; Shi, L.; Zhang, J. Carbon nanotube-assisted synthesis and high catalytic activity of CeO_2 hollow nanobeads. *Mater. Chem. Phys.* **2009**, *113*, 527–530. [[CrossRef](#)]
53. Wang, Z.; Yu, R. Hollow Micro/Nanostructured Ceria-Based Materials: Synthetic Strategies and Versatile Applications. *Adv. Mater.* **2019**, *31*, e1800592. [[CrossRef](#)] [[PubMed](#)]
54. Devaraju, M.K.; Liu, X.; Yin, S.; Sato, T. A rapid solvothermal synthesis of cerium oxide hollow spheres and characterization. *J. Solid. State Chem.* **2012**, *194*, 43–47. [[CrossRef](#)]
55. Chen, G.; Rosei, F.; Ma, D. Interfacial Reaction-Directed Synthesis of Ce-Mn Binary Oxide Nanotubes and Their Applications in CO Oxidation and Water Treatment. *Adv. Funct. Mater.* **2012**, *22*, 3914–3920. [[CrossRef](#)]
56. Chiu, K.-I.; Kwong, F.-I.; Ng, D.H.L. Enhanced oxidation of CO by using a porous biomorphic CuO/ CeO_2 / Al_2O_3 compound. *Microporous Mesoporous Mater.* **2012**, *156*, 1–6. [[CrossRef](#)]
57. Yoon, K.; Yang, Y.; Lu, P.; Wan, D.; Peng, H.-C.; StammMasias, K.; Fanson, P.T.; Campbell, C.T.; Xia, Y. A highly reactive and sinter-resistant catalytic system based on platinum nanoparticles embedded in the inner surfaces of CeO_2 hollow fibers. *Angew. Chem. Int. Edit.* **2012**, *51*, 9543–9546. [[CrossRef](#)]
58. Chen, C.; Fang, X.; Wu, B.; Huang, L.; Zheng, N. A Multi-Yolk-Shell Structured Nanocatalyst Containing Sub-10 nm Pd Nanoparticles in Porous CeO_2 . *ChemCatChem* **2012**, *4*, 1578–1586. [[CrossRef](#)]
59. Mai, H.-X.; Sun, L.-D.; Zhang, Y.-W.; Si, R.; Feng, W.; Zhang, H.-P.; Liu, H.-C.; Yan, C.-H. Shape-Selective Synthesis and Oxygen Storage Behavior of Ceria Nanopolyhedra, Nanorods, and Nanocubes. *J. Phys. Chem. B* **2006**, *109*, 24380–24385. [[CrossRef](#)]
60. Wu, Z.; Li, M.; Overbury, S.H. On the structure dependence of CO oxidation over CeO_2 nanocrystals with well-defined surface planes. *J. Catal.* **2012**, *285*, 61–73. [[CrossRef](#)]
61. Tana; Zhang, M.; Li, J.; Li, H.; Li, Y.; Shen, W. Morphology-dependent redox and catalytic properties of CeO_2 nanostructures: Nanowires, nanorods and nanoparticles. *Catal. Today* **2009**, *148*, 179–183. [[CrossRef](#)]

62. Gao, Y.; Wang, W.; Chang, S.; Huang, W. Morphology Effect of CeO₂ Support in the Preparation, Metal–Support Interaction, and Catalytic Performance of Pt/CeO₂ Catalysts. *ChemCatChem* **2013**, *5*, 3610–3620. [[CrossRef](#)]
63. Han, X.; Li, L.; Wang, C. Template-free synthesis of uniform single-crystal hollow cerium dioxide nanocubes and their catalytic activity. *Nanoscale* **2013**, *5*, 7193–7196. [[CrossRef](#)] [[PubMed](#)]
64. Zhang, J.; Yang, H.; Wang, S.; Liu, W.; Liu, X.; Guo, J.; Yang, Y. Mesoporous CeO₂ nanoparticles assembled by hollow nanostructures: Formation mechanism and enhanced catalytic properties. *CrystEngComm* **2014**, *16*, 8777–8785. [[CrossRef](#)]
65. Mu, G.; Wei, Q.; Huang, Y. Facile fabrication of CeO₂ hollow microspheres with yeast as bio-templates. *J. Rare Earths* **2015**, *33*, 1329–1334. [[CrossRef](#)]
66. Li, B.X.; Shao, X.K.; Hao, Y.G.; Zhao, Y. Ultrasonic-Spray-Assisted Synthesis of Metal Oxide Hollow/Mesoporous Microspheres for Catalytic CO Oxidation. *RSC Adv.* **2015**, *5*, 85640–85645. [[CrossRef](#)]
67. Shen, G.; Liu, H.; Wang, Q.; Wang, Z.; Chen, Y. Self-template hydrothermal synthesis of CeO₂ hollow nanospheres. *J. Nanopart Res.* **2012**, *14*, 954. [[CrossRef](#)]
68. Li, Z.; Han, F.; Li, C.; Jiao, X.; Chen, D. Hollow CeO₂ dodecahedrons: One-step template synthesis and enhanced catalytic performance. *RSC Adv.* **2016**, *6*, 60975–60982. [[CrossRef](#)]
69. Wei, J.; Wang, S.; Sun, S.; Yang, Z.; Yang, Y. Formation of catalytically active CeO₂ hollow nanoparticles guided by oriented attachment. *Mater. Lett.* **2012**, *84*, 77–80. [[CrossRef](#)]
70. Wang, H.; Mao, D.; Qi, J.; Zhang, Q.; Ma, X.; Song, S.; Gu, L.; Yu, R.; Wang, D. Hollow Multishelled Structure of Heterogeneous Co₃O₄–CeO_{2-x} Nanocomposite for CO Catalytic Oxidation. *Adv. Funct.* **2019**, *29*, 1806588. [[CrossRef](#)]
71. He, J.; Chen, D.; Li, N.; Xu, Q.; Li, H.; He, J.; Lu, J. Hollow Mesoporous Co₃O₄–CeO₂ Composite Nanotubes with Open Ends for Efficient Catalytic CO Oxidation. *ChemSusChem* **2019**, *12*, 1084–1090. [[CrossRef](#)]
72. Liu, L.; Shi, J.; Wang, R. General fabrication of MCo₂O₄@CeO₂ (M = Ni, Cu, Zn, Mn) core@shell nanospheres and their catalytic performances in CO oxidation. *Funct. Mater. Lett.* **2017**, *10*, 1850001. [[CrossRef](#)]
73. Liu, W.; Wang, W.; Tang, K.; Guo, J.; Ren, Y.; Wang, S.; Feng, L.; Yang, Y. The promoting influence of the nickel species in the controllable synthesis and catalytic property of the nickel-ceria catalysts. *Catal. Sci. Technol.* **2016**, *6*, 2427–2434. [[CrossRef](#)]
74. Liu, W.; Liu, X.; Feng, L.; Guo, J.; Xie, A.; Wang, S.; Zhang, J.; Yang, Y. The synthesis of CeO₂ nanospheres with different hollowness and size induced by copper doping. *Nanoscale* **2014**, *6*, 10693–10700. [[CrossRef](#)] [[PubMed](#)]
75. Zhang, J.; Gong, M.; Cao, Y.; Wang, C.-A. Facile synthesis of well-dispersed CeO₂–CuO_x composite hollow spheres with superior catalytic activity for CO oxidation. *RSC Adv.* **2015**, *5*, 95133–95139. [[CrossRef](#)]
76. Li, W.; Hu, Y.; Jiang, H.; Jiang, N.; Bi, W.; Li, C. Litchi-peel-like hierarchical hollow copper-ceria microspheres: Aerosol-assisted synthesis and high activity and stability for catalytic CO oxidation. *Nanoscale* **2018**, *10*, 22775–22786. [[CrossRef](#)] [[PubMed](#)]
77. Li, W.; Feng, X.; Zhang, Z.; Jin, X.; Liu, D.; Zhang, Y. A Controllable Surface Etching Strategy for Well-Defined Spiny Yolk@Shell CuO@CeO₂ Cubes and Their Catalytic Performance Boost. *Adv. Funct.* **2018**, *28*, 1802559. [[CrossRef](#)]
78. Su, Y.; Yuan, S.; Ning, D.; Zhang, Q.; Han, W.; Wang, Y. The Template-Free Synthesis of CuO@CeO₂ Nanospheres: Facile Strategy, Structure Optimization, and Enhanced Catalytic Activity toward CO Oxidation. *Eur. J. Inorg. Chem.* **2018**, *2018*, 2927–2934. [[CrossRef](#)]
79. Song, X.-Z.; Su, Q.-F.; Li, S.-J.; Liu, S.-H.; Zhang, N.; Meng, Y.-L.; Chen, X.; Tan, Z. Triple-shelled CuO/CeO₂ hollow nanospheres derived from metal–organic frameworks as highly efficient catalysts for CO oxidation. *New J. Chem.* **2019**, *43*, 16096–16102. [[CrossRef](#)]
80. Chen, G.; Guo, Z.; Zhao, W.; Gao, D.; Li, C.; Ye, C.; Sun, G. Design of Porous/Hollow Structured Ceria by Partial Thermal Decomposition of Ce-MOF and Selective Etching. *ACS Appl. Mater. Interfaces* **2017**, *9*, 39594–39601. [[CrossRef](#)] [[PubMed](#)]
81. Liu, L.; Shi, J.; Cao, H.; Wang, R.; Liu, Z. Fabrication of CeO₂–MO_x (M = Cu, Co, Ni) composite yolk-shell nanospheres with enhanced catalytic properties for CO oxidation. *Beilstein J. Nanotechnol.* **2017**, *8*, 2425–2437. [[CrossRef](#)]
82. Zhang, J.; Cao, Y.; Wang, C.-A.; Ran, R. Design and Preparation of MnO₂/CeO₂–MnO₂ Double-Shelled Binary Oxide Hollow Spheres and Their Application in CO Oxidation. *ACS Appl. Mater. Interfaces* **2016**, *8*, 8670–8677. [[CrossRef](#)] [[PubMed](#)]
83. Liu, L.; Shi, J.; Cao, H.; Wang, R. Fabrication of CeO₂@MnO₂ Core–Shell Nanospheres and Their Application in CO Oxidation. *Nano* **2017**, *12*, 1750039. [[CrossRef](#)]
84. Chen, G.; Song, G.; Zhao, W.; Gao, D.; Wei, Y.; Li, C. Carbon sphere-assisted solution combustion synthesis of porous/hollow structured CeO₂–MnO_x catalysts. *Chem. Eng. J.* **2018**, *352*, 64–70. [[CrossRef](#)]
85. Liu, L.; Shi, J.; Wang, R. Facile construction of Mn₂O₃@CeO₂ core@shell cubes with enhanced catalytic activity toward CO oxidation. *J. Solid. State Chem.* **2019**, *269*, 419–427. [[CrossRef](#)]
86. Feng, J.; Wang, Y.; Gao, D.; Kang, B.; Li, S.; Li, C.; Chen, G. Ce–Mn Coordination Polymer Derived Hierarchical/Porous Structured CeO₂–MnO_x for Enhanced Catalytic Properties. *Nanoscale* **2020**, *12*, 16381–16388. [[CrossRef](#)] [[PubMed](#)]
87. Liu, L.; Shi, J.; Wang, R.; Cao, H.; Liu, Z. Fabrication of double-shelled Fe₂O₃/CeO₂ boxes from CeO₂-modified Prussian blue and their enhanced performances for CO removal and water treatment. *J. Alloys Compd.* **2017**, *725*, 544–556. [[CrossRef](#)]
88. Fuente ORdl Gonzalez-Barrio, M.A.; Navarro, V.; Pabon, B.M.; Palacio, I.; Mascaraque, A. Surface defects and their influence on surface properties. *J. Phys. Condens.* **2013**, *25*, 484008. [[CrossRef](#)]
89. Liu, W.; Tang, K.; Lin, M.; June, L.T.O.; Bai, S.-Q.; Young, D.J.; Li, X.; Yang, Y.-Z.; Hor, T.S.A. Multicomponent (Ce, Cu, Ni) oxides with cage and core-shell structures: Tunable fabrication and enhanced CO oxidation activity. *Nanoscale* **2016**, *8*, 9521–9526. [[CrossRef](#)]

90. Cheng, Z.; Yu, M.; Yang, G.; Kang, L. Fabrication of NiCo₂O₄@CeO₂ Core@shell Nanotubes with Enhanced Catalytic Performances. *CrystEngComm* **2016**, *18*, 6331–6335. [[CrossRef](#)]
91. Du, C.; Guo, Y.; Guo, Y.; Gong, X.-Q.; Lu, G. Polymer-templated synthesis of hollow Pd–CeO₂ nanocomposite spheres and their catalytic activity and thermal stability. *J. Mater. Chem. A* **2015**, *3*, 23230–23239. [[CrossRef](#)]
92. Guo, H.; He, Y.; Wang, Y.; Liu, L.; Yang, X.; Wang, S.; Huang, Z.; Wei, Q. Morphology-controlled synthesis of cage-bell Pd@CeO₂ structured nanoparticle aggregates as catalysts for the low-temperature oxidation of CO. *J. Mater. Chem. A* **2013**, *1*, 7494. [[CrossRef](#)]
93. Zhang, J.; Li, T.; Wang, C.-A.; Luo, J.-L. Rational design of sandwich-like MnO₂-Pd-CeO₂ hollow spheres with enhanced activity and stability for CO oxidation. *Nanoscale* **2019**, *11*, 6776–6783. [[CrossRef](#)] [[PubMed](#)]
94. Xie, Q.; Zhao, Y.; Guo, H.; Lu, A.; Zhang, X.; Wang, L.; Chen, M.-S.; Peng, D.-L. Facile preparation of well-dispersed CeO₂-ZnO composite hollow microspheres with enhanced catalytic activity for CO oxidation. *ACS Appl. Mater. Interfaces* **2014**, *6*, 421–428. [[CrossRef](#)] [[PubMed](#)]
95. Jiao, Y.; Wang, F.; Ma, X.; Tang, Q.; Wang, K.; Guo, Y.; Yang, L. Facile one-step synthesis of porous ceria hollow nanospheres for low temperature CO oxidation. *Microporous Mesoporous Mater.* **2013**, *176*, 1–7. [[CrossRef](#)]
96. Liu, X.; Yang, H.; Han, L.; Liu, W.; Wang, S.; Zhang, C.; Zhang, X.; Yang, Y. Mesoporous-Shelled CeO₂ Hollow Nanospheres Synthesized by a One-pot Hydrothermal Route and its Catalysis Performance. *CrystEngComm* **2013**, *15*, 7769–7775. [[CrossRef](#)]
97. Zhu, F.; Chen, G.; Sun, S.; Sun, X. In situ growth of Au@CeO₂ core-shell nanoparticles and CeO₂ nanotubes from Ce(OH)CO₃ nanorods. *J. Mater. Chem. A* **2013**, *1*, 288–294. [[CrossRef](#)]
98. Du, C.; Guo, Y.; Guo, Y.; Gong, X.-Q.; Lu, G. Synthesis of hollow structured core-shell Au@CeO₂-ZrO₂ nanocatalyst and its excellent catalytic performance. *J. Mater. Chem. A* **2017**, *5*, 5601–5611. [[CrossRef](#)]
99. Wang, Z.; Qi, J.; Zhao, K.; Zong, L.; Tang, Z.; Wang, L.; Yu, R. Controlled synthesis of highly active Au/CeO₂ nanotubes for CO oxidation. *Mater. Chem. Front.* **2017**, *1*, 1629–1634. [[CrossRef](#)]
100. Wang, Y.; Song, G.; Xu, Z.; Rosei, F.; Ma, D.; Chen, G. Interfacial Reaction-Directed Synthesis of Ceria Nanotube-embedded Ultra-small Pt Nanoparticle Catalyst with High Catalytic Activity and Thermal Stability. *J. Mater. Chem. A* **2016**, *4*, 14148–14154. [[CrossRef](#)]
101. Wu, K.; Zhou, L.; Jia, C.-J.; Sun, L.-D.; Yan, C.-H. Pt-embedded-CeO₂ hollow spheres for enhancing CO oxidation performance. *Mater. Chem. Front.* **2017**, *1*, 1754–1763. [[CrossRef](#)]
102. Chen, G.; Yang, Y.; Guo, Z.; Gao, D.; Zhao, W.; Yan, H.; Wang, W.-W.; Jia, C.-J.; Sun, G. Thermally Stable and Highly Active Pt/CeO₂@SiO₂ Catalysts with a Porous/Hollow Structure. *Catal. Sci. Technol.* **2018**, *8*, 4413–4419. [[CrossRef](#)]
103. Chen, G.Z.; Wang, Y.; Wei, Y.W.; Zhao, W.; Gao, D.W.; Yang, H.X.; Li, C.C. Successive Interfacial Reaction-Directed Synthesis of CeO₂@Au@CeO₂-MnO₂ Environmental Catalyst with Sandwich Hollow Structure. *ACS Appl. Mater. Interfaces* **2018**, *10*, 11595–11603. [[CrossRef](#)] [[PubMed](#)]
104. Qi, J.; Chen, J.; Li, G.; Li, S.; Gao, Y.; Tang, Z. Facile synthesis of core-shell Au@CeO₂ nanocomposites with remarkably enhanced catalytic activity for CO oxidation. *Energy Environ. Sci.* **2012**, *5*, 8937. [[CrossRef](#)]
105. Chen, Z.; Wang, Y.; Liang, Q.; Chen, L.; Zhan, W.; Li, Y. Structure-induced hollow Co₃O₄ nanoparticles with rich oxygen vacancies for efficient CO oxidation. *Sci. China Mater.* **2019**, *63*, 267–275. [[CrossRef](#)]
106. Zhang, C.; Zhang, L.; Xu, G.; Ma, X.; Xu, J.; Zhang, L.; Qi, C.; Xie, Y.; Sun, Z.; Jia, D. Hollow and Core-Shell Nanostructure Co₃O₄ Derived from a Metal Formate Framework toward High Catalytic Activity of CO Oxidation. *ACS Appl. Nano Mater.* **2018**, *1*, 800–806. [[CrossRef](#)]
107. Zeng, L.; Li, K.; Wang, H.; Yu, H.; Zhu, X.; Wei, Y.; Ning, P.; Shi, C.; Luo, Y. CO Oxidation on Au/ α -Fe₂O₃-Hollow Catalysts: General Synthesis and Structural Dependence. *J. Phys. Chem. C* **2017**, *121*, 12696–12710. [[CrossRef](#)]
108. Du, X.; Dong, F.; Tang, Z.; Zhang, J. The synthesis of hollow In₂O₃@Pd-Co₃O₄ core/shell nanofibers with ultra-thin shell for the low-temperature CO oxidation reaction. *Appl. Surf. Sci.* **2020**, *505*, 144471. [[CrossRef](#)]
109. Zhang, J.; Gu, F.; Wang, C.-A. Facile synthesis of multi-shelled MnO₂-Co₃O₄ hollow spheres with superior catalytic activity for CO oxidation. *Ceram. Int.* **2021**, *47*, 18411–18416. [[CrossRef](#)]
110. Wei, Y.; Zhao, D.; Wang, D. Mesoscience in Hollow Multi-Shelled Structures. *Adv. Sci.* **2023**, *11*, 2305408. [[CrossRef](#)]
111. Barth, J.O.; Jentys, A.; Lercher, J.A. Elementary Reactions and Intermediate Species Formed during the Oxidative Regeneration of Spent Fluid Catalytic Cracking Catalysts. *Ind. Eng. Chem. Res.* **2004**, *43*, 3097–3104. [[CrossRef](#)]
112. Ma, K.; Guo, K.; Li, L.; Zou, W.; Tang, C.; Dong, L. Cavity size dependent SO₂ resistance for NH₃-SCR of hollow structured CeO₂-TiO₂ catalysts. *Catal. Commun.* **2019**, *128*, 105719. [[CrossRef](#)]
113. Shao, J.; Lin, F.; Huang, Y.; Wang, Z.; Li, Y.; Chen, G.; Cen, K. MnO_x fabrication with rational design of morphology for enhanced activity in NO oxidation and SO₂ resistance. *Appl. Surf. Sci.* **2020**, *503*, 144064. [[CrossRef](#)]
114. Shi, Y.; Yi, H.; Gao, F.; Zhao, S.; Xie, Z.; Tang, X. Facile synthesis of hollow nanotube MnCoO_x catalyst with superior resistance to SO₂ and alkali metal poisons for NH₃-SCR removal of NO_x. *Sep. Purif.* **2021**, *265*, 118517. [[CrossRef](#)]
115. Katare, S.R.; Patterson, J.E.; Laing, P.M. Diesel Aftertreatment Modeling: A Systems Approach to NO_x Control. *Ind. Eng. Chem. Res.* **2007**, *46*, 2445–2454. [[CrossRef](#)]
116. Vélez, R.P.; Ellmers, I.; Huang, H.; Bentrup, U.; Schünemann, V.; Grünert, W.; Brückner, A. Identifying active sites for fast NH₃-SCR of NO/NO₂ mixtures over Fe-ZSM-5 by operando EPR and UV-vis spectroscopy. *J. Catal.* **2014**, *316*, 103–111. [[CrossRef](#)]

117. Li, C.; Tang, X.; Yi, H.; Wang, L.; Cui, X.; Chu, C.; Li, J.; Zhang, R.; Yu, Q. Rational design of template-free MnO_x-CeO₂ hollow nanotube as de-NO_x catalyst at low temperature. *Appl. Surf. Sci.* **2018**, *428*, 924–932. [[CrossRef](#)]
118. Xie, C.; Yang, S.; Shi, J.-W.; Niu, C. Constructing hollow silk worm structure in MnO_x-TiO₂ catalysts for improving the performance in selective catalytic reduction of NO by NH₃. *React. Kinet. Mech. Catal.* **2019**, *128*, 681–693. [[CrossRef](#)]
119. Liu, C.; Gao, G.; Shi, J.-W.; He, C.; Li, G.; Bai, N.; Niu, C. MnO_x-CeO₂ shell-in-shell microspheres for NH₃-SCR de-NO_x at low temperature. *Catal. Commun.* **2016**, *86*, 36–40. [[CrossRef](#)]
120. Guo, R.-T.; Chen, Q.-L.; Ding, H.-L.; Wang, Q.-S.; Pan, W.-G.; Yang, N.-Z.; Lu, C.-Z. Preparation and characterization of CeO_x@MnO_x core-shell structure catalyst for catalytic oxidation of NO. *Catal. Commun.* **2015**, *69*, 165–169. [[CrossRef](#)]
121. Shen, Q.; Zhang, L.; Sun, N.; Wang, H.; Zhong, L.; He, C.; Wei, W.; Sun, Y. Hollow MnO_x-CeO₂ mixed oxides as highly efficient catalysts in NO oxidation. *Chem. Eng. J.* **2017**, *322*, 46–55. [[CrossRef](#)]
122. Ma, K.; Zou, W.; Zhang, L.; Li, L.; Yu, S.; Tang, C.; Gao, F.; Dong, L. Construction of hybrid multi-shell hollow structured CeO₂-MnO_x materials for selective catalytic reduction of NO with NH₃. *RSC Adv.* **2017**, *7*, 5989–5999. [[CrossRef](#)]
123. Han, Y.; Mu, J.; Li, X.; Gao, J.; Fan, S.; Tan, F.; Zhao, Q. Triple-Shelled NiMn₂O₄ Hollow Spheres as an Efficient Catalyst for Low-Temperature Selective Catalytic Reduction of NO_x with NH₃. *Chem. Commun.* **2018**, *54*, 9797–9800. [[CrossRef](#)]
124. Cheng, S.; Shao, J.; Huang, B.; Guan, J.; Zhou, L. Promotion effect of urchin-like MnO_x@PrO_x hollow core-shell structure catalysts for the low-temperature selective catalytic reduction of NO with NH₃. *RSC Adv.* **2020**, *10*, 13855–13865. [[CrossRef](#)] [[PubMed](#)]
125. Liu, J.; Du, Y.; Liu, J.; Zhao, Z.; Cheng, K.; Chen, Y.; Wei, Y.; Song, W.; Zhang, X. Design of MoFe/Beta@CeO₂ catalysts with a core-shell structure and their catalytic performances for the selective catalytic reduction of NO with NH₃. *Appl. Catal. B* **2017**, *203*, 704–714. [[CrossRef](#)]
126. Zhan, S.; Shi, Q.; Zhang, Y.; Li, Y.; Tian, Y. Preparation of novel CeMo(x) hollow microspheres for low-temperature SCR removal of NO_x with NH₃. *RSC Adv.* **2016**, *6*, 59185–59194. [[CrossRef](#)]
127. Hao, Z.; Jiao, Y.; Shi, Q.; Zhang, H.; Zhan, S. Improvement of NH₃-SCR performance and SO₂ resistance over Sn modified CeMoO_x electrospun fibers at low temperature. *Catal. Today* **2019**, *327*, 37–46. [[CrossRef](#)]
128. Zhao, Y.; Cai, W.; Chen, M.; Bu, Y. Turning the activity of Cr-Ce mixed oxide towards thermocatalytic NO oxidation and photocatalytic CO₂ reduction via the formation of yolk shell structure hollow microspheres. *J. Alloys Compd.* **2020**, *829*, 154508. [[CrossRef](#)]
129. Chi, B.; Qu, H.; Xing, X.; Zhong, Q. Assembly of hollow CeO₂@Fe-ZSM-5 and SCR performance. *J. Alloys Compd.* **2017**, *726*, 906–912. [[CrossRef](#)]
130. Chen, X.; Liu, Q.; Wu, Q.; Luo, Z.; Zhao, W.; Chen, J.; Li, J. A hollow structure WO₃@CeO₂ catalyst for NH₃-SCR of NO_x. *Catal. Commun.* **2021**, *149*, 106252. [[CrossRef](#)]
131. Zhu, H.; Wang, R. Rational design of porous Ce_xNb_{1-x} oxide hollow nanospheres as a novel NH₃-SCR catalyst. *J. Mater. Chem. A* **2022**, *10*, 12269–12277. [[CrossRef](#)]
132. Gong, P.; Xie, J.; Fang, D.; He, F.; Li, F.; Qi, K. Enhancement of the NH₃-SCR property of Ce-Zr-Ti by surface and structure modification with P. *Appl. Surf. Sci.* **2020**, *505*, 144641. [[CrossRef](#)]
133. Wang, H.; Jin, B.; Wang, H.; Ma, N.; Liu, W.; Weng, D.; Wu, X.; Liu, S. Study of Ag promoted Fe₂O₃@CeO₂ as superior soot oxidation catalysts: The role of Fe₂O₃ crystal plane and tandem oxygen delivery. *Appl. Catal. B* **2018**, *237*, 251–262. [[CrossRef](#)]
134. Li, W.-J.; Wey, M.-Y. Core-shell design and well-dispersed Pd particles for three-way catalysis: Effect of halloysite nanotubes functionalized with Schiff base. *Sci. Total Environ.* **2019**, *675*, 397–407. [[CrossRef](#)] [[PubMed](#)]
135. He, H.; Dai, H.X.; Au, C.T. An investigation on the utilization of perovskite-type oxides La_{1-x}Sr_xMO₃ (M = Co_{0.77}Bi_{0.20}Pd_{0.03}) as three-way catalysts. *Appl. Catal. B* **2001**, *33*, 65–80. [[CrossRef](#)]
136. Zhao, H.; Li, H.; Pan, Z.; Feng, F.; Gu, Y.; Du, J.; Zhao, Y. Design of CeMnCu ternary mixed oxides as soot combustion catalysts based on optimized Ce/Mn and Mn/Cu ratios in binary mixed oxides. *Appl. Catal. B* **2020**, *268*, 118422. [[CrossRef](#)]
137. Li, W.-J.; Wey, M.-Y. Sintering-resistant, highly thermally stable and well-dispersed Pd@CeO₂/halloysite as an advanced three-way catalyst. *Sci. Total Environ.* **2020**, *707*, 136137. [[CrossRef](#)]
138. Zhou, Z.; Ouyang, J.; Yang, H.; Tang, A. Three-way catalytic performances of Pd loaded halloysite-Ce_{0.5}Zr_{0.5}O₂ hybrid materials. *Appl. Clay Sci.* **2016**, *121–122*, 63–70. [[CrossRef](#)]
139. Feng, N.J.; Zhu, Z.J.; Zhao, P.; Wang, L.; Wan, H.; Guan, G.F. Facile fabrication of trepan-like CeO₂@MnO₂ nanocomposite with high catalytic activity for soot removal. *Appl. Surf. Sci.* **2020**, *515*, 146013. [[CrossRef](#)]
140. Fang, F.; Zhao, P.; Feng, N.; Chen, C.; Li, X.; Liu, G.; Wan, H.; Guan, G. Construction of a hollow structure in La_{0.9}K_{0.1}CoO_{3-δ} nanofibers via grain size control by Sr substitution with an enhanced catalytic performance for soot removal. *Catal. Sci. Technol.* **2019**, *9*, 4938–4951. [[CrossRef](#)]
141. Yu, Y.; Ma, Q.; Tan, C.; Wang, H.; Hu, Z.; Zhang, Q.; Zhang, H.; Zhang, B. Preparation of hierarchical hollow structures assembled from porous NiCo₂O₄ nanosheets for diesel soot elimination. *EcoMat* **2020**, *2*, e12041. [[CrossRef](#)]
142. Scire, S.; Liotta, L.F. Supported gold catalysts for the total oxidation of volatile organic compounds. *Appl. Catal. B* **2012**, *125*, 222–246. [[CrossRef](#)]
143. Lyu, J.; Zhou, L.; Shao, J.; Zhou, Z.; Gao, J.; Li, J.; Dong, Y.; Wang, Z. Synthesis of TiO₂/H₂Ti₃O₇ composite with nanoscale spiny hollow hierarchical structure for photocatalytic mineralization of VOCs. *Chem. Eng. J.* **2020**, *400*, 125927. [[CrossRef](#)]
144. Kondratowicz, T.; Drozdek, M.; Michalik, M.; Gac, W.; Gajewska, M.; Kuśtrowski, P. Catalytic activity of Pt species variously dispersed on hollow ZrO₂ spheres in combustion of volatile organic compounds. *Appl. Surf. Sci.* **2020**, *513*, 145788. [[CrossRef](#)]

145. Qi, L.; Cheng, B.; Yu, J.; Ho, W. High-surface area mesoporous Pt/TiO₂ hollow chains for efficient formaldehyde decomposition at ambient temperature. *J. Hazard. Mater.* **2016**, *301*, 522–530. [[CrossRef](#)] [[PubMed](#)]
146. Levasseur, B.; Kaliaguine, S. Effects of iron and cerium in La_{1-y}Ce_yCo_{1-x}Fe_xO₃ perovskites as catalysts for VOC oxidation. *Appl. Catal. B* **2009**, *88*, 305–314. [[CrossRef](#)]
147. Feng, Z.; Ren, Q.; Peng, R.; Mo, S.; Zhang, M.; Fu, M.; Chen, L.; Ye, D. Effect of CeO₂ morphologies on toluene catalytic combustion. *Catal. Today* **2019**, *332*, 177–182. [[CrossRef](#)]
148. Li, D.; Yang, J.; Tang, W.; Wu, X.; Wei, L.; Chen, Y. Controlled synthesis of hierarchical MnO₂ microspheres with hollow interiors for the removal of benzene. *RSC Adv.* **2014**, *4*, 26796. [[CrossRef](#)]
149. Fang, W.; Chen, J.; Zhou, X.; Chen, J.; Ye, Z.; Li, J. Zeolitic Imidazolate Framework-67-Derived CeO₂@Co₃O₄ Core-Shell Microspheres with Enhanced Catalytic Activity toward Toluene Oxidation. *Ind. Eng. Chem. Res.* **2020**, *59*, 10328–10337. [[CrossRef](#)]
150. Dong, F.; Han, W.; Zhao, H.; Zhang, G.; Tang, Z. The Porous hollow CoInO_x nanocubes as a highly efficient catalyst for the catalytic combustion of toluene. *Nanoscale* **2019**, *11*, 9937–9948. [[CrossRef](#)]
151. Gu, W.X.; Li, C.Q.; Qiu, J.H.; Yao, J.F. Facile fabrication of flower-like MnO₂ hollow microspheres as high-performance catalysts for toluene oxidation. *J. Hazard. Mater.* **2021**, *408*, 124458. [[CrossRef](#)] [[PubMed](#)]
152. Zhao, J.H.; Tang, Z.C.; Dong, F.; Zhang, J.Y. Controlled porous hollow Co₃O₄ polyhedral nanocages derived from metal-organic frameworks (MOFs) for toluene catalytic oxidation. *Mol. Catal.* **2019**, *463*, 77–86. [[CrossRef](#)]
153. Liao, Y.N.; Zhang, X.; Peng, R.S.; Zhao, M.Q.; Ye, D.Q. Catalytic properties of manganese oxide polyhedra with hollow and solid morphologies in toluene removal. *Appl. Surf. Sci.* **2017**, *405*, 20–28. [[CrossRef](#)]
154. Mo, S.; Zhang, Q.; Zhang, M.; Zhang, Q.; Li, J.; Fu, M.; Wu, J.; Chen, P.; Ye, D. Elucidating the special role of strong metal-support interactions in Pt/MnO₂ catalysts for total toluene oxidation. *Nanoscale Horiz.* **2019**, *4*, 1425–1433. [[CrossRef](#)]
155. Xiao, Z.; Yang, J.; Ren, R.; Li, J.; Wang, N.; Chu, W. Facile synthesis of homogeneous hollow microsphere Cu-Mn based catalysts for catalytic oxidation of toluene. *Chemosphere* **2020**, *247*, 125812. [[CrossRef](#)] [[PubMed](#)]
156. Li, L.; Zhang, C.; Yan, J.; Wang, D.; Peng, Y.; Li, J.; Crittenden, J. Distinctive Bimetallic Oxides for Enhanced Catalytic Toluene Combustion: Insights into the Tunable Fabrication of Mn–Ce Hollow Structure. *ChemCatChem* **2020**, *12*, 2872–2879. [[CrossRef](#)]
157. Zhao, L.; Zhang, Z.; Li, Y.; Leng, X.; Zhang, T.; Yuan, F.; Niu, X.; Zhu, Y. Synthesis of Ce_aMnO_x hollow microsphere with hierarchical structure and its excellent catalytic performance for toluene combustion. *Appl. Catal. B* **2019**, *245*, 502–512. [[CrossRef](#)]
158. Zhao, J.H.; Han, W.L.; Tang, Z.C.; Zhang, J.Y. Carefully Designed Hollow Mn_xCo_{3-x}O₄ Polyhedron Derived from in Situ Pyrolysis of Metal-Organic Frameworks for Outstanding Low-Temperature Catalytic Oxidation Performance. *Cryst. Growth Des.* **2019**, *19*, 6207–6217. [[CrossRef](#)]
159. Yang, S.L.; Yang, H.C.; Yang, J.Y.; Qi, H.L.; Kong, J.; Bo, Z.; Li, X.D.; Yan, J.H.; Cen, K.F.; Tu, X. Three-dimensional hollow urchin α-MnO₂ for enhanced catalytic activity towards toluene decomposition in post-plasma catalysis. *Chem. Eng. J.* **2020**, *402*, 126154. [[CrossRef](#)]
160. Xu, Y.; Dhainaut, J.; Rochard, G.; Dacquin, J.-P.; Mamede, A.-S.; Giraudon, J.-M.; Lamonier, J.-F.; Zhang, H.; Royer, S. Hierarchical porous ε-MnO₂ from perovskite precursor: Application to the formaldehyde total oxidation. *Chem. Eng. J.* **2020**, *388*, 124146. [[CrossRef](#)]
161. Dong, C.; Qu, Z.; Qin, Y.; Fu, Q.; Sun, H.; Duan, X. Revealing the Highly Catalytic Performance of Spinel CoMn₂O₄ for Toluene Oxidation: Involvement and Replenishment of Oxygen Species Using In Situ Designed-TP Techniques. *ACS Catal.* **2019**, *9*, 6698–6710. [[CrossRef](#)]
162. Huang, Y.; Fan, W.; Long, B.; Li, H.; Qiu, W.; Zhao, F.; Tong, Y.; Ji, H. Alkali-modified non-precious metal 3D-NiCo₂O₄ nanosheets for efficient formaldehyde oxidation at low temperature. *J. Mater. Chem. A* **2016**, *4*, 3648–3654. [[CrossRef](#)]
163. Li, L.; Zhang, C.; Chen, F.; Xiang, Y.; Yan, J.; Chu, W. Facile fabrication of hollow structured Cu-Ce binary oxides and their catalytic properties for toluene combustion. *Catal. Today* **2020**, *376*, 239–246. [[CrossRef](#)]
164. Kamal, M.S.; Razzak, S.A.; Hossain, M.M. Catalytic oxidation of volatile organic compounds (VOCs)—A review. *Atmos. Environ.* **2016**, *140*, 117–134. [[CrossRef](#)]
165. Le, Y.; Qi, L.; Wang, C.; Song, S. Hierarchical Pt/WO₃ nanoflakes assembled hollow microspheres for room-temperature formaldehyde oxidation activity. *Appl. Surf. Sci.* **2020**, *512*, 145763. [[CrossRef](#)]
166. Wang, C.; Liu, N.; Zhang, C.; Liu, X.; Li, X.; Zhao, X.S. Ruthenium/cobalt binary oxides supported on hollow alumina microspheres as highly efficient catalyst for vinyl chloride oxidation. *Appl. Surf. Sci.* **2019**, *497*, 143776. [[CrossRef](#)]
167. Chen, H.M.; He, J.H.; Zhang, C.B.; He, H. Self-Assembly of Novel Mesoporous Manganese Oxide Nanostructures and Their Application in Oxidative Decomposition of Formaldehyde. *J. Phys. Chem. C* **2007**, *111*, 18033–18038. [[CrossRef](#)]
168. Pang, G.; Wang, D.; Zhang, Y.; Ma, C.; Hao, Z. Catalytic activities and mechanism of formaldehyde oxidation over gold supported on MnO₂ microsphere catalysts at room temperature. *Front. Environ. Sci. Eng.* **2015**, *10*, 447–457. [[CrossRef](#)]
169. Nie, L.H.; Meng, A.Y.; Yu, J. Hierarchically macro-mesoporous Pt/γ-Al₂O₃ composite microspheres for efficient formaldehyde oxidation at room temperature. *Sci. Rep.* **2013**, *3*, 3215. [[CrossRef](#)]
170. Qi, L.; Cheng, B.; Ho, W.; Liu, G.; Yu, J. Hierarchical Pt/NiO Hollow Microspheres with Enhanced Catalytic Performance. *ChemNanoMat* **2015**, *1*, 58–67. [[CrossRef](#)]
171. Zhou, J.; Zhao, Y.; Qin, L.F.; Zeng, C.; Xiao, W. Hollow structured CoSn(OH)₆-supported Pt for effective room-temperature oxidation of gaseous formaldehyde. *Funct. Mater. Lett.* **2017**, *09*, 1642009. [[CrossRef](#)]

172. Lv, T.; Peng, C.; Zhu, H.; Xiao, W. Heterostructured Fe₂O₃@SnO₂ core-shell nanospindles for enhanced Room-temperature HCHO oxidation. *Appl. Surf. Sci.* **2018**, *457*, 83–92. [[CrossRef](#)]
173. Zhang, C.B.; He, H.; Tanaka, K.-i. Perfect catalytic oxidation of formaldehyde over a Pt/TiO₂ catalyst at room temperature. *Catal. Commun.* **2005**, *6*, 211–214. [[CrossRef](#)]
174. Zhang, C.B.; He, H.; Tanaka, K.-i. Catalytic performance and mechanism of a Pt/TiO₂ catalyst for the oxidation of formaldehyde at room temperature. *Appl. Catal. B* **2006**, *65*, 37–43. [[CrossRef](#)]
175. Khalifeh, R.; Karimi, M.; Rajabzadeh, M.; Hafizi, A.; Nogorani, F.S. Synthesis and morphology control of nano CuAl₂O₄ hollow spheres and their application as an efficient and sustainable catalyst for CO₂ fixation. *J. CO₂ Util.* **2020**, *41*, 101233. [[CrossRef](#)]
176. Prasad, D.; Patil, K.N.; Bhanushali, J.T.; Nagaraja, B.M.; Jadhav, A.H. Sustainable fixation of CO₂ into epoxides to form cyclic carbonates using hollow marigold CuCo₂O₄ spinel microspheres as a robust catalyst. *Catal. Sci. Technol.* **2019**, *9*, 4393–4412. [[CrossRef](#)]
177. Bian, Y.; Xu, C.; Wen, X.; Xu, L.; Cui, Y.; Wang, S.; Wu, C.-E.; Qiu, J.; Cheng, G.; Chen, M. CO₂ methanation over the Ni-based catalysts supported on nano-CeO₂ with varied morphologies. *Fuel* **2023**, *331*, 125755. [[CrossRef](#)]
178. Cui, Y.; Lian, X.; Xu, L.; Chen, M.; Yang, B.; Wu, C.-E.; Li, W.; Huang, B.; Hu, X. Designing and Fabricating Ordered Mesoporous Metal Oxides for CO₂ Catalytic Conversion: A Review and Prospect. *Materials* **2019**, *12*, 276. [[CrossRef](#)]
179. Heydari, P.; Hafizi, A.; Rajabzadeh, M.; Karimi, M.; Khalifeh, R.; Rahimpour, M.R. Synthesis and application of nanoporous triple-shelled CuAl₂O₄ hollow sphere catalyst for atmospheric chemical fixation of carbon dioxide. *J. Taiwan Inst. Chem. Eng.* **2020**, *114*, 81–90. [[CrossRef](#)]
180. Ion, A.; Parvulescu, V.; Jacobs, P.; Vos, D.D. Synthesis of symmetrical or asymmetrical urea compounds from CO₂ via base catalysis. *Green. Chem.* **2007**, *9*, 158–161. [[CrossRef](#)]
181. Leitner, W. Carbon Dioxide as a Raw Material: The Synthesis of Formic Acid and Its Derivatives from CO₂. *Angew. Chem. Int. Ed. Engl.* **1995**, *34*, 2207–2221. [[CrossRef](#)]
182. Qian, Q.; Zhang, J.; Cui, M.; Han, B. Synthesis of acetic acid via methanol hydrocarboxylation with CO₂ and H₂. *Nat. Commun.* **2016**, *7*, 11481. [[CrossRef](#)]
183. Witoon, T.; Permsirivanich, T.; Donphai, W.; Jaree, A.; Chareonpanich, M. CO₂ hydrogenation to methanol over Cu/ZnO nanocatalysts prepared via a chitosan-assisted co-precipitation method. *Fuel Process. Technol.* **2013**, *116*, 72–78. [[CrossRef](#)]
184. Tian, H.-F.; Yu, L.; Ding, J.; Zha, F.; Tang, X.-H.; Chang, Y. Synthesis of hollow CuO/ZnO/Al₂O₃ composite microspheres for catalysing carbon dioxide hydrogenation. *Micro Nano Lett.* **2019**, *14*, 932–936. [[CrossRef](#)]
185. Han, X.; Li, M.; Chang, X.; Hao, Z.; Chen, J.; Pan, Y.; Kawi, S.; Ma, X. Hollow structured Cu@ZrO₂ derived from Zr-MOF for selective hydrogenation of CO₂ to methanol. *J. Energy Chem.* **2022**, *71*, 277–287. [[CrossRef](#)]
186. Cui, W.G.; Zhang, Q.; Zhou, L.; Wei, Z.C.; Yu, L.; Dai, J.J.; Zhang, H.; Hu, T.L. Hybrid MOF Template-Directed Construction of Hollow-Structured In₂O₃@ZrO₂ Heterostructure for Enhancing Hydrogenation of CO₂ to Methanol. *Small* **2022**, *19*, 2204914. [[CrossRef](#)] [[PubMed](#)]
187. Cargnello, M.; Jaén, J.J.D.; Garrido, J.C.H.; Bakhmutsky, K.; Montini, T.; Gámez, J.J.C.; Gorte, R.J.; Fornasiero, P. Exceptional activity for methane combustion over modular Pd@CeO₂ subunits on functionalized Al₂O₃. *Science* **2012**, *337*, 713–717. [[CrossRef](#)] [[PubMed](#)]
188. Du, X.; Zhang, D.; Shi, L.; Gao, R.; Zhang, J. Morphology Dependence of Catalytic Properties of Ni/CeO₂ Nanostructures for Carbon Dioxide Reforming of Methane. *J. Phys. Chem. C* **2012**, *116*, 10009–10016. [[CrossRef](#)]
189. Li, Z.W.; Kawi, S. Multi-Ni@Ni phyllosilicate hollow sphere for CO₂ reforming of CH₄: Influence of Ni precursors on structure, sintering and carbon resistance. *Catal. Sci. Technol.* **2018**, *8*, 1915–1922. [[CrossRef](#)]
190. Wang, G.; Liang, Y.; Song, J.; Li, H.; Zhao, Y. Study on High Activity and Outstanding Stability of Hollow-NiPt@SiO₂ Core-Shell Structure Catalyst for DRM Reaction. *Front. Chem.* **2020**, *8*, 220. [[CrossRef](#)]
191. Sheng, K.F.; Luan, D.; Jiang, H.; Zeng, F.; Wei, B.; Pang, F.; Ge, J.P. Ni_xCo_y Nanocatalyst Supported by ZrO₂ Hollow Sphere for Dry Reforming of Methane: Synergetic Catalysis by Ni and Co in Alloy. *ACS Appl. Mater. Interfaces* **2019**, *11*, 24078–24087. [[CrossRef](#)]
192. Kathiraser, Y.; Wang, Z.; Kawi, S. Oxidative CO₂ reforming of methane in La_{0.6}Sr_{0.4}Co_{0.8}Ga_{0.2}O₃-delta (LSCG) hollow fiber membrane reactor. *Environ. Sci. Technol.* **2013**, *47*, 14510–14517. [[CrossRef](#)]
193. Li, Z.; Sibudjing, K. Facile Synthesis of Multi-Ni-Core@Ni Phyllosilicate@CeO₂ Shell Hollow Spheres with High Oxygen Vacancy Concentration for Dry Reforming of CH₄. *ChemCatChem* **2018**, *10*, 2994–3001. [[CrossRef](#)]
194. Zhang, Q.; Feng, X.; Liu, J.; Zhao, L.; Song, X.; Zhang, P.; Gao, L. Hollow hierarchical Ni/MgO-SiO₂ catalyst with high activity, thermal stability and coking resistance for catalytic dry reforming of methane. *Int. J. Hydrogen Energy* **2018**, *43*, 11056–11068. [[CrossRef](#)]
195. Lu, Y.; Guo, D.; Zhao, Y.; Moyo, P.S.; Zhao, Y.; Wang, S.; Ma, X. Enhanced catalytic performance of Ni_x-V@HSS catalysts for the DRM reaction: The study of interfacial effects on Ni-VO_x structure with a unique yolk-shell structure. *J. Catal.* **2021**, *396*, 65–80. [[CrossRef](#)]
196. Xu, Y.; Zhang, Y.; Zhou, Y.; Xiang, S.; Wang, Q.; Zhang, C.; Sheng, X. CeO₂ hollow nanospheres synthesized by a one pot template-free hydrothermal method and their application as catalyst support. *RSC Adv.* **2015**, *5*, 58237–58245. [[CrossRef](#)]
197. Chen, C.; Li, D.; Wang, A.; Guo, J.; Dong, S.; Chen, D.; Jiao, X.; Xia, Y. Interfacial enhancement for hydrogen radical transfer on hollow Cu₂O/rGO nanohybrid with efficient catalytic reduction activity. *Appl. Catal. A Gen.* **2020**, *590*, 117331. [[CrossRef](#)]

198. Wang, Y.; Li, L.; Wang, C.; Wang, T. Facile approach to synthesize uniform Au@mesoporous SnO₂ yolk-shell nanoparticles and their excellent catalytic activity in 4-nitrophenol reduction. *J. Nanopart Res.* **2015**, *18*, 2. [[CrossRef](#)]
199. Zhang, S.F.; Zhao, D.Y.; Hou, C.; Liang, C.; Li, H. Facile one-pot synthesis of cellulose nanocrystal-supported hollow CuFe₂O₄ nanoparticles as efficient catalyst for 4-nitrophenol reduction. *J. Nanopart Res.* **2018**, *20*, 161. [[CrossRef](#)]
200. Xia, Q.D.; Fu, S.S.; Ren, G.J.; Chai, F.; Jiang, J.J.; Qu, F.Y. Fabrication of Fe₃O₄@Au hollow spheres with recyclable and efficient catalytic properties. *New J. Chem.* **2016**, *40*, 818–824. [[CrossRef](#)]
201. Chen, Y.; Zhang, Y.; Kou, Q.; Liu, Y.; Han, D.; Wang, D.; Sun, Y.; Zhang, Y.; Wang, Y.; Lu, Z.; et al. Enhanced Catalytic Reduction of 4-Nitrophenol Driven by Fe₃O₄-Au Magnetic Nanocomposite Interface Engineering: From Facile Preparation to Recyclable Application. *Nanomaterials* **2018**, *8*, 353. [[CrossRef](#)]
202. Ma, M.L.; Yang, Y.Y.; Feng, R.J.; Jia, L.; Chen, G.P.; Li, W.T.; Lyu, P. Preparation and characterization of magnetic hollow Fe₃O₄/P(GMA-EGDMA)-SO₃H/Au-PPy recyclable catalyst for catalytic reduction of 4-nitrophenol. *Appl. Organomet. Chem.* **2018**, *32*, e4534. [[CrossRef](#)]
203. Cheng, J.C.; Zhao, S.L.; Gao, W.B.; Jiang, P.B.; Li, R. Au/Fe₃O₄@TiO₂ hollow nanospheres as efficient catalysts for the reduction of 4-nitrophenol and photocatalytic degradation of rhodamine B. *React. Kinet. Mech. Catal.* **2017**, *121*, 797–810. [[CrossRef](#)]
204. Zhang, D.F.; Zhang, G.Z.; Zhang, L. Multi-shelled FeCo₂O₄ hollow porous microspheres/CCFs magnetic hybrid and its dual-functional catalytic performance. *Chem. Eng. J.* **2017**, *330*, 792–803. [[CrossRef](#)]
205. Gao, Q.; Sun, Z.Q. Facile Fabrication of Uniform MFe₂O₄ (M = Co, Ni, Cu) Hollow Spheres and Their Recyclable Superior Catalytic Activity Towards 4-Nitrophenol Reduction. *J. Nanosci. Nanotechnol.* **2018**, *18*, 5645–5653. [[CrossRef](#)] [[PubMed](#)]
206. Zhang, Q.Z.; Jin, X.; Xu, Z.H.; Zhang, J.M.; Rendon, U.F.; Razzari, L.; Chaker, M.; Ma, D.L. Plasmonic Au Loaded Hierarchical Hollow Porous TiO₂ Spheres: Synergistic Catalysts for Nitroaromatic Reduction. *J. Phys. Chem. Lett.* **2018**, *9*, 5317–5326. [[CrossRef](#)] [[PubMed](#)]
207. Wu, G.; Liang, X.; Zhang, L.; Tang, Z.; Al-Mamun, M.; Zhao, H.; Su, X. Fabrication of Highly Stable Metal Oxide Hollow Nanospheres and Their Catalytic Activity toward 4-Nitrophenol Reduction. *ACS Appl. Mater. Interfaces* **2017**, *9*, 18207–18214. [[CrossRef](#)] [[PubMed](#)]
208. Zeng, J.; Zhang, Q.; Chen, J.Y.; Xia, Y.N. A comparison study of the catalytic properties of Au-based nanocages, nanoboxes, and nanoparticles. *Nano Lett.* **2010**, *10*, 30–35. [[CrossRef](#)] [[PubMed](#)]
209. Ma, X.D.; Feng, X.; Guo, J.; Cao, H.Q.; Suo, X.Y.; Sun, H.W.; Zheng, M.H. Catalytic oxidation of 1,2-dichlorobenzene over Ca-doped FeO_x hollow microspheres. *Appl. Catal. B* **2014**, *147*, 666–676. [[CrossRef](#)]
210. Wen, J.X.; Guo, H.W.; Ma, X.D.; Wei, Z.Z.; He, X.; Zhang, L.L.; Li, B.D.; Wang, T.; Cheng, Y.H. Mesoporous Ce-doped ZnO hollow microspheres for oxidation of 1, 2-dichlorobenzene. *Catal. Sci. Technol.* **2020**, *10*, 3739–3747. [[CrossRef](#)]
211. Zhao, B.; Shao, Q.; Hao, L.; Zhang, L.; Liu, Z.; Zhang, B.; Ge, S.; Guo, Z. Yeast-template synthesized Fe-doped cerium oxide hollow microspheres for visible photodegradation of acid orange 7. *J. Colloid. Interface Sci.* **2018**, *511*, 39–47. [[CrossRef](#)] [[PubMed](#)]
212. Zhang, S.W.; Fan, Q.H.; Gao, H.H.; Huang, Y.S.; Liu, X.; Li, J.X.; Xu, X.J.; Wang, X.K. Retraction: Formation of Fe₃O₄@MnO₂ ball-in-ball hollow spheres as a high performance catalyst for enhanced catalytic performances. *J. Mater. Chem. A* **2022**, *4*, 1414–1422. [[CrossRef](#)]
213. Lin, C.J.; Yang, W.-T.; Chou, C.-Y.; Liou, S.Y.H. Hollow mesoporous TiO₂ microspheres for enhanced photocatalytic degradation of acetaminophen in water. *Chemosphere* **2016**, *152*, 490–495. [[CrossRef](#)]
214. Chen, L.; Zuo, X.; Yang, S.; Cai, T.; Ding, D. Rational design and synthesis of hollow Co₃O₄@Fe₂O₃ core-shell nanostructure for the catalytic degradation of norfloxacin by coupling with peroxymonosulfate. *Chem. Eng. J.* **2019**, *359*, 373–384. [[CrossRef](#)]
215. Liu, Y.; Yang, J.; Wu, B.; Zhang, W.; Zhang, X.; Shan, C.; Liu, Q. CeO₂/Co₃O₄ hollow microsphere: Pollen-biotemplated preparation and application in photo-catalytic degradation. *Colloids Surf.* **2020**, *586*, 124193. [[CrossRef](#)]
216. Lee, D.-E.; Moru, S.; Jo, W.-K.; Tonda, S. Porous g-C₃N₄-encapsulated TiO₂ hollow sphere as a high-performance Z-scheme hybrid for solar-induced photocatalytic abatement of environmentally toxic pharmaceuticals. *J. Mater. Sci. Technol.* **2021**, *82*, 21–32. [[CrossRef](#)]
217. Xu, H.; Wang, X.; Dai, M.; Wang, W.; Lu, D.; Zhang, M.; Chen, Y.; Song, H. Resin microsphere templates for TiO₂ hollow structure with uniform mesopores: Preparation and photocatalytic application. *Mater. Chem. Phys.* **2021**, *260*, 124158. [[CrossRef](#)]
218. Chen, Z.; Zheng, Y.; Liu, Y.; Zhang, W.; Wang, Y.; Guo, X.; Tang, X.; Zhang, Y.; Wang, Z.; Zhang, T. Magnetic Mn-Doped Fe₃O₄ hollow Microsphere/RGO heterogeneous Photo-Fenton Catalyst for high efficiency degradation of organic pollutant at neutral pH. *Mater. Chem. Phys.* **2019**, *238*, 121893. [[CrossRef](#)]
219. Wu, X.; Xia, F.; Nan, Z. Facile synthesis of double-mesoporous-shelled hollow spheres of Cu–CuFe₂O₄/SiO₂ composite as excellent Fenton catalyst. *Mater. Chem. Phys.* **2020**, *242*, 122490. [[CrossRef](#)]
220. He, F.; Ji, Y.; Wang, Y.; Zhang, Y. Preparation of bifunctional hollow mesoporous Fe⁰@C@MnFe₂O₄ as Fenton-like catalyst for degradation of Tetrabromobisphenol A. *J. Taiwan Inst. Chem. Eng.* **2017**, *80*, 553–562. [[CrossRef](#)]
221. Ding, R.-R.; Li, W.-Q.; He, C.-S.; Wang, Y.-R.; Liu, X.-C.; Zhou, G.-N.; Mu, Y. Oxygen vacancy on hollow sphere CuFe₂O₄ as an efficient Fenton-like catalysis for organic pollutant degradation over a wide pH range. *Appl. Catal. B* **2021**, *291*, 120069. [[CrossRef](#)]

Disclaimer/Publisher’s Note: The statements, opinions and data contained in all publications are solely those of the individual author(s) and contributor(s) and not of MDPI and/or the editor(s). MDPI and/or the editor(s) disclaim responsibility for any injury to people or property resulting from any ideas, methods, instructions or products referred to in the content.